การวิเคราะห์เชิงสมรรถนะและการควบคุมเซลล์เชื้อเพลิงชนิดออกไซด์แข็ง ที่มีการรีฟอร์มมิงภายใน

นางสาวนริศรา ฉัตรรัตนเวช

วิทยานิพนธ์นี้เป็นส่วนหนึ่งของการศึกษาตามหลักสูตรปริญญาวิศวกรรมศาสตรดุษฎีบัณฑิต
สาขาวิชาวิศวกรรมเคมี ภาควิชาวิศวกรรมเคมี
คณะวิศวกรรมศาสตร์ จุฬาลงกรณ์มหาวิทยาลัย
ปีการศึกษา 2557

PERFORMANCE ANALYSIS AND CONTROL OF SOLID OXIDE FUEL CELLS WITH DIRECT INTERNAL REFORMING

Miss Narissara Chatrattanawet

A Dissertation Submitted in Partial Fulfillment of the Requirements
for the Degree of Doctor of Engineering Program in Chemical Engineering
Department of Chemical Engineering
Faculty of Engineering
Chulalongkorn University
Academic Year 2014

Thesis Title	PERFORMANCE ANALYSIS AND CONTROL OF SOLID OXIDE FUEL CELLS WITH DIRECT INTERNAL REFORMING
By	Miss Narissara Chatrattanawet
Field of Study	Chemical Engineering
Thesis Advisor	Assistant Professor Amornchai Arpornwichanop, D.Eng.

Accepted by the Faculty of Engineering, Chulalongkorn University in Partial Fulfillment of the Requirements for the Doctoral Degree

.....Dean of the Faculty of Engineering
(Professor Bundhit Eua-arporn, Ph.D.)

THESIS COMMITTEE

.....Chairman
(Associate Professor Anongnat Somwangthanaroj, Ph.D.)
.....Thesis Advisor
(Assistant Professor Amornchai Arpornwichanop, D.Eng.)
.....Examiner
(Associate Professor Soorathep Kheawhom, Ph.D.)
.....External Examiner
(Assistant Professor Woranee Paengjuntuek, D.Eng.)
.....External Examiner
(Veerayut Lersbamrungsuk, D.Eng.)

นริศรา ฉัตรรัตนเวช : การวิเคราะห์เชิงสมรรถนะและการควบคุมเซลล์เชื้อเพลิงชนิดออกไซด์แข็งที่มีการรีฟอร์มมิงภายใน (PERFORMANCE ANALYSIS AND CONTROL OF SOLID OXIDE FUEL CELLS WITH DIRECT INTERNAL REFORMING) อ.ที่ปรึกษาวิทยานิพนธ์หลัก: ผศ. ดร.อมรชัย อาภรณ์วิชานพ , 4 หน้า.

งานวิจัยนี้นำเสนอการวิเคราะห์เชิงสมรรถนะและการควบคุมของเซลล์เชื้อเพลิงชนิดออกไซด์แข็งที่มีการรีฟอร์มมิงของเชื้อเพลิงภายใน ในส่วนแรกของงานได้ศึกษาหาสภาวะการดำเนินงานที่เหมาะสมที่สภาวะคงตัว โดยการออกแบบเซลล์เชื้อเพลิงชนิดออกไซด์แข็ง ร่วมกับการเกิดกระบวนการรีฟอร์มมิงของก๊าซมีเทนภายใน ซึ่งจะทำให้สามารถประหยัดพลังงานที่ใช้ในการผลิตไฟฟ้าและทำให้ประสิทธิภาพของระบบสูงขึ้น เนื่องจากสามารถนำความร้อนที่เกิดขึ้นจากปฏิกิริยาไฟฟ้าเคมีภายในเซลล์เชื้อเพลิงมาใช้ในกระบวนการรีฟอร์มมิงเพื่อผลิตก๊าซไฮโดรเจนได้ อย่างไรก็ตามการผลิตไฟฟ้าดังกล่าวเป็นกระบวนการที่มีความซับซ้อน ดังนั้นการศึกษาผลของตัวแปรดำเนินงานที่มีต่อประสิทธิภาพของเซลล์เชื้อเพลิงชนิดออกไซด์แข็งที่เกิดการรีฟอร์มมิงภายในจึงมีความสำคัญต่อการออกแบบระบบการควบคุมที่เหมาะสมของเซลล์เชื้อเพลิง จากการศึกษาตัวแปรต่างๆ ที่สภาวะพลวัต พบว่าการเปลี่ยนแปลงของค่าความหนาแน่นของกระแส อัตราการไหลของเชื้อเพลิงและอากาศขาเข้า และอุณหภูมิของเชื้อเพลิงและอากาศขาเข้า ส่งผลต่ออุณหภูมิและค่าความต่างศักย์ไฟฟ้าของเซลล์เชื้อเพลิง ในส่วนที่สองของงานวิจัยนั้นได้ทำการออกแบบโครงสร้างการควบคุมเซลล์เชื้อเพลิง เพื่อหาตัวแปรที่จะถูกควบคุมและตัวแปรปรับที่เหมาะสม ซึ่งจะทำให้ระบบควบคุมมีประสิทธิภาพมากขึ้น โดยที่การวิเคราะห์ความสามารถในการควบคุมเพื่อกำหนดคู่ตัวแปรปรับและตัวแปรควบคุมถูกวิเคราะห์ด้วยอัตราการขยายสัมพัทธ์ จากการศึกษาพบว่าอัตราการไหลเชิงโมลของอากาศและเชื้อเพลิงขาเข้าเป็นตัวแปรปรับเพื่อควบคุมอุณหภูมิของเซลล์เชื้อเพลิงและสัดส่วนโมลของก๊าซมีเทนตามลำดับ ส่วนสุดท้ายของงานวิจัยจะมุ่งเน้นในด้านการออกแบบตัวควบคุมเพื่อควบคุมอุณหภูมิของเซลล์เชื้อเพลิง สัดส่วนเชิงโมลของก๊าซมีเทน และค่าความต่างศักย์ไฟฟ้า โดยใช้ตัวควบคุมทั่วใช้และเทคนิคการควบคุมขั้นสูงอย่างตัวควบคุมแบบโมเดลพรีดิกทีฟ ซึ่งตัวควบคุมแบบโมเดลพรีดิกทีฟนั้นต้องการแบบจำลองที่มีความแม่นยำและน่าเชื่อถือ อย่างไรก็ตามแบบจำลองที่เกี่ยวข้องกับเซลล์เชื้อเพลิงที่เกิดกระบวนการรีฟอร์มมิงภายในมีความซับซ้อนและเกี่ยวข้องกับพารามิเตอร์ที่มีความไม่แน่นอน ดังนั้นในงานวิจัยนี้จึงได้นำเสนอการควบคุมแบบโมเดลพรีดิกทีฟที่มีเงื่อนไขบังคับคงทนเชิงออฟไลน์ มาประยุกต์ใช้เพื่อควบคุมเซลล์เชื้อเพลิงที่ทำการศึกษา โดยแบบจำลองที่ทำการศึกษา จะถูกจัดให้อยู่ในรูปแบบจำลองเชิงเส้นที่เปลี่ยนแปลงตามเวลา และแบบจำลองเชิงเส้นที่เปลี่ยนแปลงตามพารามิเตอร์ จากการศึกษาภายใต้แบบจำลองที่มีความไม่แน่นอนพบว่าตัวควบคุมที่นำเสนอมีสมรรถนะการควบคุมที่ดี สามารถควบคุมตัวแปรควบคุมต่างๆ ได้ นอกจากนี้ตัวควบคุมซึ่งใช้แบบจำลองเชิงเส้นที่เปลี่ยนแปลงตามพารามิเตอร์มีสมรรถนะการควบคุมที่ดีกว่าตัวควบคุมที่ใช้แบบจำลองเชิงเส้นที่เปลี่ยนแปลงตามเวลา เนื่องจากระบบที่เปลี่ยนแปลงตามพารามิเตอร์นั้นจะคำนวณพารามิเตอร์ที่ใช้ในแบบจำลองใหม่

ภาควิชา วิศวกรรมเคมี ลายมือชื่อนิสิต .....

สาขาวิชา วิศวกรรมเคมี ลายมือชื่อ อ.ที่ปรึกษาหลัก .....

ปีการศึกษา 2557

5171846821 : MAJOR CHEMICAL ENGINEERING
KEYWORDS: SOLID OXIDE FUEL CELL / INTERNAL REFORMING / CONTROL STRUCTURE DESIGN / ROBUST MODEL PREDICTIVE CONTROL

NARISSARA CHATRATTANAWET: PERFORMANCE ANALYSIS AND CONTROL OF SOLID OXIDE FUEL CELLS WITH DIRECT INTERNAL REFORMING. ADVISOR: ASST. PROF. AMORNCHAI ARPORNWICHANOP, D.Eng., 4 pp.

This research focuses on the performance analysis and control of a solid oxide fuel cell (SOFC) with direct internal reforming using methane as fuel. Firstly, the steady state analysis is performed to design the optimal operational condition for this system. The direct internal reforming of methane in SOFC can utilize the heat from the exothermic electrochemical reaction to produce hydrogen-rich gas, leading to an increasing system efficiency. However, the coupling of the endothermic reforming and electrochemical reactions results in a complicated dynamic response. Therefore, the effect of input variables on the cell temperature and cell voltage is analyzed to investigate the dynamic behavior that is important for design a controller. It is found that the cell operating temperature and cell voltage are dependent on the fuel and air inlet temperature as well as the current density. Next, to achieve the efficient control system, the control structure design of the SOFC is considered to identify good controlled variables and manipulated variables. The concept of a controllability analysis is applied to the control system design of the SOFC for the selection of input-output pairings by considering the relative gain array (RGA). The result shows that the inlet molar flow rates of air and fuel are manipulated variables to control the cell temperature and the content of fuel, respectively. Finally, the conventional and advanced control techniques are designed and implemented to control the cell temperature, the content of methane and the cell voltage. In this research, the model predictive control (MPC) that is a model-based control strategy is proposed for SOFC control. In general, MPC requires the accurate and reliable model of the process to be controlled. However, the SOFC model is complicated and involves uncertain parameters. Therefore, an off-line robust MPC algorithm is developed and employed for controlling the SOFC. The robust MPC algorithm based on linear time-varying (LTV) and linear parameter varying (LPV) systems is also studied. The simulation results show that under the model uncertainty, the proposed robust MPC can control the SOFC and guarantee the stability of the SOFC. The robust MPC algorithm using the LPV model of the SOFC can achieve a better control performance because the model parameters are on-line updated and used in the control calculation.

Department:	Chemical Engineering	Student's Signature	.....
Field of Study:	Chemical Engineering	Advisor's Signature	.....
Academic Year:	2014		

ACKNOWLEDGEMENTS

I would first like to express my sincere gratitude to my thesis advisor, Assistant Professor Amornchai Arpornwichanop, for giving me the possibility to complete this thesis. His valuable guidance, great enthusiasm, and warm encouragement have inspired and motivated me so much during the course of my dissertation. It has been great opportunity and experience to work with him.

I would also like to especially thank all members of my thesis committee, Associate Professor Anongnat Somwangthanaroj, Asssociate Professor Soorathep Kheawhom, Assistant Professor Woranee Paengjuntuek, and Dr. Veerayut Lersbamrungsuk for their valuable comments and suggestions on this thesis.

My sincere gratitude is expressed to Professor Sigurd Skogestad who provides me an opportunity to join his research group at Norwegian University of Science and Technology (NTNU), Trondheim, Norway, to broaden my knowledge in the field of control structure design. He has guided and encouraged me during my research work there. Furthermore, I would also like to thank all of my friends in Norway for their assistance and friendship during my visit to Norway.

I would also like to acknowledge the Thailand Research fund (TRF) through the Royal Golden Jubilee Ph.D. program for their grant support to this research. Support from the Ratchadaphiseksomphot Endowment Fund of Chulalongkorn University, the Graduate School of Chulalongkorn University (Conference Grant for Ph.D. Student) and the Computational Process Engineering Research Unit is also gratefully acknowledged.

I am also very grateful to Assistant Professor Yaneeporn Patcharavorachot, Dr. Suthida Authayanun, Dr. Dang Saebea and all my colleagues in the Control and Systems Engineering Research Center for their friendship and kind assistance. Finally, I would like to thankful my beloved family for their eternal love and encouragement during my study. My research work would not have finished without their support.

CONTENTS

Page

Page

LIST OF TABLES

LIST OF FIGURES

NOMENCLATURES

A	reaction area (m^2)
A_i	vertices in the convex hull
B_i	vertices in the convex hull
Co	convex hull
Cp	heat capacity (kJ kg^{-1} K^{-1})
CV	controlled variable
$D_{eff,anode}$	effective diffusivity coefficient in the anode (m s^{-1})
$D_{eff,cathode}$	effective diffusivity coefficient in the cathode (m s^{-1})
d	disturbance
$E_{electrode}$	activation energy of the electrode exchange current density (kJ mol^{-1})
E_0	open-circuit voltage at the standard pressure (V)
E_{OCV}	open-circuit voltage (V)
E_r	standard reversible voltage (V)
e	error
F	Faraday constant (C mol^{-1})
F	state feedback gains
G	non-singular square complex matrix
g_{ij}	ij th element of G
$\hat{g}_{ij}$	inverse of the ji th element of G^{-1}
h	channel height (mm)
J	cost function
j	current density (A cm^{-2})
$j_{0,\ electrode}$	exchange current density of electrode (A m^{-2})
K_c	proportional gain
k	plant gain
$k_{electrode}$	pre-exponential factor of electrode (A m^{-2})
L	cell length (m)
LHV_i	low heating value of component i

loss L	*Loss*
$\dot{m}_f$	mass flow rate of fuel (kg s^{-1})
N_{ss}	number of steady-state degrees of freedom
N_{valves}	numbers of dynamic DOFs or numbers of valves
N_{0y}	numbers of controlled variables
$N_{0,valves}$	numbers of purely dynamic control DOFs
n	number of electrons transferred
$\dot{n}$	molar flow rate (mol s^{-1})
P	pressure (bar)
P_{FC}	power density (W m^{-2})
p	scheduling parameter
p_i	partial pressure of component *i* (bar)
Q	weighting matrix
Q_i	enthalpy flow of component *i* (kJ s^{-1})
R	gas constant (kJ mol^{-1} K^{-1})
R	weighting matrix
R_k	rate of reaction *k* (mol s^{-1} m^{-2})
R_{Ohm}	internal resistance of the cell (Ω m^{-2})
T_{FC}	fuel cell temperature (K)
t	time (s)
U_a	air utilization factor
U_{fuel}	fuel utilization factor
u	degrees of freedom
u_j	control input
V	volume (m^3)
V_{FC}	fuel cell voltage (V)
W	cell width (m)
W_{elec}	electrical work (W)
x	state variables
x_i	molar fraction of component *i*
y_j	plant output

Greek symbols

α	transfer coefficient
ε_{SOFC}	fuel cell efficiency
ΔG	Gibbs free energy change
ΔH	heat of reaction (kJ mol^{-1})
η	overpotentials (V)
λ	uncertain parameter vector
λ_{air}	excess air ratio
λ_{ij}	relative gain
θ	time delay
ρ	density (kg m^{-3})
σ_{anode}	electronic conductivity of anode (Ω^{-1} m^{-2})
$\sigma_{cathode}$	electronic conductivity of cathode (Ω^{-1} m^{-2})
$\sigma_{electrolyte}$	ionic conductivity of electrolyte (Ω^{-1} m^{-2})
Ω	polytope for polytopic systems
τ_1	time constant
τ_2	second-order lag time constant
τ_{anode}	anode thickness (m)
τ_c	response time constant
$\tau_{cathode}$	cathode thickness (m)
τ_D	derivative gain
$\tau_{electrolyte}$	electrolyte thickness (m)
τ_I	integral gain
$\upsilon_{i,k}$	stoichiometric coefficient of component *i* in reaction *k*

Superscripts

0	feed conditions (fuel and air channel inlet)
in	inlet
T	transpose of matrix

-1	inverse of matrix

Subscripts

a	air channel
act	activation
conc	concentration
f	fuel channel
i	chemical component
in	inlet
K	reaction
k	sampling time
M	control horizon
Ohm	Ohmic
Opt	optimal value
out	outlet
P	prediction horizon
ref	reference
SOFC	solid oxide fuel cell
ss	steady state condition
TPB	three-phase boundary

CHAPTER I

INTRODUCTION

1.1 Research background and motivation

Fuel cell are electrochemical devices that can convert the chemical energy of fuels (often in the form of hydrogen) directly to electrical energy by electrochemical reactions without the combustion reaction (Yamamoto, 2000). In general, the fuel cells are classified fundamentally by electrolyte types corresponding to their operating temperature range. Among the currently available fuel cells, a solid oxide fuel cell (SOFC) is regarded as the most promising fuel cell types with possibility of its use in co-generation applications and a wide range of commercial applications. It operates at high temperatures (typically 873-1273 K), which leads to a high energy conversion efficiency, the flexibility of using various fuel types, and the prospect for combined heat and power systems. The attractive features of fuel cells include no moving parts, quiet operation, low environmental pollution, high reliability over conventional power generation equipment, and high energy conversion efficiency. However, the high-temperature operation cause some problems such as the requirement for high performance of materials, sealing problems caused by thermal expansion, high manufacturing cost and difficulties in thermal management (Yang et al., 2009).

The structure of SOFC consists of interconnects, two porous electrodes (anode and cathode) separated by a dense ceramic electrolyte. Because of no liquid components, the SOFC can be fabricated into various shapes such as planar, tubular, and monolithic configurations. The planar SOFC has been received much attention due to its compactness, high power density, and ease of mass production (Hu et al., 2008). The most important design feature of the planar SOFC relates to gas flow configurations: co-flow, counter-flow, and cross-flow. The co-flow configuration gives a uniform current density distribution among the three flow configurations (Hu et al., 2008). In addition, SOFC can also be designed either with electrolyte support or electrode support (Xin et al., 2006).

Further, SOFC can use various fuel types such as methane, methanol, ethanol and other hydrocarbons and the heat generated from SOFC can be used in the heat and power systems (Casas et al., 2011, Varbanov and Friedler, 2009). Steam reforming process is an interesting strategy because this reaction can produce the highest H_2 yield and cleanest exhaust. Due to its high-temperature operation, it can directly convert hydrocarbon fuels via internal reforming process to generate hydrogen-rich gas within the fuel cell stack. This operational strategy is known as a direct internal reforming solid oxide fuel cell (DIR-SOFC). The total heat produced in fuel cell can be used for the endothermic steam reforming reaction, eliminating the requirement of a separate fuel reformer. This leads to a more attractive and efficient SOFC system design (Aguiar et al., 2004). In addition, the steam required for the reforming reaction can be obtained from the electrochemical oxidation of hydrogen and, because of the continuing consumption of hydrogen, the equilibrium of the reforming reaction may be further shifted to the product side, increasing the methane conversion and leading to a more evenly distributed load of hydrogen (Aguiar et al., 2004). However, carbon deposition on the anode and subsequent electro-catalyst deactivation can be found in DIR-SOFC, leading to loss of cell performance and poor durability. To avoid this problem, the DIR cell operation requires a large amount of steam in addition to the fuel (Laurencin et al., 2008). Furthermore, the direct internal reforming reaction at the anode side causes a temperature gradient and thermal stress due to the endothermic cooling effect in the fuel cell stack. In addition, the coupling of the reforming and electrochemical reactions results in a complicated dynamic response. As a result, an efficient control is necessary for this process to avoid thermal cracking and ensure system stability.

To develop the SOFC performance, a dynamic model is considered an essential tool. It is used to design for fuel cell improvement and to predict the time-dependent behavior of the SOFC system due to step changes in input variables. The model must be robust and accurate and be able to provide solutions to fuel cell performance under a wide range of fuel cell operating conditions. Achenbach (1994) presented a three dimensional dynamic model for a planar SOFC with inclusion of the internal reforming effect and examined the transient cell voltage response to load changes as well as the influence of several design parameters on the transient performance. Jayasankar et al. (2009) studied the identifiability and estimability of parameters in SOFC via the

dynamic model that provides a detailed description of the diffusion process of different species and that of the inherent impedance.

The dynamic modeling is especially beneficial for steady-state and dynamic system analysis as well as control design to improve the system transient performance and investigate dynamic responses. SOFC operations are often subjected to transient condition, fuel cell dynamics have been increasingly considered in modeling activities (Chaisantikulwat et al., 2008). Simple and accurate SOFC dynamic model is very important for optimizing the system as well as for developing control strategies (Kang et al., 2009). To date, various SOFC models have been reported, ranging from one to three dimensional models that describe the spatially distributed nature of SOFC variables and the internal complex transport processes within the SOFC. However, it is difficult to build and solve due to complex form and also spend time-consuming. To cope with these difficulties, Murshed et al. (2007) developed a control relevant model of the hybrid SOFC system using a lumped parameter modeling concept. Compared with a very detailed model of SOFC, the developed SOFC model can captures the dynamics of the SOFC and thus can be used to design a control structure. The understanding of steady-state and dynamic behavior is thus an essential necessity for the nonlinear control system design and for design of efficient controllers.

In recent years, SOFC has received much attention on its operation and design, but the control study has less focus, including control structure design, controllability analysis, and the tuning design of the controllers. Controllability plays an important role in designing a control system as it demonstrates the ability to move system outputs to specified bounds using available inputs. Controllability analysis can offer insights for identifying the inherent properties of a process and how they limit control performance (Morari, 1983, Skogestad and Postlethwaite, 1996). Morari (1983) has reported that controllability is an inherent property of the process itself and should be considered at the design stage before the control system design is fixed. The comparison and selection of different control structures and the validation of the controlled system were studied for the controllability analysis of decentralized linear controllers (García et al., 2010, Serra et al., 2005). In addition, a controllability analysis is generally applied for selection of the best controlled and manipulated variable pairing within one process and evaluation of control properties for two or more process alternatives (Skogestad and

Postlethwaite, 1996). Therefore, the theory of controllability analysis is interesting and challenging for SOFC.

To design an efficient control system, it is essential to first decide the control structure design. Control structure design deals with the structural decisions of the control system, including the selection of manipulated variables, controlled variables, control configuration, and controller type and what to control and how to pair the variables to form control loops (Skogestad and Postlethwaite, 1996). The self-optimizing control is implemented to select the good controlled variable which can be kept constant at setpoints without the need to re-optimize when disturbance occur.

Recently, several works have been concentrated on the dynamic modeling and control of solid oxide fuel cell. Owning to high-temperature operation of SOFC, temperature gradients in a fuel cell stack need to be carefully monitored to avoid any thermally induced fractures on its ceramic components, with a consequent cell failure (Aguiar et al., 2004). Therefore, the cell temperature should be kept as constant as possible. Moreover, it is necessary to maintain a constant voltage in the presence of load changes. Hajimolana and Soroush (2009) showed the inlet temperatures of air and fuel strongly affect the dynamics of the fuel system, so proportional-integral (PI) controllers are implemented and simulated to study the control of the outlet cell voltage and cell-tube temperature. Kaneko et al. (2006) showed the power and temperature were controlled in a biomass gas fuels SOFC and micro gas turbine hybrid system, using PID control. Chaisantikulwat et al. (2008) presented the development of a SOFC dynamic model and a feedback control scheme by maintaining output voltage despite load changes, using PI controllers. Li et al. (2005) studied the control of an SOFC power by implementing proportional-integral (PI) controllers to maintain fuel utilization and voltage when the stack current changes. Furthermore, a dynamic model was used to study the dynamics of the SOFC stack and to design control strategies (Aguiar et al., 2004). A PID controller was implemented to maintain the outlet fuel temperature and the fuel utilization during load changes. Stiller et al. (2006) developed a dynamic model for control of a SOFC and gas turbine hybrid system. The SOFC power, fuel utilization, air flow and cell temperature were controlled using a proportional–integral–derivative (PID) type controller.

There are many different control algorithms that can be implemented but model predictive control (MPC) has presented itself as the most successful process control technology. MPC can handle a multivariable problem and incorporate physical limitations. MPC is a multivariable control algorithm which generally uses a linear model to predict the output trajectory of the process in the future and to compute a controller action (Qin and Badgwell, 2003). Golbert and Lewin (2004) used the model predictive controller for the regulation of a PEM fuel cell described by a model which accounted for spatial dependencies of voltage, current, temperature, and materials flow. Murshed et al. (2010) described the application of a nonlinear model predictive control applied on the fuel cell system by utilizing estimated states from the unscented Kalman filter.

However, many real chemical processes are highly nonlinear and involve many uncertain parameters. As a traditional MPC algorithm is incompetent to deal with plant model uncertainties, a number of studies have been focused on the development of robust MPC to handle nonlinear systems and guarantee its stability. Kothare et al. (1996) synthesized the robust MPC algorithm that allows an explicit incorporation of plant model uncertainties. The state feedback control law was obtained by minimizing the worst-case performance cost. The convex optimization problem with linear matrix inequalities (LMIs) constraints was formulated. Bumroongsri and Kheawhom (2012) proposed a robust MPC for uncertain polytopic discrete-time systems. The robust MPC algorithm was also developed by Pannocchia (2004) to stabilize the system described by a linear time-varying (LTV) model. Kouramas et al. (2011) focused on the design of MPC controller to control the cell voltage and cell temperature. Because the SOFC model involves many uncertain parameters, the control design should take a model uncertainty into account. For an on-line synthesis approach, the requirement of optimality leads to high on-line MPC computational time. When MPC incorporates the model uncertainty, the resulting on-line computation will grow significantly with the number of vertices of the uncertainty set. As a result, an off-line synthesis approach to the robust MPC for uncertain model is focused. With the off-line approach, the computation of the robust MPC is reduced significantly with minor loss in its control performance.

1.2 Research objective

The objective of this research is to concentrate on the performance analysis and control and to study the control structure design and controllability analysis of solid oxide fuel cell with direct internal reforming of methane.

1.3 Dissertation overview

This dissertation is organized as follows:

Chapter I presents the research background and motivation of this research. The research objective and dissertation overview are also presented.

Chapter II reviews a literature for work related to design and modeling of SOFC, control structure design, and control algorithm based on robust model predictive control (robust MPC).

Chapter III discusses a general basic principle of fuel cells and SOFC. SOFC design involved an internal reforming process is also given in this research. The theory of control structure design, controllability analysis, and robust MPC algorithm is described.

Chapter IV explains a mathematical model of SOFC derived from mass and energy balances and electrochemical model.

Chapter V presents the design and dynamic modeling of SOFC with direct methane steam reforming. The operating condition is selected from the steady state analysis and the dynamic behavior is investigated.

Chapter VI focuses on control structure design and controllability analysis for SOFC. A procedure for select an active constraint and a self-optimizing variables is presented. Moreover, the relative gain array (RGA) considered as a controllability index for the selection of input-output pairings is also implemented.

Chapter VII presents the controller design for control the cell temperature and cell voltage. The simulation studies of PID using SIMC tuning rules are discussed.

Chapter VIII describes the implementation of an off-line robust MPC algorithm using linear time-varying (LTV) and linear parameter varying (LPV) systems for the internal reforming SOFC. The state feedback control law is implemented to the process.

Chapter IX gives the conclusions and recommendation of this dissertation.

CHAPTER II

LITERATURE REVIEWS

This chapter presents a literature review of solid oxide fuel cells (SOFCs). The design, modeling, and control of SOFC are explained in the first part. The second part presents the important of control structure design. Finally, the control algorithm based on model predictive control (MPC) is presented.

2.1 Solid oxide fuel cell (SOFC)

Many researches have discussed the considerable environmental benefits of fuel cell technology (Hall and Kerr, 2003). The advantage of using a solid oxide fuel cell (SOFC) technology involves a reduction of greenhouse gas emissions (Casas et al., 2011). Moreover, the development of fuel cell technology as a replacement for the internal combustion engine is interesting (Van den Hoed, 2007). Therefore, the SOFC technology is the interested energy conversion device.

2.1.1 Design and modeling of SOFC

Recently, there have been several publications concentrating on SOFC designs. The cell configurations of SOFC can be classified into planar, tubular, and monolithic configurations. One of these configurations, the planar configuration is quite simple, relatively easy and inexpensive to construct, high power density, and simplicity of mass production. Furthermore, the planar design provides very high volumetric power densities and simpler to fabricate than tubular configuration (Kakac et al., 2007). Laurencin et al. (2008) implemented a planar SOFC directly fed with methane to study the thermal and electrochemical behavior. The important design feature of the planar SOFC relates to gas flow configuration which can be arranged in several ways such as cross-flow, co-flow or counter-flow. Aguiar et al. (2004) has studied the system behavior under co-flow and counter-flow operations. The results showed the co-flow configuration was better than the counter-flow because the counter-flow leads to steep temperature gradients with a consequent uneven current density distribution. Moreover,

a planar SOFC with co-flow was implemented to evaluate the accuracy and applicability of the current dynamic model (Zhang et al., 2006).

Because of the high operating temperatures, the materials used in the cell components are limited by chemical stability in oxidizing and reducing environments, chemical stability of contacting materials, etc. Therefore, the developing cells with compositions of oxide and metals that operate at intermediate temperatures have been investigated. A SOFC electrolyte is yttria-stabilised zirconia (YSZ), an oxide ion conductor at elevated temperatures. The anode is usually a nickel/zirconia cermet, which provides high electrochemical performance, good chemical stability, and low cost, and the cathode is a perovskite material, such as strontium doped lanthanum manganite, often mixed with YSZ in the form of a composite (Aguiar et al., 2004). However, it is usually observed that the intermediate temperature operation causes an increase of internal resistance of cell. Therefore, there are several researchers analyzing the performance of a planar IT-SOFC with different support structures such as electrolyte-supported and electrode-supported. Patcharavorachot et al. (2008) studied the role of support structures which the result showed that an anode-supported SOFC is superior to an electrolyte-supported and cathode-supported SOFC. Chan et al. (2001) presented the tests of sensitivity to indicate the effect of the thickness of the respective fuel cell components on the cell voltage dropped. The results showed the performance of an anode-supported solid oxide fuel cell was superior to that using cathode as the support under elevated operating pressure in the cathode compartment.

Mathematical models are essential tool for design the optimum operating conditions of SOFC and for studying and development the performance of SOFC. In general, the modeling of SOFC consists of mass and energy balances and an electrochemical model. There are several works focusing on the development of mathematical models for SOFC. Many researcher have been used the mathematical models to study the complicated interactions between the various phenomena occurring inside the cell and to optimize the system performance. Moreover, the physical and electrochemical processes can be analyzed exactly, which is instructional and significant for the manufacture of the electrodes and electrolytes when dynamic characteristics of fuel cells are considered accurately.

The performance of a fuel cell can be expressed by the polarization curve. It is necessary for optimization of fuel cell operating points, design of the power conditioning units, design of simulators for fuel cell stack systems, and design of system controllers. Therefore, it should be noted that the accurate electrochemical model is required to study and improve the fuel cell performance. The electrochemical modeling and parametric study of methane fed solid oxide fuel cells have been presented by Ni et al. (2009). An important feature of this model is that the effects of electrode structural parameters on both the exchange current density and gas diffusion coefficients are fully taken into consideration. The simulation results of parametric analyses showed that all the overpotentials decreased with increasing cell temperature. This is different from previous analyses on hydrogen (H_2) fed SOFCs, in which the concentration overpotentials are slightly increases with increasing temperature. Moreover, it is found that although increasing electrode porosity or pore size decreases the concentration overpotentials, an increase in activation overpotentials of methane fed SOFCs is observed. At low current densities, low porosity, and pore sizes are desirable to reduce the total electrode overpotentials as concentration overpotentials are insignificant compared with activation overpotentials. At high current densities, the total overpotentials can be minimized at optimal porosities and pore sizes. Chan et al. (2001) presented a complete polarization model of a solid oxide fuel cell (SOFC) that eliminates the ambiguity of the suitability of such model when used under different design and operating conditions. The Butler-Volmer equation is used in the model to describe the activation overpotential instead of using simplified expressions such as the Tafel equation and the linear current-potential equation. In the concentration overpotential, both ordinary and Knudsen diffusions are considered to cater for different porous electrode designs.

A model for anode performance of a planar anode-supported SOFC was studied (Kulikovsky, 2009). The models include Butler–Volmer equation, Ohm's law, and mass balance equation of hydrogen in the anode channel. The results showed that the anode operation regime depends on the relation between the cell current density and the critical current density. Analytical solutions to the system of governing equations for the case of low current density and high current density are derived. The cell voltage is proportional to cell current at the low current density, which explains the concept of

anodic activation resistivity. In case of the high-current density, the voltage depends on cell current, with the apparent Tafel slope being twice the kinetic value. Furthermore, a performance analysis of a planar solid oxide fuel cell (SOFC) with different support structures was presented (Patcharavorachot et al., 2008). To analyze the characteristics of the planar SOFC, the structural and operational parameters and gas diffusion at the electrodes was used and taken into an electrochemical model. The analysis result of cell voltage loss indicated that the ohmic losses affect the performance of an electrolyte-supported SOFC whereas the activation and ohmic overpotentials constitute the major losses in an electrode-supported counterpart. Sensitivity analysis of the anode-supported SOFC showed that decreasing in the electrolyte and anode thickness can improve cell performance.

Aguiar et al. (2004) has been studied the performance of an anode-supported intermediate temperature direct internal reforming planar solid oxide fuel cell. The model developed consists of mass and energy balances, and an electrochemical model that relates the fuel and air gas composition and cell temperature to cell voltage, current density, and other variables. The electrochemical performance of the fuel cell was analyzed and the cell performance at steady state, the effect of the inlet temperatures of fuel and air, fuel utilization, current density, and flow configurations were studied. The results showed that the activation overpotentials at cathode represented the major source of voltage loss, followed by anode activation overpotentials and ohmic losses.

2.1.2 Dynamic and control of SOFC

In the research field of modeling of fuel cells, there are many considerable works on modeling steady-state behavior whereas there are a few studied concentrated on dynamic models. The models can be developed to simulate steady-state or dynamic behavior and can range from zero-dimensional to three-dimensions. For SOFC system, simple and accurate SOFC dynamic models are very valuable because the model-based simulation is a valid tool for optimizing the system parameters and flow sheet, as well as for developing control strategies (Cao et al., 2010, Kang et al., 2009). Further, it is essential for the prediction of the cell response under transient conditions when load changes occur and systems also start-up or shut down.

The dynamic modeling of electrical characteristics of SOFCs using fractional derivatives has been proposed (Cao et al., 2010). A dynamic model is established by a transient equivalent circuit, and then a fractional order dynamic model is done in the perspective of the fractional derivatives theory. Then the parameters of the dynamic models were optimized via genetic algorithms according to electrochemical impedance spectroscopy (EIS) experimental data. Finally, the dynamic response from the models were studied. The results showed the fractional order dynamic model has higher accuracy for representing the dynamics of the SOFC electrical characteristics, which lays a solid foundation for the controller based on the accurate model.

Moreover, the dynamics behavior of a tubular SOFC was studied (Hajimolana and Soroush, 2009). The response of cell voltage, current, and the tube temperature of fuel cell to step changes in external load resistance and conditions of the feed streams were presented. Simulation results showed that the fuel cell was a multi-time scale system; the cell output responses exhibit consecutive apparent dominant time constants. The temperature and pressure of the inlet air and fuel stream strongly affected the dynamics of the fuel cell system. The temperature of the inlet air stream had also the strongest effect on the cell performance; however, the velocity effects of inlet air and fuel on the cell responses were weaker than the inlet feed pressures and temperatures.

Kang et al. (2009) concentrated on one-dimensional dynamic modeling and simulation of a co-flow planar direct internal reforming solid oxide fuel cell. The model based on mass and energy balances, and electrochemical model were implemented. The steady-state performances of SOFC under specified initial operating conditions and the dynamic response to introduced operating parameter disturbances were studied. The dynamic responses of SOFC, such as cell temperature, current density, and cell voltage were all investigated when the SOFC was subjected to the step changes in the load current and the flow rates of inlet fuel and air. The results indicated the rapid dynamics of the current density and the cell voltage were mainly influenced by the gas composition, particularly the H_2 molar fraction in anode gas channels, while the slow dynamics were both dominated by the solid (including the PEN and interconnects) temperature.

For the development of a 3D dynamic model of an anode-supported planar SOFC, Chaisantikulwat et al. (2008) studied the dynamic responses to determine the

solutions of coupled partial differential equations derived from conservation laws of charges, mass, momentum and energy equations. To obtain the performance curve, the dynamic model was subjected to varying load current for different fuel specifications. Finally, the voltage responses to step changes in the fuel concentration and load current were determined.

Solid oxide fuel cell (SOFC) stacks are at the core of complex and efficient energy conversion systems for distributed power generation. Therefore, Salogni and Colonna (2010) presented modeling of solid oxide fuel cells for dynamic simulations of integrated systems. For the simplest SOFC configurations, and more so for complex integrated systems, the dynamic operation of the power plant is challenging, especially because the fluctuating electrical load of distributed energy systems demand for reliable transient operation. Issues related to dynamic operation must be studied in the early design stage and simulation results can be used to optimize the system configuration, taking into account transient behavior.

Lumped-parameter modeling considered only time changes is the simple approach to describe the dynamic modeling of solid oxide fuel cell. Xi et al. (2010) showed that lumped-parameter models are adequately accurate for systems-level analysis and control through experimental validation. Moreover, the lumped model was implemented for analysis and control of the planar SOFC systems (Murshed et al., 2007). Consequently, this work has used the lumped-parameter model for analysis, design, and control of the dynamic SOFC model.

Dynamic models are necessary for system design, and system optimization that take into account requirements of dynamic performance. Moreover, Dynamic model are especially beneficial for the design of the control system in the development stage of SOFCs. To devise appropriate control algorithms for fuel cells, it is essential to understand the nature of the control problem first. Once the application environment of fuel cells has been clearly described, it is then necessary to identify the best control variables so that the system will behave as required.

A control of a tubular solid oxide fuel cell system was studied by Hajimolana and Soroush (2009). A simple control system was then implemented to control the cell output voltage and cell-tube temperature via manipulating the pressure and temperature of the inlet air stream, respectively. The results showed that the performance of control

system can successfully reject unmeasured disturbances in the load resistance, the velocity of the inlet air and fuel stream, and the pressure and temperature of fuel stream. Two PI controllers were then implemented and simulated to study control of the fuel cell outlet voltage and cell-tube temperature.

Aguiar et al. (2005) investigated the open-loop and closed-loop response of a planar anode-supported intermediate-temperature direct internal reforming solid oxide fuel cell due to load changes. A typical feedback PID temperature controller that, given the outlet fuel temperature had been implemented by manipulating the air ratio and imposing current density as disturbance (keeping the fuel utilization and air ratio constant). This research further proved the need for process control to enhance the reliability and minimize the degradation of a SOFC. However, an adjustable set-point control strategy was more effective in avoiding oscillatory control action for the load changes of higher magnitude. This leads to operation failure, as well as in preventing potentially damaging temperature gradients that lead to cell breakdown.

The development of control relevant models for a SOFC combined with a gas turbine (GT) in an autonomous power system was presented (Kandepu et al., 2007). The results in a SOFC system showed that the power output and the cell temperature can be controlled by manipulating the fuel and air feed flow rates, using proportional-integral (PI) control, respectively. The controller provides satisfactory performance for load changes at the cost of efficiency.

Chaisantikulwat et al. (2008) developed a dynamic model of a SOFC and a feedback control scheme by implementing PI controllers. The control objective was to maintain a cell voltage in the existence of load changes by manipulating the fuel concentration which was hydrogen. Load change resulted in voltage drops; therefore, the load current was considered to be a disturbance to the SOFC system. Low-order dynamic models that were sufficient for feedback control design were derived from the step responses. However, the feedback PI controller was able to maintain a SOFC voltage for small changes in the load current.

Furthermore, Kaneko et al. (2006) presented the power and temperature control of fluctuating biomass gas fueled solid oxide fuel cell (SOFC). A power controller was designed and implemented by using a standard PID control strategy and manipulating inlet fuel flow rate for controlling the power output of the system. In addition, the cell

temperature was controlled by manipulating a bypass valve around the recuperator. By releasing excess heat to the exhaust, the bypass valve provided the control means to avoid the self-exciting behavior of system temperature and stabilized the temperature of SOFC.

A hierarchical modeling as a suitable methodology to perform control-oriented analysis of planar solid oxide fuel cells was proposed (Sorrentino et al., 2008). The development of a PI controller to limit temperature rise from cell inlet to outlet. The implement of the controller allowed dropping voltage relaxation time, while bounding in a safe range the temperature rise subsequent to a load change. Moreover, the comparison between controlled and uncontrolled system indicated the need of solving the trade-off between safe operation of cell components and cell performance, with the latter being lowered by temperature rise control.

Besides that, there are many different control algorithms that can be implemented. Among various types of the control algorithms, Model Predictive Control (MPC) has presented itself as the most successful process control technology.

Danzer et al. (2009) implemented model predictive control to prevent oxidant starvation and to allow for a dynamic operation of the fuel cell. The starvation of fuel becomes high significant at fast load changes. This can be limiting the dynamics of load changes or decoupling the desired load from the effective load. Therefore, the oxygen excess ratio, the fuel cell pressure, and the effective current were the control variables. This goal was to achieve the control design by using MPC controller that incorporates actuator limitations and state constraints. The results showed that the application of model based controller to the nonlinear model of the fuel cell system increased the dynamics, the reliability and the durability of the fuel cell.

The solid oxide fuel cell system was estimated and controlled by nonlinear model predictive control (NMPC) which is able to handle multivariate objective and constraints (Murshed et al., 2010). The structure of the fuel cell related components imposed certain restrictions on the system operation. NMPC were implemented on the fuel cell system by using the unscented Kalman filter to utilize estimated states. A control relevant dynamic model was required to predict the cell output voltage and the component temperatures of the system as well as can be used to design controller. The results showed the linear MPC can stabilize the system for a small load change;

however, it cannot control the system for higher load disturbances. This has motivated to operate nonlinear MPC which is not restricted by the operating region. It showed that NMPC can handle the voltage to its target.

As a nonlinear power generation device, the solid oxide fuel cell (SOFC) often operates under small window of operating conditions due to the constraints stemming from the environmental and safety considerations. The nonlinear model predictive control (NMPC) appears to be well suited control algorithm for this application. NMPC is a closed-loop feedback control scheme that predicts the open-loop optimal input based on the measurements and the setting trajectory. Zhang et al. (2008) developed a closed-loop feedback control strategy based on the NMPC controller for a planar SOFC. The current density and the molar flow rates of fuel and air were selected as manipulated variables to control the output power, fuel utilization, and cell temperature. The mole fraction of the exit gases and temperature were defined as the state variables. The moving horizon estimation (MHE) method was implemented to estimate the variables. The robustness and stability of the controller here were shown, a typical case study had been conducted with the power output changes under constant fuel utilization and temperature. The simulation results showed the NMPC controller succeeded pleasantly following the setting output trajectory.

Kouramas et al. (2011) focused on the design of MPC controller to control the cell voltage and cell temperature. The result showed that the controller can manage the SOFC voltage and temperature at its desired value. A solid oxide fuel cell using neural network predictive control (NNPC) was studied (Hajimolana et al., 2013). The SOFC temperature was controlled for thermal stress management using a NNPC and the temperature of the inlet air stream is manipulate variable. The performance of the control system showed that NNPC can assure less oscillating control responses with shorter settling times in comparison to the proportional-integral (PI) controller.

Because the SOFC model involves many uncertain parameters, the control design should take a model uncertainty into account.

2.2 Control structure design

To design an efficient control system, the structural decisions of control structure design is interested. Skogestad (2004) has proposed a procedure for control

structure design for complete chemical plants. At the beginning of the procedure, the operational and economic objectives, and degree of freedom was carefully defined. Control structure design deals with the structural decisions of the control system, including the selection of manipulated variables, controlled variables, control configuration, and controller type and what to control and how to pair the variables to form control loops (Skogestad and Postlethwaite, 1996). The self-optimizing control was implemented to select the good controlled variable which can be kept constant at setpoint without the need to re-optimize when disturbance occur. Panahi et al. (2010) studied self-optimizing and control structure design for a CO_2 capturing plant. To validate the proposed structure, dynamic simulation and performance of the control structure was studied. The result found that the temperature closed to the top of the stripper to be a good controlled variable for the remaining unconstrained degree of freedom. Moreover, the control structure design for an ethanol production plant was presented (Andrade and Lima, 2009). The obtained control structure was tested to verify its performance in the presence of external disturbances. The result showed the control structure presented good results. Dwivedi et al. (2013) implemented the control structure selection for four-product Petlyuk column. Four decentralized control structures were proposed and tested against a wide range of disturbances. Control structure design for the ammonia synthesis process was studied (Araújo and Skogestad, 2008). The final control structures resulted in good dynamic performance for all cases.

Furthermore, controllability analysis for identifying the inherent properties of a process and how they limit control performance has an important role in designing a control system (Skogestad, 2004). Morari (1983) has reported that controllability is an inherent property of the process itself and should be considered at the design stage before the control system design is fixed. The comparison and selection of different control structures and the validation of the controlled system were studied for the controllability analysis of decentralized linear controllers (Serra et al., 2005). García et al. (2010) presented dynamic modeling and controllability analysis of a low temperature ethanol reformer for fuel cell application. The controllability analysis was focused on mass balances and based on a linearization of the complex non-linear model of the reformer. Analysis tools such as Relative Gain Array (RGA), Condition Number (CN), and Morari Resiliency Index (MRI) were applied to the linear model suggesting.

Controllability of an ethanol steam reforming process for hydrogen production was proposed (García et al., 2011). The sensitivity and controllability were studied to investigate the influence of the temperature on the output variables. The controllability result was used for the identification of the best control structures.

2.3 Control algorithms

2.3.1 Basic principle of MPC

Model predictive control (MPC) algorithms have been known as effective tools for handling some of the difficult control problems in industry (Temeng et al., 1995). It is also known as moving horizon control or receding horizon control, which control inputs are computed based on an optimization problem over a prediction horizon. Moreover, an explicit model is used to predict the effect of future inputs on states or outputs. The overall objectives of an MPC controller have been summarized (Qin and Badgwell, 2003) such as to prevent violations of input and output constraints, to drive some output variables to their optimal set points, while maintaining other outputs within specified ranges. Moreover, MPC controller can prevent excessive movement of the input variables and control as many process variables as possible when a sensor or actuator is not available.

Two popular variations of MPC algorithm are dynamic matrix control (DMC) and model algorithmic control (MAC) (García et al., 1989). The primary strategy of MPC algorithms is to use a model to predict the future output trajectory of the process and compute a controller action to minimize the difference between the predicted trajectory and specified trajectory. In general, MPC can be divided into linear model predictive control (LMPC) and nonlinear model predictive control (NMPC). First approach is to use linear models in prediction and optimization to predict the dynamic system although the dynamic models is nonlinear. For other approach, the dynamic models, objective function, and constraints is nonlinear function. However, LMPC algorithm would decompose when it is applied to processes with highly nonlinear process dynamics.

The most chemical processes, however, is highly nonlinear model and the linear models cannot explain the behavior of process. The procedure of linear controllers in these industries which exhibit severe nonlinear behavior can lead to poor performance,

particularly when the system moves away from its nominal point (Pinheiro and Kershenbaum, 1999). Several works have been made to extend MPC techniques to nonlinear systems. Model predictive control is suitable methods for the control engineer, particularly in the process industries where plants being controlled are slow sufficiently to permit its implementation (Mayne et al., 2000). MPC controller may be valuably employed include unconstrained nonlinear plants, for which offline computation of a control law usually requires the plant dynamics to keep a structure, and time-varying plants.

Seki et al. (2001) developed a model predictive control and apply to an industrial polypropylene semi-batch reactor process and a high density polyethylene (HDPE) continuous stirred tank reactor process. The NMPC algorithm was developed and described. The simulation result showed that the NMPC successfully prohibited thermal runaway of the reactor temperature control due to the heat removal constraint; however, it was difficult with conventional operations (LMPC).

2.3.2 Robustness of MPC

It is extremely important for model predictive control to be robust to model uncertainties. As a traditional MPC algorithm is incompetent to deal with plant model uncertainties, a number of studies have been focused on the development of robust MPC to handle nonlinear systems and guarantee its stability. Therefore, the development of MPC algorithm to robustness issue is also significant. García and Morari (1985) have been analyzed the robustness properties of unconstrained MPC in the internal model control and developed tuning to guarantee robust stability.

Kothare et al. (1996) synthesized the robust MPC algorithm that allows an explicit incorporation of plant model uncertainties. The state feedback control law was obtained by minimizing the worst-case performance cost. The convex optimization problem with linear matrix inequalities (LMIs) constraints was formulated. The algorithm was proved to guarantee robust stability. The robust MPC algorithm was also developed by Pannocchia (2004) to stabilize the system described by a linear time-varying (LTV) model. The proposed algorithm is efficient since the on-line implementation only requires one to solve a convex quadratic program with a number of decision variables.

For an on-line synthesis approach, the requirement of optimality leads to high on-line MPC computational time. When MPC incorporates model uncertainty, the resulting on-line computation will grow significantly with the number of vertices of the uncertainty set. As a result, an off-line synthesis approach to robust MPC for uncertain model is presented. With the off-line approach, the computation of robust MPC is reduced significantly with minor loss in performance. Bumroongsri and Kheawhom (2012) proposed an off-line robust MPC for uncertain polytopic discrete-time systems. Moreover, an ellipsoidal off-line MPC strategy for linear parameter varying (LPV) systems was studied. At each sampling, the smallest ellipsoid containing the presently measured state was determined in each sequence of ellipsoids and the scheduling parameter for LPV was measured on-line. Liu (1968) has shown that every trajectory (x, u) of a nonlinear system is a trajectory of linear time-varying system in the polytope (Ω). An efficient off-line formulation of robust model predictive control using linear matrix inequalities (LMIs) was studied (Wan and Kothare, 2003). The concept of an asymptotically stable invariant ellipsoid was developed to a robust constrained MPC algorithm. This off-line approach for model uncertainty descriptions can guarantee robust stability of the closed-loop system and substantial reduction of the on-line MPC computation. This results assured robust MPC that is very attractive control method.

Recently, the controller synthesis based on a linear parameter varying (LPV) system has been received considerable attention. Casavola et al. (2012) proposed a fast ellipsoidal MPC strategy to feedback regulation problems for constrained polytopic linear parameter varying (LPV) systems subject to bounded disturbances. The LPV model was used to explain a nonlinear plant in the MPC algorithm. A computationally low-demanding MPC algorithm was presented base on the off-line computation of an ellipsoidal approximations. Chang et al. (2014) presented a multi-parametric model predictive controller (mpMPC) for discrete-time linear parameter-varying (LPV) systems based on the discrete-time linear time-invariant (LTI) systems solution with application to anaesthesia. The result showed the mpMPC for LPV systems can reduce the 60% of the reference tracking error compared with LTI systems.

Moreover, finite horizon control laws for the performance objective have been known to have poor nominal stability properties owning to need the imposition of the

terminal state constraint (Rawlings and Muske, 1993). The infinite horizon control laws have been shown to guarantee nominal stability.

CHAPTER III

THEORY

In this chapter, a background of theory of a fuel cell that consists of the basic principle of fuel cell, type of fuel cells, and its advantages is presented in Section 3.1. Section 3.2 begins with the details of the solid oxide fuel cell (SOFC) such as advantage, features, and materials of SOFC, design of SOFC, and internal reforming of SOFC. Further, the description of control structure design and controllability analysis is explained in Section 3.3 and 3.4, respectively whereas the detail of robust model predictive control including model description, Lyapunov theory, and robust MPC algorithm is shown in Section 3.5.

3.1 Basic principle of fuel cell

A fuel cell is an electrochemical device which can convert a chemical energy of fuels directly into an electrical energy (electricity) by the electrochemical reaction and producing water and heat as by-products. It operates like batteries but the fuel cell can produce continuously electricity as long as both fuel and oxidant are supplied to the electrodes. Moreover, it is unlike internal combustion engines where there are losses due to Carnot cycle efficiency limitation and mechanical losses. To produce electricity by combustion engines, fuel energy is converted to thermal energy by combusting fuel with oxygen and then the thermal energy is used to generate electricity. Thus, the internal combustion energy efficiency is lower than the fuel cell efficiency that can be as high as 40–55%. The basic physical structure of fuel cell composes of an electrolyte layer sandwiched between two electrodes, anode and cathode. A general schematic of fuel cell operation is illustrated in Figure 3.1. This figure presents the flow directions of the reactant/product and the ions/protons conduction through the electrolyte. For the operation of fuel cell, fuels (such as hydrogen or hydrocarbon) are continuously fed to the anode side and an oxidant (such as air or oxygen) is continually supplied to the cathode side. The electrochemical reactions take place at the electrodes to produce an electricity. The ions/protons can diffuse through the electrolyte and the electrons can transport through the external circuit providing electrical energy. Byproducts (i.e.

water, exhaust gases, and heat) are also produced by the fuel cell. Therefore, fuel cells are considered to be a non-emission power generator.

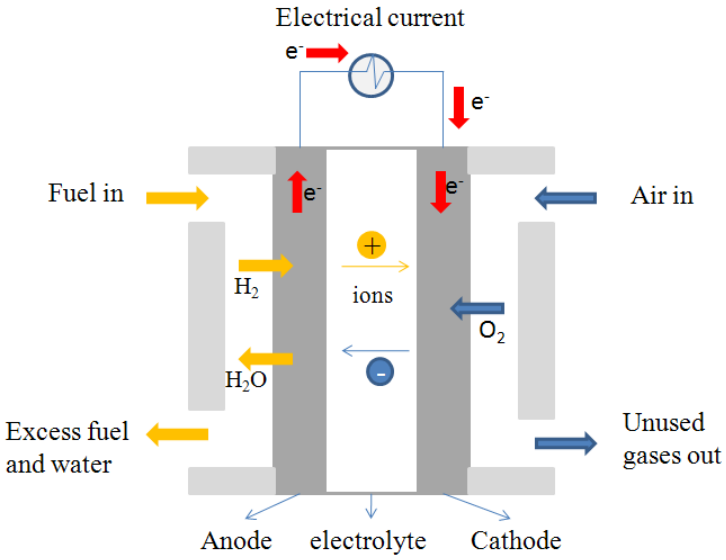

Figure 3. 1 A schematic of fuel cell operation.

3.1.1 Type of fuel cells

Fuel cells can be generally classified by the various types of electrolyte, fuel, and oxidant, whether the fuel feeding is managed outside (external reforming) or inside (internal reforming) the cell, and the operating temperature. Furthermore, there are the kind of chemical reactions that take place in the cell, the kind of catalysts required, the fuel required, and other factors. There are several types of fuel cells currently under development for applications as small as a cellular phone to as large as a small power plant for an industrial factory, each with its own advantages, limitations, and potential applications. The most common classification of fuel cells is by the type of electrolyte used in the cell that includes polymer electrolyte membrane fuel cell or proton exchange membrane fuel cell (PEMFC), alkaline fuel cell (AFC), phosphoric acid fuel cell (PAFC), molten carbonate fuel cell (MCFC), and solid oxide fuel cell (SOFC).

The operating temperature and useful life of fuel cell dictate the physicochemical and thermos-mechanical properties of materials used in the cell components such as electrodes, electrolyte, interconnect, and current collector. The operating temperature also plays an important role in dictating the type of fuel cell. The low-temperature fuel cells such as PEMFC, AFC, and PAFC with aqueous electrolytes

are in most practical applications and restricted to hydrogen as a fuel. For the high-temperature fuel cells (i.e., MCFC and SOFC), CO and even CH_4 can be used as fuel because of the inherently rapid electrode kinetics and the lesser need for high catalytic activity at high temperature. Details of the various fuel cells are presented in Table 3.1. The applications of the fuel cell and the advantages and disadvantages for each type of fuel cells are illustrated in Table 3.2.

3.1.2 Advantage of fuel cells

Fuel cells are defined as the power generation of the future. The interests in fuel cells have increased due to many advantages that consist of:

- Low pollutant emissions due to by-products as water and heat.
- High-energy efficiency (Direct energy conversion, no combustion).
- The possibility of using various fuel types.
- No moving parts in the energy converter, thus reducing noise pollution and low maintenance cost.
- Quickly recharged.
- The utilization of waste heat in a cogeneration and bottom recycle.

3.2 Solid oxide fuel cell (SOFC)

As mentioned above, solid oxide fuel cell (SOFC) is one of the most efficient device since it composes of a ceramic ions-conducting electrolyte such as yttria-stabilized zirconia (YSZ). It operates at high temperature which offers several advantages as shortly described. Although the basic advantages of SOFC are similar to other fuel cells, SOFC presents more benefits, for example:

- SOFCs can be operated with many common hydrocarbon fuels such as natural gas, gasoline, biofuels, and alcohol without reforming of such fuel into pure hydrogen before feeding to the SOFCs.
- The high temperature exhaust gases and heat generation in the SOFCs can be used for cogeneration applications and bottoming recycles (Saebea et al., 2012). This leads to increasing overall efficiency of SOFC system.

Table 3. 1 Description of Major Fuel Cell Types.

Types of fuel cells / Details	Low-temperature fuel cells			High-temperature fuel cells	
	polymer electrolyte membrane fuel cell (PEMFC)	**alkaline fuel cell (AFC)**	**phosphoric acid fuel cell (PAFC)**	**molten carbonate fuel cell (MCFC)**	**solid oxide fuel cell (SOFC)**
Operating Temperature (°C)	80	60-220	200	650	600-1000
Electrolyte	Polymer membrane	Liquid KOH (immobilized)	Liquid H_3PO_4 (immobilized)	Molten carbonate	Ceramic
Charge carrier	H^+	OH^-	H^+	CO^{2-}_3	O^{2-}
Cell component	Carbon based	Carbon based	Carbon based	Stainless based	Ceramic based
Interconnect	Carbon	Metal	Graphite	Stainless steel or Nickel	Nickel, ceramic, or steel
Electrode	Carbon	Transition metals	Carbon	Nickel and Nickel Oxide	Perovskite and perovskite/metal cermet
Catalyst	Platinum	Platinum	Platinum	Stainless based	Ceramic based
Fuel compatibility	H_2, methanol	H_2	H_2	H_2, CH_4	H_2, CH_4, CO
Product Water Management	Evaporative	Evaporative	Evaporative	Gaseous Product	Gaseous Product
Product Heat Management	Process Gas + Liquid Cooling Medium	Process Gas + Electrolyte Circulation	Process Gas + Liquid cooling medium or steam generation	Internal Reforming + Process Gas	Internal Reforming + Process Gas
Balance of Plant	Low-moderate	Moderate	Moderate	Complex	Moderate
Efficiency	40%	60%	40%	55%	55%
Size (MW)	0.25	very small	11	2	1-2

Table 3. 2 The applications of the fuel cell, the advantage and disadvantage for each type of fuel cells.

Types of fuel cells	Advantage	Disadvantage	Application
PEMFC	- Highest power density of all the fuel classes - Good start-stop capabilities - Suitable for portable applications	- Uses expensive platinum catalyst - Expensive polymer membrane and ancillary components - Required active water management - Very poor CO and S tolerance	- Transportation: cars, buses, boats - Residential: household electrical power needs - Portable: laptop computers, cell phones, medical equipment
AFC	- Improved cathode performance - non-precious metal catalysts - Low materials costs	- Must use pure H_2-O_2 - Must remove water from anode	- NASA space program: space vehicles
PAFC	- Mature technology - Excellent reliability/long term performance - Relatively low-cost electrolyte	- Expensive platinum catalyst - Susceptible to CO and S poisoning - Corrosive-liquided electrolyte	- Landfill/wastewater treatment facilities: To generate power from methane gas
MCFC	- Fuel flexibility - non-precious metal catalysts - High-quality waste heat	- Corrosive, molten electrolyte - Degradation/lifetime issues - Relatively expensive materials	- Commercial: utility power plants, airport terminals, schools, office buildings, hotels, hospitals
SOFC	- Fuel flexibility - non-precious metal catalysts - High-quality waste heat - Solid electrolyte - Relatively high power density	- Significant high-temperature materials issues - Sealing issues - Relatively expensive components/fabrication	- Commercial: utility power plants, airport terminals, public and commercial office buildings, hotels, hospitals

- SOFCs are no need to use precious metals as catalysts and thus, there are potentially lower cost compared with PEMFC and PAFC in which platinum is used as a catalyst. SOFCs have all-solid-state construction which in turn both electrodes and electrolyte are solid state ceramic cells. Accordingly, there are no problems in terms of material corrosion and electrolyte management.

3.2.1 Principle of SOFC

SOFC is currently the highest-temperature fuel cell which can be operated over a wide temperature range between 600ºC and 1000ºC and atmospheric or elevated pressures. As mentioned above, the structure of SOFC is the solid state character of all SOFC components. This means, in principle, there is no restriction on the cell configuration. The SOFC structure consists of two porous electrodes, anode and cathode, which are separated by ceramic ions-conducting electrolyte (denoted as the PEN, Positive electrode-Electrolyte-Negative electrode) and can be expressed in Figure 3.2. In general, a single unit of SOFC cannot produce adequate power and thus, it is necessary to stack SOFCs to increase the voltage and power. The interconnection in fuel cell stacks is desired to connect each cell in series or parallel, so that the electricity each cell generated from fuel cell can be combined. Figure 3.3 shows a schematic view of basic SOFC operation.

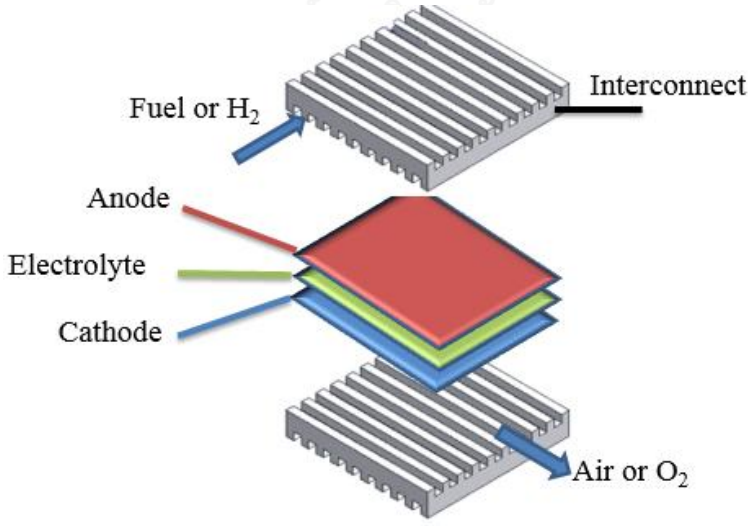

Figure 3. 2 The structure of solid oxide fuel cell.

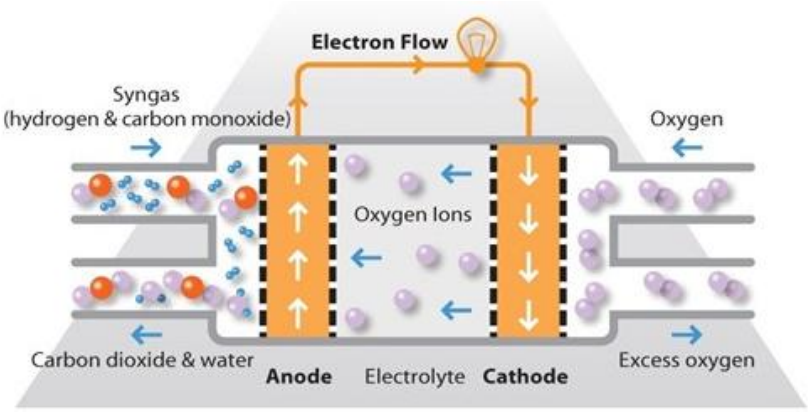

Figure 3. 3 A schematic view of basic solid oxide fuel cell operation.

(http://www.fuelcelltoday.com/technologies/sofc)

Fuels such as hydrogen, methane, ethanol, carbon monoxide or hydrocarbons are directly fed at the anode side and air or oxygen used as oxidant is continuously fed at the cathode side for generating electricity. At the cathode side, the reduction reaction occurs when oxygen is reduced, and formed into oxygen ions. Then oxygen ions can diffuse through the ceramic ions-conducting electrolyte to the anode/electrolyte interface where they react chemically with hydrogen held in the fuel. The dense structure of the electrolyte does not allow the passage of the cathodic gas through it, while the high ionic conductivity and the high electrical resistance allow only oxygen ions to migrate from the cathode to the anode. The electrons are produced afterward via the electrochemical reaction between the hydrogen and oxygen on the anode side. The electrons transport through the anode via the external circuit, providing electrical energy and back to the cathode/electrolyte interface. Water and heat as by-product are also given.

The electrochemical reactions occurring in SOFC from the utilization of H_2 and O_2 are expressed as Eqs. (3.1) and (3.2).

At the anode, oxygen ion reacts with hydrogen producing water and electrons.

$$H_2 + O^{2-} \rightarrow H_2O + 2e^- \qquad (3.1)$$

At the cathode, the reduction of oxygen occurs via

$$\frac{1}{2}O_2 + 2e^- \rightarrow O^{2-} \qquad (3.2)$$

The overall reaction occurring in the cell is exothermic.

$$H_2 + \frac{1}{2}O_2 \rightarrow H_2O \qquad (3.3)$$

Because of the high operating temperatures of present SOFC (approximately 800 ºC-1000 ºC), the materials used in the cell components are limited by chemical stability in oxidizing, reducing environments and chemical stability of contacting materials. The properties of SOFC material should be high electrical conductivity for the electrodes and almost zero electrical conductivity for the electrolyte. In order to avoid mechanical fracture and material delimitation, the thermal expansion of each material composing the stack must be as close as possible. These limitations have prompted investigations of developing cells with compositions of oxide and metals. The traditional materials for SOFC are summarized in Table 3.3.

Table 3. 3 Summarizes traditional materials for SOFC.(Sammes, 2006).

Component composition	**Specific conductivity (S/m) at SOFC running temperature**	**Conductivity depends upon**
Anode: Ni/YSZ cermet	400-1000	Particle size ratio Ni content
Cathode: $Sr_xLa_{1-x}MnO_{3-\delta}$	6-60	Cathode Porosity Sr content
Electrolyte: Y_2O_3-ZrO_2	10-15	Electrolyte Density

The most used material for the anode is currently a composite of Ni/YSZ (i.e. Ni with 8% mole of YSZ). Ni/YSZ cermet provides the anode with high electrical conductivity, an adequate ionic conductivity, and a high activity for the electrochemical reactions and reforming reaction. Moreover, the mechanical characteristics enable the anode to be the supporting structure of the entire cell, thus realizing anode supported cells. The anode layer must be very porous to allow the fuel to diffuse towards the electrolyte.

The typical material for the cathode is the strontium doped $LaMnO_3$ (LSM). LSM presents good electrochemical activity for oxygen reduction, a thermal expansion close to that of YSZ, and good stability when the fuel cell operates at about 1000°C.

The solid oxide electrolyte must be free of porosity that permits gas to permeate from one side of the electrolyte layer to the other, and it should be thin to minimize ohmic loss. Yttria-stabilized zirconia (YSZ) is currently the most widely employed material for the electrolyte manufacture. YSZ presents good ionic conductivity and negligible electronic conductivity at high temperature (above 700°C), it is chemical stable at the SOFC operating conditions, and presents a thermal expansion that is compatible with the anode and the cathode.

There are two main types of materials employed for the interconnect manufacture: ceramic, which are suitable for high temperature usage and metallic alloys for intermediate temperature. When the operating temperature is lower, the use of metallic interconnects becomes feasible. Compared to ceramic materials, metallic alloys are relatively inexpensive and easy to process.

3.2.2 SOFC design

SOFC configuration can be classified into two classes that consist of self-supporting and those requiring external support. In the first class, the cell components, often the thickest layer acts as the cell structural support such as electrolyte-supported, anode-supported, or cathode-supported. In the latter class, the single cell is configured as thin layers on the interconnection or a porous substrate. It is necessary to stack SOFCs to increase the voltage and power being produced. Because there are no liquid components, the SOFC can be shaped into flexible shapes such as flat planar, tubular, and monolithic. Each type is different and can be description.

Flat Planar: The flat planar structure is the common configuration for fuel cell stacks. Fabrication and assembly appear to be simpler for the flat plate design as compared with the other designs. In a planar SOFC, cell components such as the electrodes, electrolyte, and current collectors are configured as a flat planar geometry, and arranged in the ‘typical’ sandwich configuration that can be presented in Figure 3.4. This configuration is quite simple, relatively easy and inexpensive to construct, and the associated power density can be relatively high.

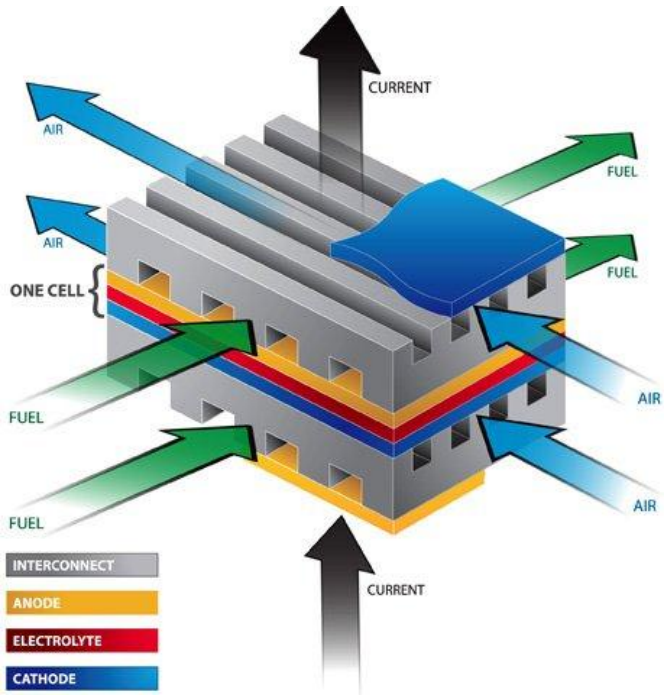

Figure 3. 4 A schematic of planar SOFC design.

(https://www.egcfe.ewg.apec.org)

The most important design feature of the planar SOFC relates to gas flow configuration and gas manifolding which can be arranged in several ways, as shown in Figure 3.5. Flow configurations of planar SOFC consist of co-flow, counter-flow, and cross flow. The selection of a particular flow configuration has significant effects on temperature and current distribution within the stack, depending on the precise stack design.

Although flat planar design has many advantages, it offers disadvantages. Firstly, the different thermal expansion of the components can lead to cracking problems and thus, the maximum active surface is usually limited. Another disadvantage is the high contact resistance between electrolyte and electrodes, due to the geometrical configuration and the all solid state components.

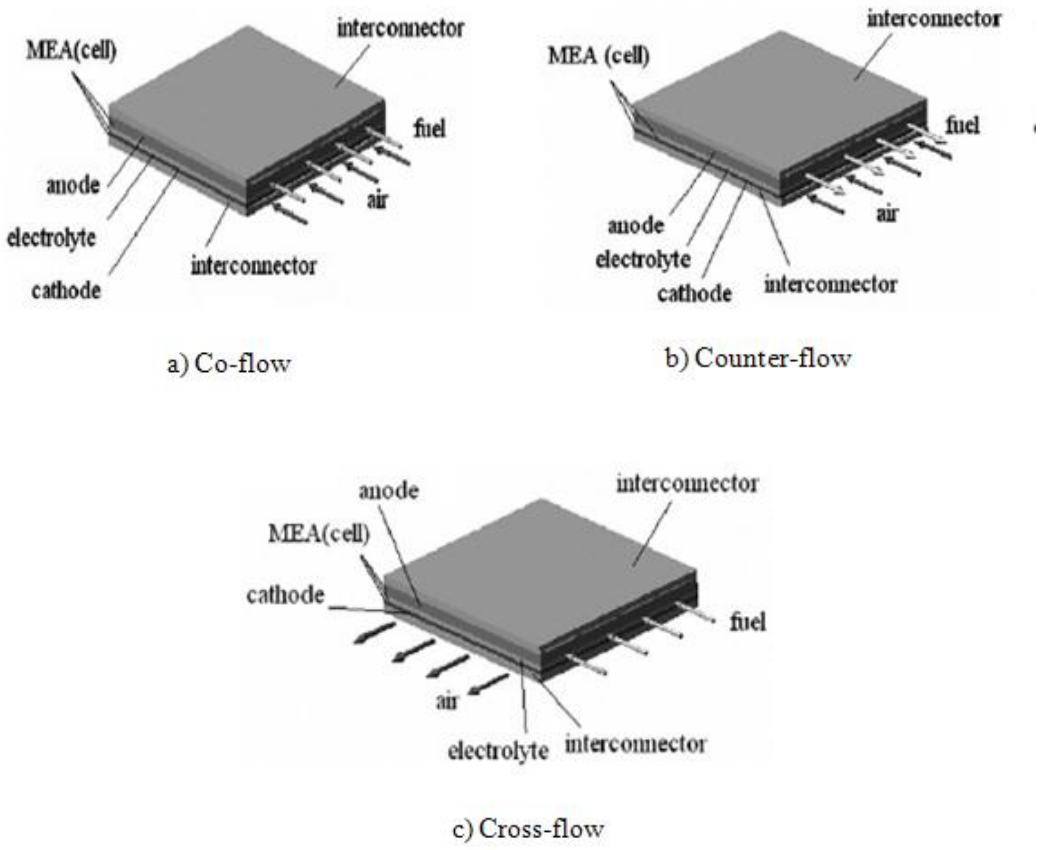

Figure 3. 5 Flow configurations of planar SOFC (Rahimpour and Lotfinejad, 2008).

Tubular design: In tubular design, individual fuels cells are arranged in bands along the support tube and are connected in series by a ceramic interconnect material. In general, the tubular SOFC is cathode-supported SOFC and thin electrolyte and anode layers cover the cathode, as demonstrated in Figure 3.6. A major advantage is that relatively large single tubular cells can be constructed in which the successive active layers. The tubular approach with one closed end eliminates the requirement of gas seals between cells. One attractive feature of this design is that it eliminates the need for leak-free gas manifolding of the fuel and oxidant streams. However, the seal less tubular design results in a relatively long current path around the circumference of the cell to the interconnection, resulting in the limitation of cell performance. Other drawbacks of the tubular design are the low volumetric power density, and the high manufacturing costs.

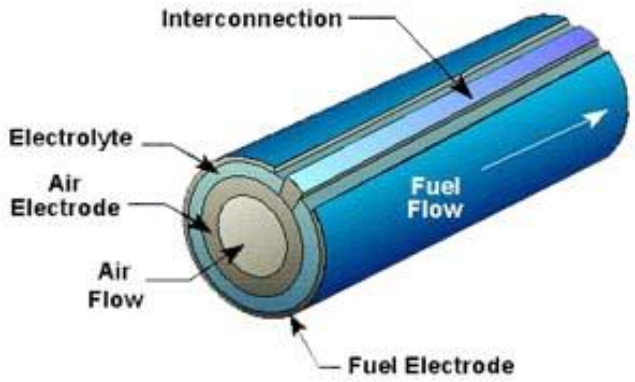

Figure 3. 6 A schematic of tubular SOFC design.

(http://www.netl.doe.gov/publications/press/2000/tl_sofcdemo.html)

3.2.3 Internal reforming SOFC

Due to the high operating temperature of SOFC, it can directly run on hydrocarbon fuels which are internally reformed to generate hydrogen-rich gas within a fuel cell stack. The method can be called reforming which can be split into internal reforming and external reforming. In this part, we will explain only internal reforming. The internal reforming occurring inside the fuel itself (at the surface of anode's catalysts) is divided into indirect internal reforming (IIR) and direct internal reforming (DIR). The primary conversion may be accomplished with or without a catalyst via one of three major types of fuel reforming processes, i.e., steam reforming (SR), partial oxidation (POX) reforming, and autothermal reforming (AR).

Chemical reaction characteristics of three primary fuel reforming reactions are shown in Table 3.4 whereas Table 3.5 presents advantages and disadvantages of three primary H_2 production methods. The steam reforming reaction produces the highest H_2 yield and cleanest exhaust. The low H_2 yield for another is a result of their intake of air; the oxygen in air partially oxidizes the fuel while the nitrogen in air dilutes the hydrogen composition in the outlet gas. For all three reactions, the H_2 yield can be increased by downstream use of the water gas shift reaction.

Table 3. 4 Comparison of Chemical reaction characteristics of three primary fuel reforming reactions (O'Hayre et al., 2006).

Type	Chemical Reaction	Temperature Range (°C)	Outlet Gas Composition (with Natural Gas Fuel)					Exothermic or Endothermic?
			H_2	CO	CO_2	N_2	Others	
Steam reforming	$C_xH_y + xH_2O\,(g) \leftrightarrow xCO + (\frac{1}{2}y + x)H_2$ $\Rightarrow CO, CO_2, H_2, H_2O$	700-1000	76%	9%	15%	0%	Trace NH_3, CH_4, SO_x	Endothermic
Partial oxidation	$C_xH_y + \frac{1}{2}xO_2 \leftrightarrow xCO + \frac{1}{2}yH_2$	>1000	41%	19%	1%	39%	Some NH_3, CH_4, SO_x, HC	Exothermic
Autothermal reforming	$C_xH_y + zH_2O\,(g) + (x - \frac{1}{2}z)O_2$ $\leftrightarrow xCO + (z + \frac{1}{2}y)H_2$ $\Rightarrow CO, CO_2, H_2, H_2O$	600-900	47%	3%	15%	34%	Trace NH_3, CH_4, SO_x, HC	Neutral

Table 3. 12 Advantages and disadvantages of three primary H_2 production processes (O'Hayre et al., 2006).

Type	Advantages	Disadvantages
Steam reforming	- Highest H_2 yield	- Requires careful thermal management to provide heat for reaction especially for (a) start-up and (b) dynamic response - Only works on certain fuel
Partial oxidation	- Quick to start and respond because reaction is exothermic - Quick dynamic response - Less careful thermal management required - - Works on many fuels	- Lowest H_2 yield - Highest pollutant emissions (HCs, CO)
Autothermal reforming	- Simplification of thermal management by combining exothermic and endothermic reactions in same process - Compact due to reduction in heat generation - Quick to start	- Low H_2 yield - Requires careful control-system design to balance exothermic and endothermic processes during load changes and start-up

The steam reforming of hydrocarbons are required for SOFC. Internal reforming of the hydrocarbon fuels in SOFC systems increases the system efficiency by recuperating waste heat from the stack into the fuel supply, whereas at the same time substantially reducing the complexity and cost of the system by elimination of the external reformer and associated heating arrangements and by reduction in the stack cooling air requirements and associated equipment. Thus, internal reforming SOFCs offer significantly higher system efficiencies and reduced complexity compared to lower temperature fuel cells, as well as offer flexibility in the choice of fuel.

Direct Internal Reforming SOFC (DIR-SOFC): The reforming takes place directly on the anode and the fuels are supplied directly into the cell. This type offers the simplest and most cost effective design for an SOFC system. High-efficiency of using DIR-SOFC results from utilizing the heat from the exothermic electrochemical oxidation reaction to reform the hydrocarbon fuel which is a strongly endothermic reaction. The advantage of direct internal reforming is that by consuming the hydrogen to form steam, which can then reform more of the hydrocarbon fuel, the electrochemical reactions help drive the reforming reaction to completion.

However, the problems with direct internal reforming is that it gives rise to a sharp endothermic cooling effect at the cell inlet, generating inhomogeneous temperature distributions and a steep temperature gradient along the length of the anode. This problem is very difficult to control and can result in cracking of the anode and electrolyte materials.

Indirect Internal Reforming SOFC (IIR-SOFC): the reformer unit is separated from the fuel cell but adjacent to the fuel cell anode. The heat from the exothermic fuel cell reaction is still utilized. Although indirect internal reforming is less efficient and less straightforward than direct reforming, it still represents a more efficient, simpler and more cost-effective approach than using an external reformer. The advantage of indirect internal reforming is much easier to control from a thermodynamic standpoint. Moreover, it is easier to develop dispersed catalysts which do not promote carbon deposition to the same extent as the nickel anode. Nevertheless the conversion of fuels to hydrogen is not promoted to the same extent as with direct internal reforming. A schematic of IIR/DIR SOFC is illustrated in Figure 3.7.

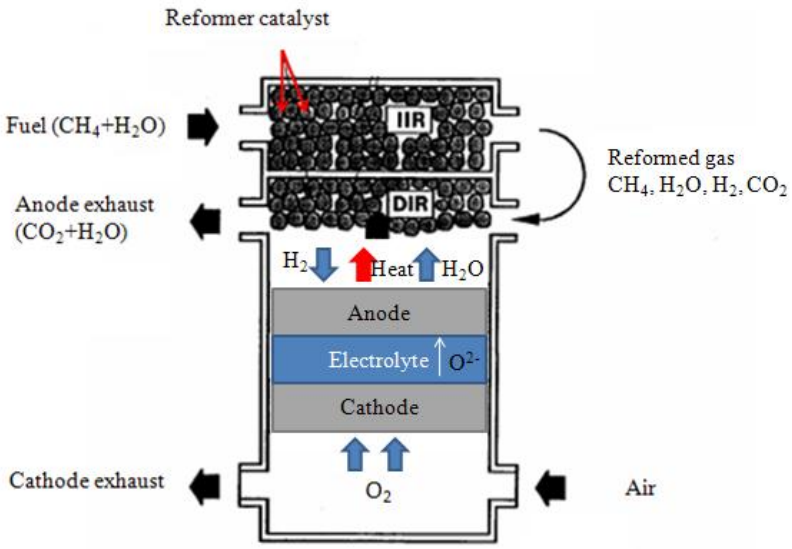

Figure 3. 7 A schematic of IIR/DIR SOFC.

3.3 Control structure design

To design an efficient control system, it is necessary to first decide the control structure design. Control structure design deals with the structural decisions of the control system, including the selection of manipulated variables (inputs), controlled variables (output), measurements, control configuration, and controller type and what to control and how to pair the variables to form control loops (Skogestad and Postlethwaite, 1996). Control structure selection points are identified as important also in many industries and the most important control aspect has been to select the correct controlled variables. The key to the control design is selecting the variables to be regulated and the controls to perform regulation (Balas, 2003). Moreover, the self-optimizing control is implemented to select the good controlled variable which can be kept constant at setpoints without the need to re-optimize when disturbance occur.

The control structure design procedure can follow the stepwise of Skogestad (2004). The procedure is divided in two main parts: Top-down analysis and Bottom-up design of the control system that include the purpose and typical model requirements for each layer, implementing decentralized (single loop) control or multivariable control (e.g. MPC) in the supervisory control layer. The first part including definition of operational objectives, consideration of degrees of freedom available, and selection

of controlled variables and production rate. The second part shows the detail of the stabilizing control layer. The step of control structure design can be shown as follow:

Step 1. Definition of operational objectives.

It must be distinctly defined for design a control system. Moreover, operational constraints and a scalar cost function *J* to be minimized should be identified. In general, function J may be selected as the operational cost; however, it can be formulated as constraints.

The general operational objective function is defined as *J* (u, x, d). The variable u refers to degrees of freedom, x refers to state variables, and d refers to disturbances variable. The operational objective function *J* optimized to be minimize with respect to u for given d can be expressed as:

$$\min_{u} J(u, x, d) \tag{3.4}$$

Subject to: Model equations

Operational constraints

Step 2. Selection of manipulated variables and degrees of freedom.

The dynamic and steady-state degrees of freedom (DOFs) are identified. The number of control variables is equal to the number of steady-state degrees of freedom, N_{ss} and can be calculated from Eq. (3.5).

$$N_{ss} = N_{valves} - (N_{0y} + N_{0,valves}) \tag{3.5}$$

where N_{valves} represents the numbers of dynamic DOFs (counting valves) that is equal to the number of manipulated variables, N_{0y} represents the numbers of controlled variables (liquid levels) with no steady-state effect, and $N_{0,valves}$ represents the numbers of purely dynamic control DOFs.

Step 3. Selection of primary controlled variables.

Which variables should be controlled? We needs to control the variables that relate to ensuring optimal economic operation. The control active constraints variable and control self-optimizing variable are identified and controlled to their setpoints. The

variable needed to remain constant is active constraint. Self-optimizing control is achieved an acceptable loss L (without the need to reoptimize when disturbances occur) with constant setpoint values for the controlled variables. The concept of self-optimizing control can be shown in Figure 3.8. The loss L is defined as the difference between the actual value ($J(d)$) of the cost function and the optimal value ($J_{opt}(d)$) and can be express as:

$$\text{Loss } L = J(d) - J_{opt}(d) \tag{3.6}$$

Loss imposed by keeping constant setpoint for the controlled variable, $C_{1,s}$ is better self-optimizing controlled variable than $C_{2,s}$. d^* represents its nominal optimal operating point.

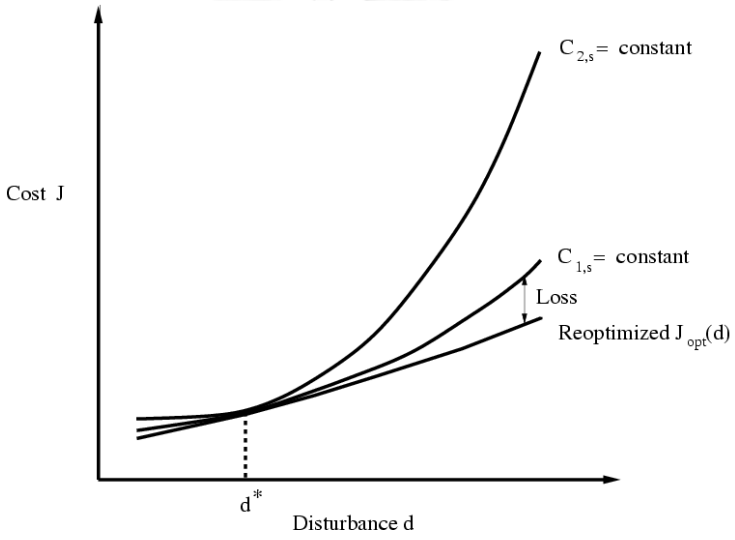

Figure 3. 8 The concept of self-optimizing control.

Step 4. Definition of production rate.

The production rate is usually assumed to be set at the inlet to the process and set at the throughput manipulated (TPM) located. TPM is the manipulated variable used to control throughput (controlled variable) or a degree of freedom that affects the network flow.

Step 5. Structure of stabilizing control layer.

The objective of the regulatory control layer is to select and control secondary controlled variables (measurements), so that the effect of disturbances on the primary

outputs can be handled by the layer above. Moreover, this measurements are pairing with the manipulated variables. The good secondary measurements should select the variables that easy to measure and control using the available manipulated variables.

Step 6. Supervisory control layer.

The controlled outputs are keep at optimal setpoints, using as degrees of freedom (inputs) for the regulatory layer. For decentralized (single-loop) control may use simple PI or PID controllers. The structural is to choose input-output pairing. The pairing analysis is discussed in Section 3.4 on controllability analysis.

Step 7. Optimization.

This step is to identify active constraints and to compute optimal setpoints for controlled variables. Optimization is based on nonlinear steady-state model including costs and constraints.

Step 8. Validation.

It involves nonlinear dynamic simulation of critical parts.

3.4 Controllability analysis

Controllability plays an important role in designing a control system as it demonstrates the ability to move system outputs to specified bounds using available inputs. Controllability analysis can offer insights for identifying the inherent properties of a process and how they limit control performance (Morari, 1983). It is also the ability of a process to achieve acceptable control performance; that is, to preserve the outputs with in specified bounds (Skogestad and Postlethwaite, 1996). In addition, a controllability analysis is generally applied for selection of the best controlled and manipulated variable pairing within one process and evaluation of control properties for two or more process alternatives.

It offers a numerical indication of the sensitivity balance to provide a qualitative assessment of the control properties of the alternative designs. A plant is controllable if there exists a controller that yields acceptable performance for all expected plant variations. From this, controllability is independent of the controller and a property of

the process alone. Therefore, controllability analysis is applied to a plant to find out what control performance can be expected.

In particular, in this thesis we will apply controllability analysis in the design of processes, namely such processes that are designed for dynamic and control purposes, and in the design and understanding of feedforward and multivariable controllers.

Next, the relative gain array (RGA) is considered a controllability index for the selection of input-output pairings and to describe the interactions among inputs and outputs. Furthermore, it is an analysis tool used to determine the optimal control structure of multi input multiple output (MIMO) and determine the interaction among control loops in a multivariable process (García et al., 2011). Generally, a RGA that is a normalized form of the gain matrix, close to the unity matrix at frequencies around bandwidth is preferred and in particular control structures with high RGA elements should be avoided. It is important to know that the structures with large RGA elements around the bandwidth frequency are difficult to control due to sensitivity to input uncertainty (Skogestad and Postlethwaite, 1996). The RGA of a non-singular square complex matrix (G) is defined as indicated in Eq (3.6), where x denotes element by element multiplication (the Hadamard or Schur product).

$$\mathrm{RGA}(G) = \Lambda(G) = G \times \left(G^{-1}\right)^{T} \tag{3.6}$$

The RGA of a transfer matrix is generally computed as a function of frequency. The example for a 2x2 matrix with elements g_{ij}, the RGA can be shown as:

$$\Lambda(G) = \begin{bmatrix} \lambda_{11} & \lambda_{12} \\ \lambda_{21} & \lambda_{22} \end{bmatrix}, \tag{3.7}$$

$$\lambda_{11} = \frac{1}{1 - \dfrac{g_{12}g_{21}}{g_{11}g_{22}}} \tag{3.8}$$

The RGA provides a measure of interactions (Bristol, 1996). Assume u_j and y_j refer to a particular input-output pair for the multivariable plant G and u_j is used to control y_j.

For all other loops open

$$g_{ij} = \left(\frac{\Delta y_i}{\Delta u_j} \right)_{u_k = 0, k \neq j} \tag{3.9}$$

For other loops closed

$$\hat{g}_{ij} \cong \left(\frac{\Delta y_i}{\Delta u_j} \right)_{y_k = 0, k \neq i} \tag{3.10}$$

where g_{ij} is the ij th element of G and $\hat{g}_{ij}$ is the inverse of the ji th element of G^{-1}.

$$\hat{g}_{ij} = 1/\left[G^{-1}\right]_{ji} \tag{3.11}$$

The ratio between the gains in Eqs. (3.9) and (3.10) is a useful measure of interactions, and the ij th the relative gain can be defined as:

$$\lambda_{ij} \cong \frac{g_{ij}}{\hat{g}_{ij}} = \left[G\right]_{ij}\left[G^{-1}\right]_{ji} \tag{3.12}$$

The corresponding matrix of relative gains is the RGA. From Eq. (3.12), this is identical to the definition of the RGA matrix in Eq. (3.6).

3.5 Robust model predictive control

3.5.1 Model description

In order to define the controller for robust control, a linear time-varying (LTV) system is considered for multi-model paradigm or polytopic uncertainty. The linear discrete-time model can be expressed as:

$$x(k+1) = A(k)x(k) + B(k)u(k) \tag{3.13}$$

$$y(k) = Cx(k)$$

$$\left[A(k) \quad B(k)\right] \in \Omega$$

where $x(k)$ is the state of the plant, $u(k)$ is the control input and $y(k)$ is the plant output. Furthermore, we define that the set Ω is the polytope for polytopic systems.

$$\Omega = \mathrm{Co}\{\left[A_1 \quad B_1\right], \left[A_2 \quad B_2\right], ..., \left[A_L \quad B_L\right]\} \tag{3.14}$$

where Co represents the convex hull and $[A_i\ B_i]$ are vertices in the convex hull. If the system is the nominal linear time-invariant (LTI) model, it shows that L=1.

For other cases, $[A(k)\ B(k)] \in \Omega$ defined by L vertices, we have

$$\begin{bmatrix} A(k) & B(k) \end{bmatrix} = \sum_{i=1}^{L} \lambda_i \begin{bmatrix} A_i & B_i \end{bmatrix} \tag{3.15}$$

$$\sum_{i=1}^{L} \lambda_i = 1, \qquad 0 \le \lambda_i \le 1$$

Notation: For a matrix A, A^T represents the transpose of matrix A, A^{-1} represents the inverse of matrix A, I represents the identity matrix. For a vector x, $x(k/k)$ represents the state measured at real time k, $x(k+i/k)$ represents the state at prediction time $k+i$ predicted at real time k.

3.5.2 Lyapunov theory

To determine the stability of the linear discrete-time systems, Lyapunov theorem is used as an important basic theorem and used to make conclusions about trajectories of a system without finding the trajectories. Moreover, the formulation of the Lyapunov stability constraint is implemented to guarantee robust stability of the closed-loop system. The Lyapunov stability can be extended to infinite-dimensional manifolds that relates to the behavior of different solutions to differential equations.

Suppose there is a function V such that V is a positive definite function. For the linear discrete-time system, Let

$$x(k+1) = Ax(k) \tag{3.16}$$

This system is an asymptotically stable if

$$V(x) = x^T Px > 0 \tag{3.17}$$

such that

$$V(x(k+i|k)) = 0, \text{at } x(k+i|k) = 0 \tag{3.18}$$

and

$$V(x(k+i+1|k)) - V(x(k+i|k)) < 0, \text{ for all non-zero} \tag{3.19}$$

At sampling time k,

$$x(k+i+1|k) = Ax(k+i|k) \tag{3.20}$$

by substitution Eq. (3.17) to Eq.(3.19):

$$x(k+i+1|k)^T Px(k+i+1|k) - x(k+i|k)^T Px(k+i|k) < 0 \tag{3.21}$$

Equivalent to

$$x(k+i|k)^T A^T PAx(k+i|k) - x(k+i|k)^T Px(k+i|k) < 0 \tag{3.22}$$

Pre-multiplying by $x(k+i|k)^{-T}$ and post-multiplying by $x(k+i|k)^{-1}$, and then Eq. (3.22) can be written as:

$$A^T PA - P < 0 \tag{3.23}$$

3.5.3 Model predictive control (MPC) (Seborg et al., 2003)

Model Predictive Control (MPC) is an important advanced control technique for difficult multivariable control problems. Suppose that we wish to control a multiple-input, multiple-output process while satisfying inequality constraints on the input and output variables. If a reasonably accurate dynamic model of the process is available, we can use the model and current measurement to predict future values of the outputs. Then the appropriate changes in the input variables can be calculated based on both predictions and measurements. In essence, the changes in the individual input variables are coordinated after considering the input-output relationships represented by the process model. In MPC applications, the output variables are also referred as controlled variables or CVs, while the input variables are also called manipulated variables or MVs. Measured disturbance variables are called DVs or feedforward variables.

Model predictive control offers several important advantages: (1) The process model captures the dynamic and static interactions between input, output, and disturbance variables; (2) constraints on inputs and outputs are considered in a systematic manner; (3) the control calculations can be coordinated with the calculation of optimum set points, and (4) accurate model predictions can provide early warnings of potential problem. Clearly, the success of MPC (or any other model-based approach)

depends on the accuracy of the process model. Inaccurate predictions can make matters worse, instead of better.

A block diagram of a model predictive control system is shown in Figure 3.9. A process model is used to predict the current values of the output variables. The residuals, the differences between the actual and predicted outputs, serve as a feedback signal to a prediction block. The predictions are used in two types of MPC calculations that are performed at each sampling instant: set-point calculations and control calculations. Inequality constraints on the input and output variables, such as upper and lower limits, can be included in either type of calculation. Furthermore, MPC has had a much greater impact on industrial practice because it is more suitable for constrained MIMO control problems.

The set points for the control calculations, also called targets, are calculated from an economic optimization based on a steady-state model of the process, traditionally, a linear model. Typical optimization objectives include maximizing a profit function, minimizing a cost function, or maximizing a production rate. The optimum values of set points are changed frequently owing to varying process conditions, especially changes in the inequality constraints. The constraint changes are due to variations in process conditions, equipment, and instrumentation, as well as economic data such as prices and costs. In MPC, the set points are typically calculated each time the control calculations are performed.

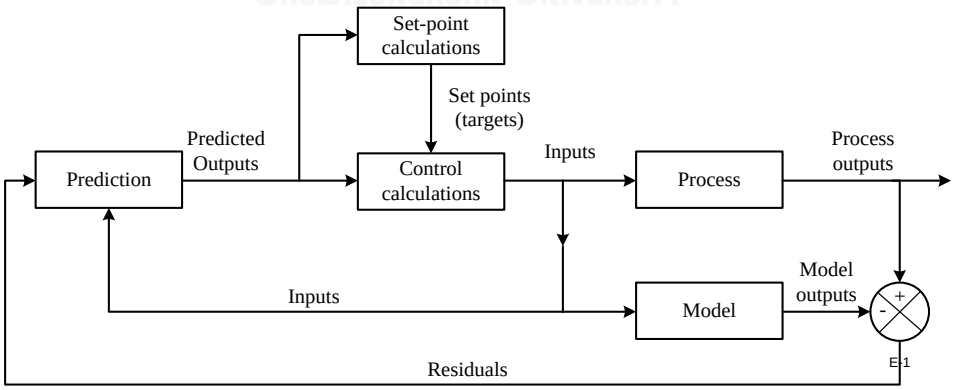

Figure 3. 9 Block diagram for model predictive control (Seborg et al., 2003).

The objective of the MPC control calculations is to determine a sequence of control moves (that is, manipulated input changes) so that the predicted response moves

to the set point in an optimal manner. The actual output, *y*, predicted output, $\hat{y}$, and manipulated input, *u*, are shown in Figure 3.10. At the current sampling instant, denoted by *k*, the MPC strategy calculates a set of M values of the input $\{u(k+i-1), i=1,2,...,M\}$. The set consists of the current input $u(k)$ and *M*-1 future inputs. The input is held constant after the M control moves. When the inputs are calculated, the set of P predicted outputs $\{\hat{y}(k+i), i=1,2,...,P\}$ reach the set point in an optimal manner. The control calculations are based on optimizing an objective function. The number of prediction P is preferred to as the prediction horizon while the number of control moves M is called the control horizon.

A distinguishing feature of MPC is its receding horizon approach. Although a sequence of M control moves is calculated at each sampling instant, only the first move is actually implemented. Then a new sequence is calculated at the next sampling instant, after new measurement become available; only the first input move is implemented. This procedure is repeated at each sampling instant.

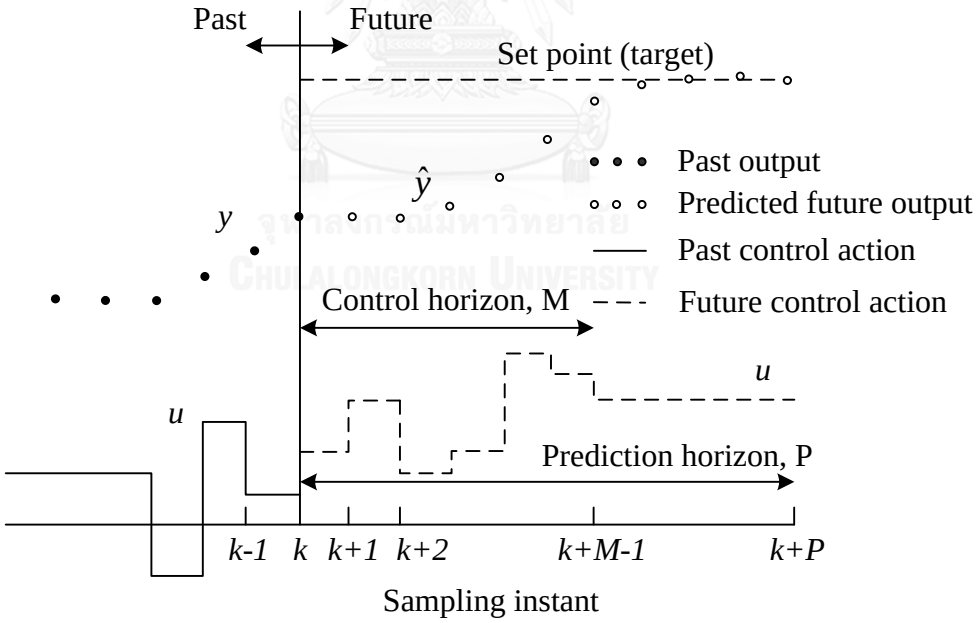

Figure 3. 10 Basic concepts for model predictive control (Seborg et al., 2003).

At each sampling time *k*, the control moves *u(k+i), i = 0, 1, …, m-1*, (control horizon, *m*) can be computed by minimizing a performance cost $J_p(k)$ over a prediction horizon *p* and expressed as:

$$\min_{u(k+i)} J_p(k) \tag{3.24}$$

Subject to constraints on the control input *u*, the state *x*, the output *y*.

In this research, the performance cost is considered following quadratic objective and shown as:

$$J_p(k) = \sum_{i=0}^{p} \left[x(k+i|k)^T Q_1 x(k+i|k) + u(k+i|k)^T Ru(k+i|k) \right] \tag{3.25}$$

where $Q_1 > 0$ and $R > 0$ are symmetric weighting matrices.

3.5.4 Robust MPC algorithm (Kothare et al., 1996)

Model predictive control (MPC) is effectively implemented to many chemical processes; however, a robust stability of the control system is not guarantee. The control performance base on MPC is significantly deteriorates and incompetence to deal with plant uncertainty. Therefore, robust MPC synthesis that allows a plant model uncertainty in the problem formulation has been proposed. The algorithm is then proved to guarantee robust stability by imposing the Lyapunov stability constraint.

This part serves as robust constrained infinite horizon model predictive control (IH-MPC) that includes input and output constraints integrated with linear matrix inequality (LMI) constraints in robust MPC problem. LMI constraints are convex quadratic inequalities. Thus, it is computationally tractable. The more details of LMI are referred to Boyd et al. (1994).

At each sampling time *k*, a robust performance objective is a min-max problem (minimization of worst-case performance cost) in term of the quadratic objective for the LTV system as given in Eq. (3.26).

$$\min_{u(k+i|k),i=0,1,\ldots,m} \quad \max_{[A(k+i) \;\; B(k+i)] \in \Omega, i \geq 0} \quad J_\infty(k) \tag{3.26}$$

where

$$J_\infty(k) = \sum_{i=0}^{\infty} \left[x(k+i|k)^T Q_1 x(k+i|k) + u(k+i|k)^T Ru(k+i|k) \right] \tag{3.27}$$

where $Q_1 > 0$ and $R > 0$ are symmetric weighting matrices.

The state feedback control law with the state feedback matrix F is defined to synthesis the robust MPC algorithm.

$$u(k+i|k) = Fx(k+i|k), \quad i \geq 0 \tag{3.28}$$

The state feedback gains F in the control law are defined as $F=YQ^{-1}$ to stabilize the closed-loop system. The matrix variables $Q>0$ and Y are achieved from the result of the linear objective minimization problem $J_{\infty}(k)$ with the upper bound $V(x(k/k))$ on the robust performance objective function at sampling time k.

The linear objective minimization problem can be expressed as:

$$\min_{\gamma,Q,Y} \gamma \tag{3.29}$$

subject to

$$\begin{bmatrix} 1 & x(k|k)^T \\ x(k|k) & Q \end{bmatrix} \geq 0 \tag{3.30}$$

and

$$\begin{bmatrix} Q & QA_j^T + Y^T B_j^T & QQ_1^{1/2} & Y^T R^{1/2} \\ A_j Q + B_j Y & Q & 0 & 0 \\ Q_1^{1/2} Q & 0 & \gamma I & 0 \\ R^{1/2} Y & 0 & 0 & \gamma I \end{bmatrix} \geq 0, \quad j = 1,2,...,L \tag{3.31}$$

Proof. See Appendix A

For input constraints, it is the limitations in the process equipment that inflict hard constraints on the manipulated variable $u(k)$.

$$\begin{bmatrix} u_{\max}^2 I & Y \\ Y^T & Q \end{bmatrix} \geq 0, \tag{3.32}$$

Performance terms inflict constraints on the process output $y(k)$ for output constraints.

$$\begin{bmatrix} Q & \left(A_j Q + B_j Y\right)^T C^T \\ C\left(A_j Q + B_j Y\right) & y_{\max}^2 I \end{bmatrix} \geq 0, \quad j = 1,2,...,L \tag{3.33}$$

In order to guarantee robust constraint satisfaction, Eq. (3.32) is expressed for guarantee input constraint satisfaction and Eq. (3.33) is expressed for guarantee output constraint satisfaction.

CHAPTER IV

MATHEMATICAL MODEL

A mathematical model is an essential tool in the design and optimization of the process system. The mathematical model of fuel cell is helpful for fuel cell developers because it can lead to improve the fuel cell design. The model should be robust and accurate and be able to provide solutions to fuel cell performance under a wide range of fuel cell operating conditions. The dynamic model of process refers to unsteady-state (or transient) process behavior. By contrast, most of the curricula emphasize steady-state and equilibrium conditions such as mass and energy balances, thermodynamics, and transport phenomena. However, the dynamic models are also very important. Transient behavior occurs during important situations such as start-ups and shutdowns, and unusual process disturbances. Consequently, this part is concerned with the process dynamic model. For this research, the mass balance in flow channel, energy balance, and electrochemical model of SOFC is also described.

4.1 Model configuration

A sketch of a planar solid oxide fuel cell is shown in Figure 4.1. The solid oxide fuel cell structure is composed of a ceramic ion-conducting electrolyte sandwiched between two porous electrodes, anode and cathode (denoted as the PEN, Positive electrode-Electrolyte-Negative electrode). Fuels such as hydrogen or hydrocarbon fuels are directly fed at the anode side and air used as oxidant at the cathode side is continuously fed into the fuel cell for generating electricity. At the cathode side, the oxygen is reduced and formed into oxygen ions which can diffuse through the ceramic ion-conducting electrolyte to the anode/electrolyte interface. The oxygen ions react with hydrogen which is supplied continuously to the anode side. Afterwards, the electrons are produced by the electrochemical reactions between hydrogen and oxygen ions on the anode side. The electrons transport through the anode via the external circuit, generating electricity and return to the cathode/electrolyte interface. Water, exhaust gases and heat as by-product are also produced.

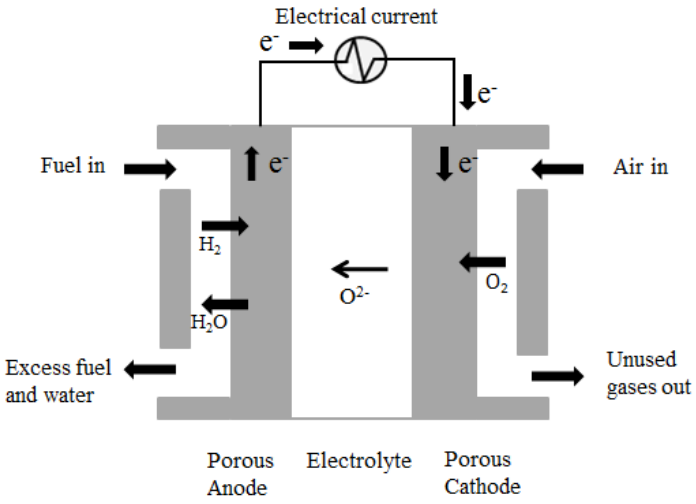

Figure 4. 1 A schematic of solid oxide fuel cell operation.

4.2 Model assumption

The mathematical model is considered for a planar direct internal reforming solid oxide fuel cell with co-flow direction of fuel and air (as shown in Figure 4.2). The fuel is directly reformed into hydrogen on the anode side by the steam reforming and water-gas shift (WGS) reactions inside the fuel cell stack (called direct internal reforming solid oxide fuel cell (DIR-SOFC)). In this work, methane, steam, and air are the main reactants for producing electricity.

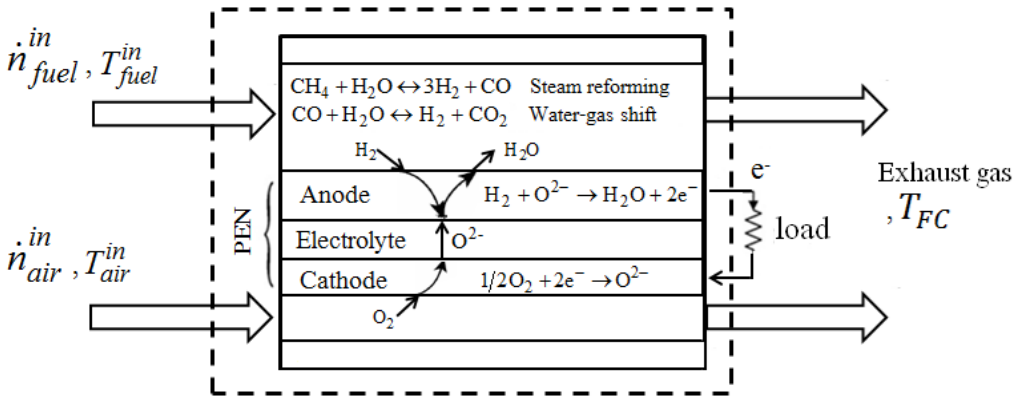

Figure 4. 2 Direct internal reforming solid oxide fuel cell.

The main assumptions are defined as follows:

1. Lumped-parameter model is considered.
2. All gas components are performed as ideal-gases.

3. Heat capacities of all components are constant.
4. Heat loss to the surrounding and distribution of pressure inside the gas channels are negligible.
5. The exit temperatures of fuel and air are same as the cell temperature.

4.3 SOFC model

The dynamic mathematical models of SOFC including mass balances in the fuel and air channels, energy balance, and electrochemical model were considered and explained in this Section.

4.3.1 Mass and energy balances

All reactions used in the mass and energy balances are presented in Table 4.1. In the fuel channel, three reactions are taken into account: (i) methane steam reforming reaction that is methane directly reformed within SOFC by the strongly endothermic reaction, (ii) water gas-shift reaction which is carbon monoxide reacted with water to produce hydrogen and carbon dioxide, and (iii) hydrogen oxidation reaction. In the air channel, only (iv) oxygen reduction reaction is considered.

Table 4. 1 Reactions considered in an SOFC.

Reaction name	No.	Reaction equation	ΔH (kJ/mol)
steam reforming	(i)	$CH_4 + H_2O \leftrightarrow 3H_2 + CO$	206.10
water-gas shift	(ii)	$CO + H_2O \leftrightarrow H_2 + CO_2$	-41.15
hydrogen oxidation	(iii)	$H_2 + O^{2-} \rightarrow H_2O + 2e^-$	-
oxygen reduction	(iv)	$1/2O_2 + 2e^- \rightarrow O^{2-}$	-
electrochemical reaction	(v)	$H_2 + 1/2O_2 \rightarrow H_2O$	-241.83

The internal methane steam reforming (MSR) reaction in porous-supported SOFC is the important factor to expose the performances of SOFC completely (Yang et al., 2009). Moreover, it is the major reaction involved in the hydrogen production. As mentioned above, the steam reforming reaction is an endothermic reaction of steam with methane as fuel. The rate expression of steam reforming reaction, $R_{(i)}$ is written as (Achenbach, 1994):

$$R_{(i)} = k_0 p_{CH_4} \exp\left(-\frac{E_a}{RT}\right) \quad (4.1)$$

where k_0 is a pre-exponential constant and equal to 4274 mol s^{-1} and E_a is an activation energy, equal to 82 kJ mol^{-1}.

Excess steam is used to prevent carbon formation on the catalyst at anode side and to force the reaction to completion. An associated reaction to the reforming reaction is the water-gas shift reaction. Unlike the steam reforming reaction, the water gas-shift reaction is an exothermic reaction. The rate expression of water gas shift reaction, $R_{(ii)}$ is written as (Haberman and Young, 2004):

$$R_{(ii)} = k_{WGSR} p_{CO}\left(1 - \frac{p_{CO_2} p_{H_2} / p_{CO} p_{H_2O}}{K_{eq}}\right) \quad (4.2)$$

$$k_{WGSR} = 0.0171\exp\left(\frac{-103191}{RT}\right) \quad (4.3)$$

$$K_{eq} = \exp\left(\frac{4276}{T} - 3.961\right) \quad (4.4)$$

Faraday's law relates the flux of reactants and products to the electric current arising from an electrochemical reaction. According to this law and when only hydrogen oxidation is present, the local amount of H_2 and O_2 consumed and H_2O produced through overall cell reaction, $R_{(v)}$ is related to the electric current density, j, produced in the cell by:

$$R_{(v)} = \frac{j}{2F} \quad (4.5)$$

Mass Balances

Methane is assumed to be only reformed to hydrogen, carbon monoxide, and carbon dioxide and, therefore, not electrochemically oxidized (Aguiar et al., 2004). Thus, the chemical species considered in the fuel channel consist of methane, water, carbon monoxide, hydrogen, and carbon dioxide (CH_4, H_2O, CO, H_2, and CO_2) whereas the chemical species in the air channel are oxygen and nitrogen (O_2 and N_2). Lumped parameter models are adequately accurate for systems-level analysis and control as confirmed through experimental validation (Xi et al., 2010).

The lumped parameter models were employed for analysis and control of SOFC systems (Muller et al., 2008, Murshed et al., 2007, Sorrentino et al., 2008). Therefore, the lumped parameter model is implemented to describe the dynamics of the fuel cell.

Hence, the lumped model of mass balances in the fuel and air channels can be defined in term the mole of component, as shown below:

In fuel channel: (i = CH_4, H_2O, CO, H_2, and CO_2)

$$\frac{dn_{i,\mathrm{f}}}{dt} = \dot{n}_{i,f}^{in} - \dot{n}_{i,f} + \sum_{\mathrm{k}\in\{(\mathrm{i}),(\mathrm{ii}),(\mathrm{v})\}} \upsilon_{i,\mathrm{k}} R_{\mathrm{k}} A \tag{4.6}$$

Initial condition for the fuel channel:

$$n_{i,f}\Big|_{t=0} = n_{i,f}^{0} \tag{4.7}$$

In air channel: (i = O_2 and N_2)

$$\frac{dn_{i,\mathrm{a}}}{dt} = \dot{n}_{i,a}^{in} - \dot{n}_{i,a} + \upsilon_{i,(\mathrm{v})} R_{(\mathrm{v})} A \tag{4.8}$$

Initial condition for the air channel:

$$n_{i,a}\Big|_{t=0} = n_{i,a}^{0} \tag{4.9}$$

where $\dot{n}_{i,f}$ and $\dot{n}_{i,a}$ (mol s^{-1}) are the molar flow rate of species i in the fuel and air channels, respectively, $\upsilon_{i,k}$ is the stoichiometric coefficient of component i in reaction k, R_k (mol s^{-1} m^{-2}) is the rate of reaction k, and A is the reaction area (m^2).

Energy Balance

It is assumed that the temperature variation inside the fuel cell is negligible for the lumped model, resulting in the following expression for the fuel cell temperature (T_{FC}):

$$\frac{dT_{FC}}{dt} = \frac{1}{\rho_{SOFC} Cp_{SOFC} V_{SOFC}} \left(\dot{Q}_{f,in} - \dot{Q}_{f,out} + \dot{Q}_{a,in} - \dot{Q}_{a,out} + \sum_{\mathrm{k}\in\{(\mathrm{i}),(\mathrm{ii}),(\mathrm{v})\}} \left(-\Delta H\right)_{\mathrm{k}} R_{\mathrm{k}} A - jAV_{FC} \right) \tag{4.10}$$

where

$$\dot{Q}_i = \sum_j \dot{n}_j Cp_j (T_i - T_{ref}) \tag{4.11}$$

Moreover, ρ_{SOFC} (kg m^{-3}), Cp_{SOFC} (kJ kg^{-1} K^{-1}), and V_{SOFC} (m^3) represent the density, heat capacity, and volume of SOFC, respectively, ΔH (kJ mol^{-1}) represents the heat of reaction, and Q_i (kJ s^{-1}) shows the enthalpy flow, and subscripts *i* and *j* in Eq. (4.11) refer to the corresponding streams (fuel or air) and components, respectively.

4.3.2 Electrochemical model

It is necessary to understand the reaction process occurring at the anode and cathode, the reaction rate to produce the electric current and the fuel cell energy conversion efficiency.

Thermodynamics is the study of energy changing from one stage to another. The conversion of the free energy change associated with a chemical reaction directly into electrical energy is the electrochemical energy conversion. Maximum electrical work (W_{elec}) is given by the negative change in Gibbs free energy change (ΔG) for the process, and can be expressed in molar quantities as:

$$W_{elec} = -\Delta G \tag{4.12}$$

The potential of a system to perform electrical work by a charge, *Q* (coulombs), through an electrical potential difference, *E* (Volts), is

$$W_{elec} = EQ \tag{4.13}$$

If the charge is assumed to be carried out by electrons:

$$Q = nF \tag{4.14}$$

where *n* is the number of electrons transferred and *F* is the Faraday's constant (96,487 coulombs per electrons). Therefore, the maximum reversible voltage can be provided by the cell can be expressed in Eq. (4.15),

$$\Delta G = -nFE_r \tag{4.15}$$

where E_r is the standard reversible potential.

For any chemical reaction

$$jA + kB \rightarrow mC + nD \tag{4.16}$$

The Gibbs free energy can be expressed in terms of the standard state Gibbs free energy and the partial pressures of the reactants and products:

$$\Delta G = \Delta G^{\mathrm{O}} + RT\ln\frac{(p_{\mathrm{c}}/\mathrm{P}_0)^{\mathrm{m}}(p_{\mathrm{D}}/\mathrm{P}_0)^{\mathrm{n}}}{(p_{\mathrm{A}}/\mathrm{P}_0)^{\mathrm{j}}(p_{\mathrm{B}}/\mathrm{P}_0)^{\mathrm{k}}} \tag{4.17}$$

The overall reaction in an SOFC is the oxidation of H_2 to form H_2O, that is,

$$\mathrm{H}_2 + \frac{1}{2}\mathrm{O}_2 \rightarrow \mathrm{H}_2\mathrm{O} \tag{4.18}$$

In this reaction, the number of electrons transferred for one mole of reacted hydrogen is 2 (n=2) and then,

$$E = -\frac{\Delta G}{nF} = -\frac{\Delta G^0}{nF} - \frac{RT}{nF}\ln\left(\frac{p_{\mathrm{H_2O}}}{p_{\mathrm{H_2}}\, p_{\mathrm{O_2}}^{1/2}}\right) \tag{4.19}$$

Thus,

$$E = E^0 - \frac{RT}{2F}\ln\left(\frac{p_{\mathrm{H_2O}}}{p_{\mathrm{H_2}}\, p_{\mathrm{O_2}}^{1/2}}\right) \tag{4.20}$$

Eq. (4.20) can be called Nernst Equation; it depends on the gas composition and cell temperature and results from the difference between the thermodynamic potentials of the electrode reactions. For this work, the Nernst equation can be express as Eq. (4.21):

$$E_{OCV} = E_0(T_{FC}) - \frac{RT_{FC}}{2F}\ln\left(\frac{p_{\mathrm{H_2O}}}{p_{\mathrm{H_2}}\, p_{\mathrm{O_2}}^{1/2}}\right) \tag{4.21}$$

The theoretical open-circuit voltage or reversible cell voltage (E_{OCV}) is the maximum voltage. E_0 is the standard-state reversible potential or the open-circuit voltage at the standard pressure and is a function of the operating temperature (T_{FC}) that can be expressed by Eq. (4.22). Whereas p_i is the partial pressure of component *i*, *R* is the universal gas constant, and T_{FC} is the operating cell temperature.

$$E_0 = 1.253 - 2.4516\times10^{-4}T_{FC}(K) \tag{4.22}$$

The theoretical open circuit voltage is the maximum voltage that can be calculated by Nernst equation. In general, the fuel cell cannot achieve maximum reversible voltage. The rate at which this work can be realized near equilibrium is essentially zero as the current flowing through the cell at open-circuit voltage (OCV). When an external load is connected, a finite, non-zero current flows through the circuit, and the process is carried out irreversibly. Thus, the operating cell voltage or the actual voltage (V_{FC}) is less than its open-circuit voltage due to ohmic resistance (η_{ohm}) and overpotentials losses that can be divided into concentration overpotentials (η_{conc}) and activation overpotentials (η_{act}). These losses depend on the cell temperature, current density, and species concentrations. Therefore, the cell operating voltage is given by subtracting the various losses from the theoretical open circuit voltage and can be shown as:

$$V_{\text{FC}} = E_{OCV} - \left(\eta_{\text{Ohm}} + \eta_{\text{conc}} + \eta_{\text{act}}\right) \tag{4.23}$$

Three major losses influence the shape of *V-i* curve (voltage-current density curve) that shows the output voltage of the fuel cell for a given current output, as illustrated in Figure 4.3.

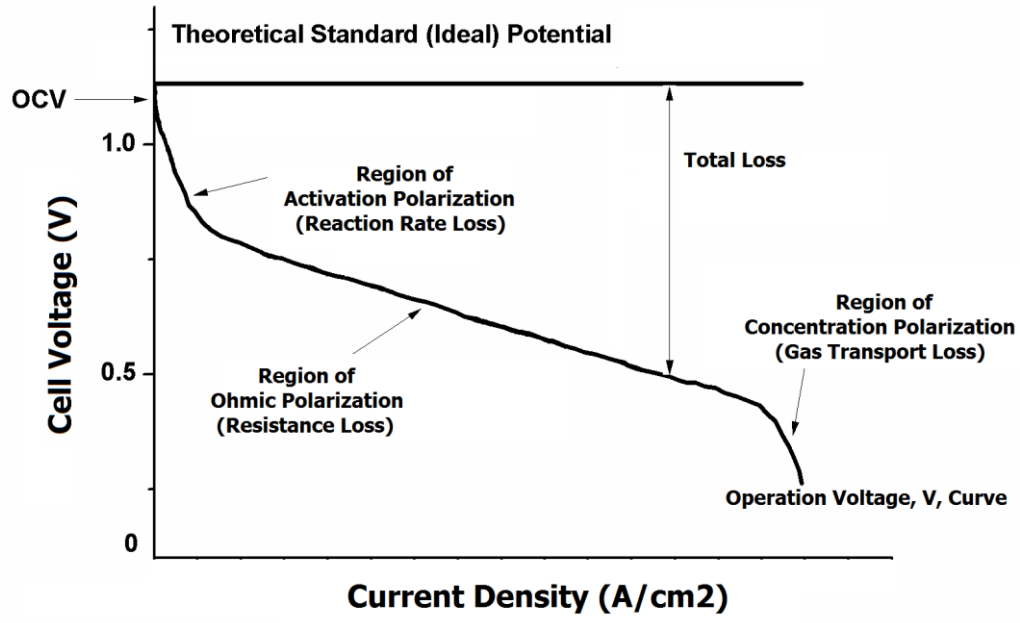

Figure 4. 3 A schematic of fuel cell *V-i* curve.

The ohmic losses (η_{Ohm}) are caused by the oxide ions transport through the electrolyte, the electrons transport through the porous electrodes (anode and cathode), and contact resistance occurs between cell components. The electronic resistivity is corrected for porosity and the possible existence of secondary, insulating phases. Ohm's law can describe the ohmic losses that can be expressed as:

$$\eta_{Ohm} = jR_{Ohm} \tag{4.24}$$

where R_{Ohm} is the internal resistance of the cell that depends on the resistivity and the thicknesses of electrodes and electrolyte. It is also calculated from the conductivity and the thickness of the individual layers as:

$$R_{Ohm} = \frac{\tau_{anode}}{\sigma_{anode}} + \frac{\tau_{electrolyte}}{\sigma_{electrolyte}} + \frac{\tau_{cathode}}{\sigma_{cathode}} \tag{4.25}$$

where τ_{anode}, $\tau_{electrolyte}$, and $\tau_{cathode}$ refer to the thickness of the anode, electrolyte, and cathode layers, respectively, σ_{anode} and $\sigma_{cathode}$ refer to the electronic conductivity of the anode and cathode, respectively, and $\sigma_{electrolyte}$ refers to the ionic conductivity of the electrolyte.

Assumption of Eq. (4.25) is negligible contact resistances, cross-plane charge flow, and series connection of resistances. General methods of reducing ohmic losses include making the electrolyte as thin layer, employing high conductivity materials, and operating cell at higher temperatures.

The concentration overpotentials (η_{conc}) are the result of practical limitations on mass transport within the cell. They can be caused when the reactants are consumed by the electrochemical reaction faster than diffusing into the porous electrode. Moreover, they can also be caused by variation in bulk flow composition because the consumption of reacting species in the reactant flows causes a drop in reactant concentration along the cell, which causes a drop in the local potential near the end of the cell. The occurrences of these losses include gas species transport in electrodes, solution of reactants into the electrolyte, dissolution of products out of the electrolyte, and diffusion of the reactants/products through the electrolyte to/from the reaction sites. At the high current densities, these overpotentials become significant because of the lacking of fuel at the reaction sites, resulting in a corresponding loss in the output voltage.

These losses involve the species concentration at the three-phase boundaries (TPB) and the bulk channel flow and current density. The Nernst equation at TPB (E_{TPB}) is written as:

$$E_{\mathrm{TPB}} = E_0(T_{FC}) - \frac{RT_{FC}}{2F}\ln\left(\frac{p_{\mathrm{H_2O,TPB}}}{p_{\mathrm{H_2,TPB}}\, p_{\mathrm{O_2,TPB}}^{1/2}}\right) \tag{4.26}$$

The difference between Equations (4.21) and (4.26) gives the departure from the theoretical voltage; therefore, the concentration overpotentials can be calculated by:

$$\eta_{\mathrm{conc}} = \frac{RT_{FC}}{2F}\ln\left(\frac{p_{\mathrm{H_2O,TPB}}\, p_{\mathrm{H_2}}}{p_{\mathrm{H_2O}}\, p_{\mathrm{H_2,TPB}}}\right) + \frac{RT_{FC}}{4F}\ln\left(\frac{p_{\mathrm{O_2}}}{p_{\mathrm{O_2,TPB}}}\right) \tag{4.27}$$

where $p_{\mathrm{i,TPB}}$ is the partial pressure of component i at three-phase boundaries (TPB).

The concentration overpotentials appeared in Eq. (4.27) can be divided into the anodic concentration overpotentials, ($\eta_{\mathrm{conc,anode}}$) occurring on the first term of right-hand side and the cathodic concentration overpotential, ($\eta_{\mathrm{conc,cathode}}$) which occurs on the second term of right-hand side.

The partial pressures of H_2, H_2O, and O_2 at the three-phase boundaries can be determined by using porous-media gas-phase transport models as shown in Eqs. (4.28) - (4.30), respectively.

$$p_{\mathrm{H_2,TPB}} = p_{\mathrm{H_2,f}} - \frac{RT_{FC}\tau_{\mathrm{anode}}}{2FD_{\mathrm{eff,anode}}}\, j \tag{4.28}$$

$$p_{\mathrm{H_2O,TPB}} = p_{\mathrm{H_2O,f}} + \frac{RT_{FC}\tau_{\mathrm{anode}}}{2FD_{\mathrm{eff,anode}}}\, j \tag{4.29}$$

$$p_{\mathrm{O_2,TPB}} = P - (P - p_{\mathrm{O_2}})\exp\left(\frac{RT_{FC}\tau_{\mathrm{cathode}}}{4FD_{\mathrm{eff,cathode}}P}\, j\right) \tag{4.30}$$

where $D_{\mathrm{eff,anode}}$ stands for the effective diffusivity coefficient in the anode (considering a binary gas mixture of H_2 and H_2O), and $D_{\mathrm{eff,cathode}}$ stands for the oxygen effective diffusivity coefficient in the cathode (binary gas mixture of O_2 and N_2). These overpotentials can be mitigated by reducing the reactant utilization fraction or increasing the electrode porosity.

The activation overpotentials (η_{act}) are the result of the kinetics involved with the electrochemical reactions at the electrode/electrolyte interface. The activation barrier is the effect of many complex electrochemical reaction steps where typically the rate limiting step is responsible for the overpotentials. The overpotentials equation shown below can be found by solving the non-linear Butler-Volmer equation, which relates the current density drawn to the activation overpotential, for a first order charge transfer controlled electrochemical reaction. These overpotentials need to determine both the exchange current density and the transfer coefficient for both the anode and the cathode reactions.

$$j = j_{0,\text{anode}}\left[\frac{p_{H_2,\text{TPB}}}{p_{H_2,\text{f}}}\exp\left(\frac{\alpha nF}{RT_{FC}}\eta_{\text{act,anode}}\right) - \frac{p_{H_2O,\text{TPB}}}{p_{H_2O,\text{f}}}\exp\left(-\frac{(1-\alpha)nF}{RT_{FC}}\eta_{\text{act,anode}}\right)\right] \tag{4.31}$$

$$j = j_{0,\text{cathode},}\left[\exp\left(\frac{\alpha nF}{RT_{FC}}\eta_{\text{act,cathode}}\right) - \exp\left(-\frac{(1-\alpha)nF}{RT_{FC}}\eta_{\text{act,cathode}}\right)\right] \tag{4.32}$$

where α is the fraction of the applied potential that promotes the transfer coefficient and usually taken to be 0.5 and n is the number of electrons transferred in the single elementary rate-limiting reaction step. The exchange current density of electrode ($j_{0,\text{electrode}}$) can be expressed by:

$$j_{0,\text{electrode}} = \frac{RT_{FC}}{nF}k_{\text{electrode}}\exp\left(-\frac{E_{\text{electrode}}}{RT_{FC}}\right), \quad \text{electrode} \in \{\text{anode, cathode}\} \tag{4.33}$$

where $E_{\text{electrode}}$ represents the activation energy of the electrode exchange current densities as 140 kJ mol^{-1} and 137 kJ mol^{-1} for anode and cathode, respectively and $k_{\text{electrode}}$ represents the pre-exponential factor of the electrode exchange current density as 6.54 x 10^{11} $\Omega^{-1}m^{-2}$ and 2.35x10^{11} $\Omega^{-1}m^{-2}$ for anode and cathode, respectively (Aguiar et al., 2004).

4.4 SOFC performance

The power density or power output of cell (P_{FC}) is the amount of power per unit area which is obtained by the product of the operating cell voltage and current density, as given by:

$$P_{FC} = jV_{FC} \tag{4.34}$$

where V_{FC} represents the operating cell voltage, and j represents the current density.

The fuel utilization factor (U_{fuel}) is the ratio of the total inlet fuel used to produce electricity in the cell and the inlet fuel flow, and is defined by:

$$U_{\text{fuel}} = \frac{jLW}{(8Fx^{0}_{\text{CH}_4} + 2Fx^{0}_{\text{H}_2} + 2Fx^{0}_{\text{CO}})\dot{n}^{\text{in}}_{\text{fuel}}} \tag{4.35}$$

Fuel utilization ratio is the amount of hydrogen that is reacted in the electrochemical reaction to the amount of hydrogen in the inlet stream, expressed as:

$$U_{\text{fuel}} = \left(\frac{\dot{m}_{\text{f,in}} - \dot{m}_{\text{f,out}}}{\dot{m}_{\text{f,in}}}\right) \times 100\% = \frac{\dot{m}_{\text{f,consumed}}}{\dot{m}_{\text{f,in}}} \times 100\% \tag{4.36}$$

where $\dot{m}_{\text{f,in}}$ is the mass flow rate of fuel inlet and $\dot{m}_{\text{f,out}}$ is the mass flow rate of fuel outlet.

The excess air is a very important process parameter for the design of the total system. The air ratio reflects the air excess which is supplied to the cell for cooling and retaining the cell temperature. Therefore, the air utilization factor can be defined as:

$$U_{\text{a}} = \left(\frac{\dot{m}_{\text{a,in}} - \dot{m}_{\text{a,out}}}{\dot{m}_{\text{a,in}}}\right) \times 100\% = \frac{\dot{m}_{\text{a,consumed}}}{\dot{m}_{\text{a,in}}} \times 100\% \tag{4.37}$$

The air ratio (λ_{air}) is the inverse of the air utilization factor, which is defined as:

$$\lambda_{air} = \frac{1}{U_a} \tag{4.38}$$

or,

$$\lambda_{\text{air}} = \frac{x^{0}_{\text{O}_2}\dot{n}^{\text{in}}_{\text{air}}}{jLW/4F} \tag{4.39}$$

For energy conversion device, the efficiency of a system is great importance. Fuel efficiency represents the capability of the total chemical energy in the inlet fuel which is converted into electricity. Fuel cell efficiency can be calculated from thermal energy of fuel fed in the cell that are methane, carbon monoxide, and hydrogen, as described below:

$$\varepsilon_{SOFC} = \frac{jV_{FC}LW}{\left(x_{CH_4}^{in} LHV_{CH_4} + x_{H_2}^{in} LHV_{H_2} + x_{CO}^{in} LHV_{CO}\right)\dot{n}_{Total,anode}^{in}} \tag{4.40}$$

4.5 Model validation

The electrochemical model allows for the computation of the SOFC voltage, current density, and power density. The model reliability has been examined by comparing the predicted results with the experimental data from Zhao and Virkar (2005). Figure 4.4 shows the operating voltage of the SOFC predicted from the model, compared with the experimental data as a function of current densities at different operating temperatures. Table 4.2 and Table 4.3 show the values of operating parameters used for model validation.

The comparison shows good agreement with the experimental data for operating at 1073 K. When operating under lower temperatures such as 873 and 973 K, it seems to have the error between the predicted results and experiment data at lower current density. This may be caused by the model parameter errors in terms of the activation overpotentials and ohmic losses. However, the predicted cell voltage have a similar shape with the experiment data. Moreover, the coefficient of determination between simulation results and experiment data can be expressed in Figure 4.5. The result shows that the coefficient of determinations are 0.9613, 0.9912, and 0.9987 for the cell temperature as 873, 973, and 1073 K, respectively. It indicates the predicted values properly fit the experiment data.

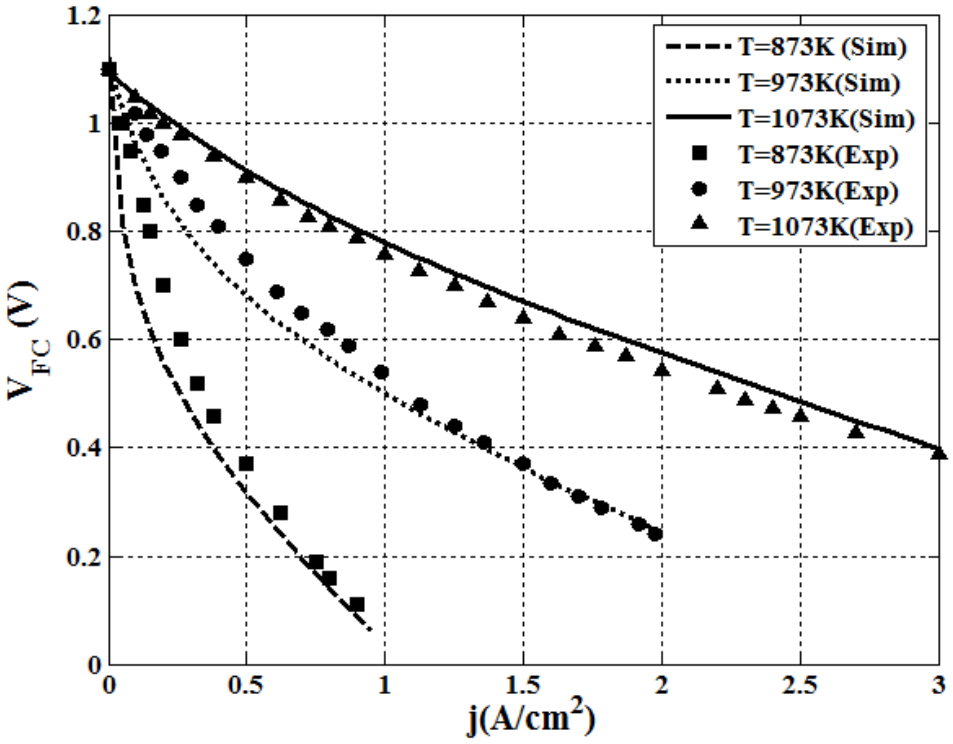

Figure 4. 4 Comparison between the model prediction and experimental data from Zhao and Virkar (2005).

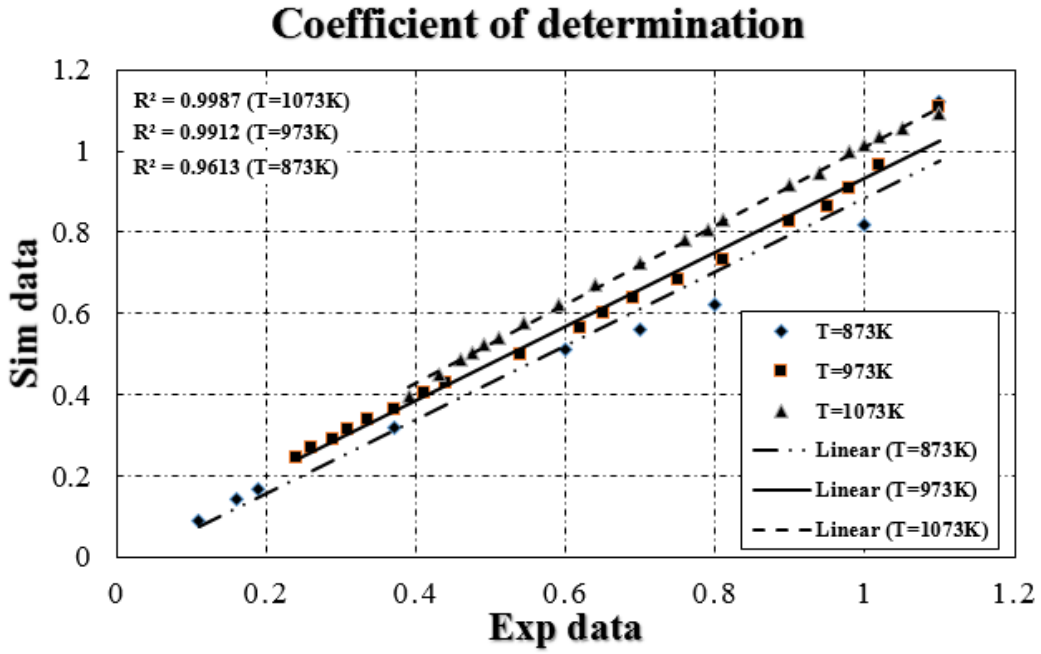

Figure 4. 5 The coefficient of determination between simulation results and experiment data.

Table 4. 2 Operating conditions for model validation (Zhao and Virkar, 2005).

Symbol	Representation	Value	Unit
P	Pressure	1	bar
T_{SOFC}	cell temperature	873, 973, 1073	K
Fuel feed		97% H_2, 3% H_2O	
Air feed		21% O_2, 79% N_2	

Table 4. 3 Structure parameters for model validation (Zhao and Virkar, 2005).

Symbol	Representation	Value	Unit
τ_{anode}	anode thickness	1000	μm
$\tau_{cathode}$	cathode thickness	20	μm
$\tau_{electrolyte}$	electrolyte thickness	8	μm
h_f	fuel channel height	1	mm
h_a	air channel height	1	mm
L	cell length	0.4	m
W	cell width	0.1	m

CHAPTER V

DESIGN AND DYNAMIC MODELING OF SOLID OXIDE FUEL CELL WITH METHANE STEAM REFORMING

This chapter presents the implementing of internal methane steam reforming for a planar solid oxide fuel cell. The operating design for SOFC is considered with the goal to select optimal operating point by using steady-state model of mass and energy balances and electrochemical model. The effect of key operating parameters on the cell temperature and cell voltage is considered by investigating the dynamic responses.

5.1 Introduction

A solid oxide fuel cell (SOFC) is regarded as the promising fuel cell technology with possibility of its use in cogeneration applications. It operates at high temperatures (typically between 1073 and 1273 K) and converts the chemical energy in the fuel directly to electrical energy by electrochemical reactions (Yamamoto, 2000). Further, SOFC can use the flexibility of various fuel types such as hydrocarbon fuels. Due to its high-temperature operation, the SOFC can internally reformed fuels to hydrogen-rich gas within a fuel cell stack. This operation is known as a direct internal reforming solid oxide fuel cell (DIR-SOFC). SOFC is not necessary to use only hydrogen as fuel that is still very difficult to produce and store hydrogen effectively and economically (Ni, 2011). In addition to hydrogen, methane that is the major component in natural gas can be used as fuel for SOFC. Ni et al. (2009) studied the performance of solid oxide fuel cells using methane as fuel with considering the direct internal methane steam reforming and water gas shift reaction. Moreover, Yang et al. (2009) investigated the methane steam reforming in planar porous support solid oxide fuel cell. The simulation result reported the reforming reaction and the distribution of hydrogen were influenced by the operating conditions such as cell temperature and steam to carbon ratio.

Many research have been studied a promising alternative to eliminate the requirement high performance materials and to prevent thermal expansion and management for high temperature SOFC. Therefore, SOFC operating at intermediate temperatures and reducing the thickness of electrolyte layer by adopting anode support structure in SOFC instead of electrolyte layer support have been investigated. The role of support structures were investigated by Patcharavorachot et al. (2008). The simulation result showed that an anode-supported SOFC was superior to an electrolyte-supported and cathode-supported SOFC under SOFC operated at intermediate temperature. The performance of an anode-supported intermediate temperature direct internal reforming planar solid oxide fuel cell was studies (Aguiar et al., 2004).

To develop the SOFC performance, a dynamic model is considered an essential tool. It is used to design for fuel cell improvement and to predict the time-dependent behavior of the SOFC system due to step changes in input variables. To date, various SOFC models have been reported, ranging from one to three dimensional models that describe the spatially distributed nature of SOFC variables and the internal complex transport processes within the SOFC. However, it is difficult to build and solve due to complex form and also spend time-consuming. To cope with these difficulties, Murshed et al. (2007) developed a control relevant model of the hybrid SOFC system using a lumped parameter modeling concept.

The purpose of this part is to analyze the performance of a planar anode-supported SOFC with direct internal reforming of methane. The optimal operating condition is selected under steady state analysis and the dynamic behavior of the SOFC is studied to investigate dynamic responses using a lumped parameter model. The effect of input variables on the cell temperature and cell voltage is investigated.

5.2 Results and discussion

5.2.1 Steady-state analysis

In order to obtain an exact solution, the electrochemical, mass and energy models are presented and solved simultaneously (Pirkandi et al., 2012). The steady state analysis is performed for the SOFC and reformer in order to select operating conditions such as the cell temperature, cell voltage, power density, and current density. This

operating condition will be the initial condition for dynamic behavior and the design of SOFC control.

The lumped parameter model of SOFC is built by relating mass and energy balances for investigating steady state and dynamic behavior.

The model parameters and cell geometry data for the SOFC are given in Table 5.1. The structure parameters, the heat capacities of all component, and the operating conditions for SOFC are presented in Tables 5.2, 5.3, and 5.4, respectively.

Table 5. 1 Kinetic and material property data for SOFC.

Symbol	Representation	Value
k_{anode}	pre-exponential factor of anode exchange current density, $\Omega^{-1}m^{-2}$	6.54×10^{11}
$k_{cathode}$	pre-exponential factor of cathode exchange current density, $\Omega^{-1}m^{-2}$	2.35×10^{11}
E_{anode}	activation energy of anode exchange current density, kJ mol^{-1}	140
$E_{cathode}$	activation energy of cathode exchange current density, kJ mol^{-1}	135
$D_{eff,anode}$	anode effective diffusivity coefficient, m^2s^{-1}	3.66×10^{-5}
$D_{eff,cathode}$	cathode effective diffusivity coefficient, m^2s^{-1}	1.37×10^{-5}
σ_{anode}	electronic conductivity of anode, $\Omega^{-1}m^{-2}$	$9.5\times10^7/T_{FC}\exp(-1150/T_{FC})$
$\sigma_{cathode}$	electronic conductivity of cathode, $\Omega^{-1}m^{-2}$	$4.2\times10^7/T_{FC}\exp(-1200/T_{FC})$
$\sigma_{electrolyte}$	ionic conductivity of electrolyte, $\Omega^{-1}m^{-2}$	$33.4\times10^3\exp(-10300/T_{FC})$

Table 5. 2 Structure parameters for SOFC.

Symbol	Representation	Value
τ_{anode}	anode thickness, μm	500
$\tau_{cathode}$	cathode thickness, μm	50
$\tau_{electrolyte}$	electrolyte thickness, μm	20
h_f	fuel channel height, mm	1
h_a	air channel height, mm	1
L	cell length, m	0.4
W	cell width, m	0.1
ρ_{SOFC}	SOFC density, kg m^{-3}	4200
Cp_{SOFC}	SOFC heat capacity, J $Kg^{-1}K^{-1}$	640

Table 5. 3 Heat capacities of each component.

Components	Cp, J $mol^{-1}K^{-1}$	Components	Cp, J $mol^{-1}K^{-1}$
CH_4	58.381	CO_2	49.561
H_2O	38.459	O_2	32.582
CO	31.374	N_2	31.394
H_2	30.236		

Table 5. 4 Operating conditions for SOFC.

Symbol	Representation	Value
P	Pressure, bar	1
T_f^0	fuel inlet temperature, K	1023
T_a^0	air inlet temperature, K	1023
U_{fuel}	fuel utilisation factor	70%
λair	air ratio	8.5
Fuel feed		S/C = 2, 10% pre-reforming
Air feed		21% O_2, 79% N_2

Figure 5.1 shows (a) the effect of the current density on the cell voltage and power density and (b) the cell temperature as a function of current density at steady state for a planar SOFC. The operating condition is desired close to the highest power production point (Georgis et al., 2011). Moreover, the cell performance will be a good compromise between cell efficiency, power density, stable operation, and so on when the cell voltage operates near 0.7 V (Aguiar et al., 2004). Therefore, the nominal steady state operating points is selected at current density, j = 0.45 A/cm^2. At this condition, it is observed that cell voltage, V_{FC} = 0.72 V, power density, P_{FC} = 0.32 W/cm^2, and cell temperature, T_{FC} = 1058 K. This is closed to the maximum power density. At this point, the SOFC is operated between 823 and 1073 K; it is called an intermediate temperature solid oxide fuel cell (IT-SOFC). The cell temperature increases with increase in the current density due to high electrochemical reactions that is exothermic reaction. However, the cell voltage depending on the cell temperature decreases rapidly at high current density due to concentration overpotentials.

5.2.1 Dynamic behavior

In this work, the model introduced in chapter 4 has been simulated using Matlab. The electrochemical model allows for the computation of the SOFC voltage, current density, and power density. The model reliability has been examined by comparing the predicted results with the experimental data from Zhao and Virkar (2005).

After we obtain the optimum operating condition on SOFC performance, it is applied as the initial condition to investigate the open-loop dynamic responses to step changes around the assumed operating point by using the nonlinear ODEs of mass and energy balances. The effects of variables are studied to investigate the responses of the cell temperature and cell voltage by changing the current density, the inlet temperatures of air and fuel, and the inlet molar flow rates of air and fuel in terms of velocity.

(a)

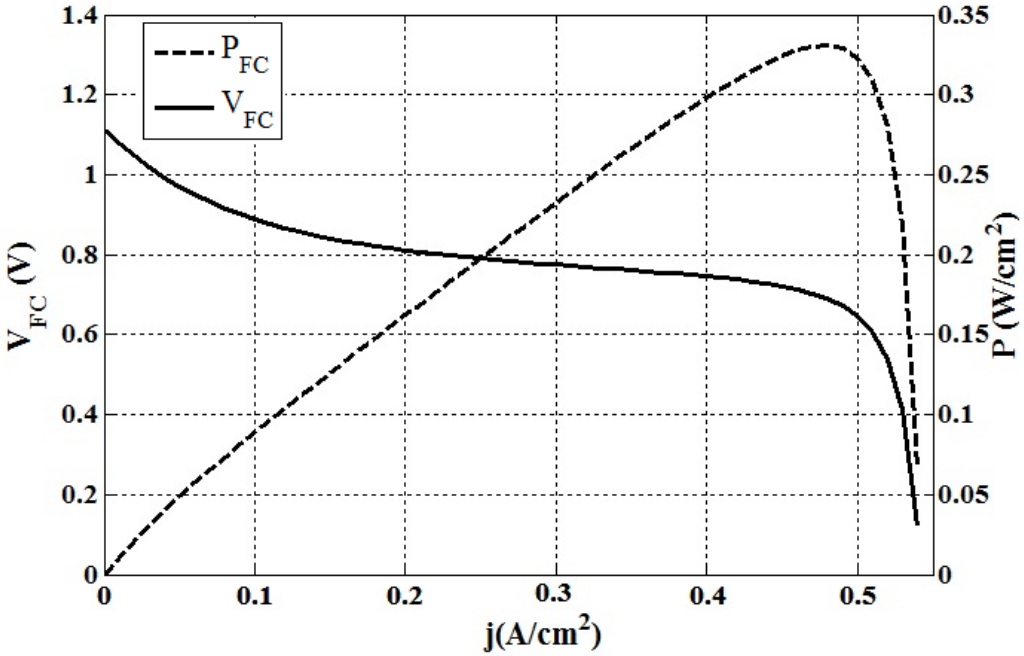

(b)

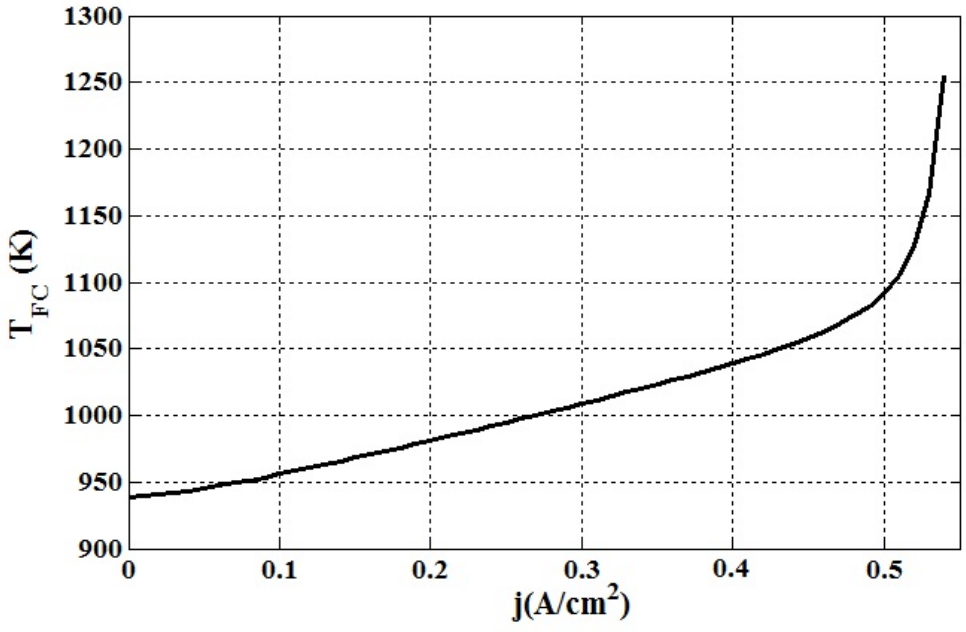

Figure 5. 1 (a) the cell voltage and power density, and (b) the cell temperature as a function of the current density at the steady-state for a planar SOFC.

The open-loop response of the fuel cell temperature and cell voltage due to step changes of ±10% in the current density is shown in Figure 5.2.

In the first period, it is the nominal operating point in the dynamic model that the cell voltage and cell temperature start from their setpoints at 0.72 V and 1058 K, respectively. The step changes of +10% in each input are presented at the second period. For the third period between 4000 and 7000 s, it shows the responses due to step changes of -10% in each input. The last period of this result is to move to the initial conditions.

As seen in Figure 5.2, the cell voltage indeed depends on the cell operating temperature which is dependent on the fuel and air inlet temperatures as well as the current density. The transient response of the cell voltage and cell temperature due to step change in current density is studied while the inlet temperatures and mole flow rates of air and fuel are maintained at the nominal values. When the SOFC is operated at the high current densities, it is observed that the cell operating temperature increases because of an instantaneous increase in hydrogen consumption in the cell. Moreover, the fuel cell voltage also sudden drops associated with the ohmic losses according to Eq. (4.24), although the increase in the cell temperature will decrease the activation overpotentials and the internal resistance in ohmic losses. The cell voltage is dependent on the magnitude of ohmic loss (Murshed et al., 2007).

The effects of the inlet temperatures of air and fuel on the both of them can be shown in Figures 5.3 and 5.4, respectively. The step changes of ±10% in the inlet temperatures of air and fuel are investigated with the different inputs kept at their nominal values. The results show that the dynamic response of fuel cell voltage and cell temperature depend on the inlet temperatures of fuel and air. The inlet temperatures of fuel and air increased cause an increase in the cell temperature and also increase in the fuel cell voltage due to the ohmic losses term decreased.

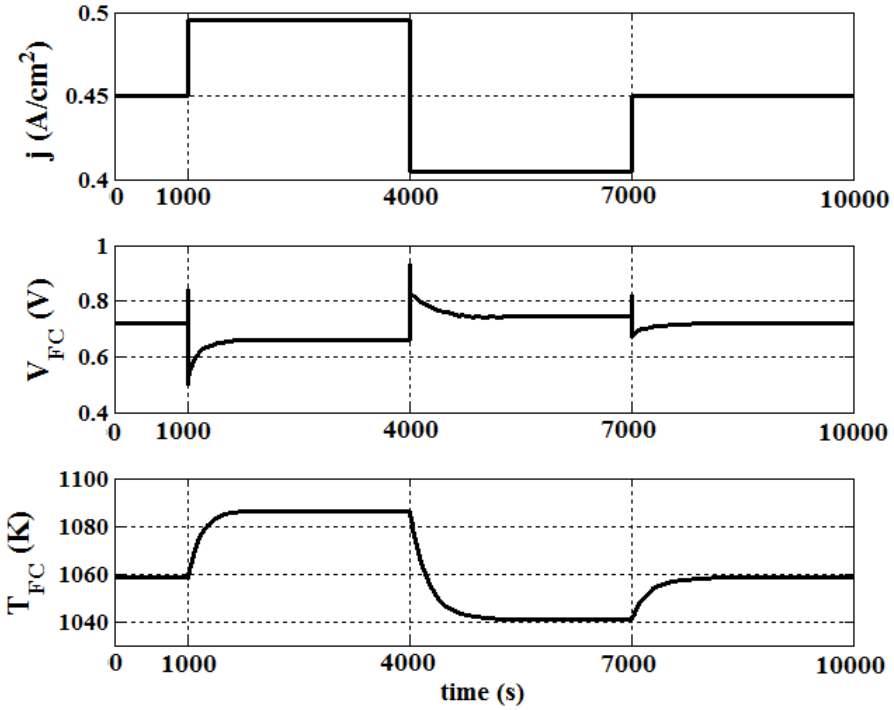

Figure 5. 2 The responses of the voltage and cell temperature due to step changes in the current density (j).

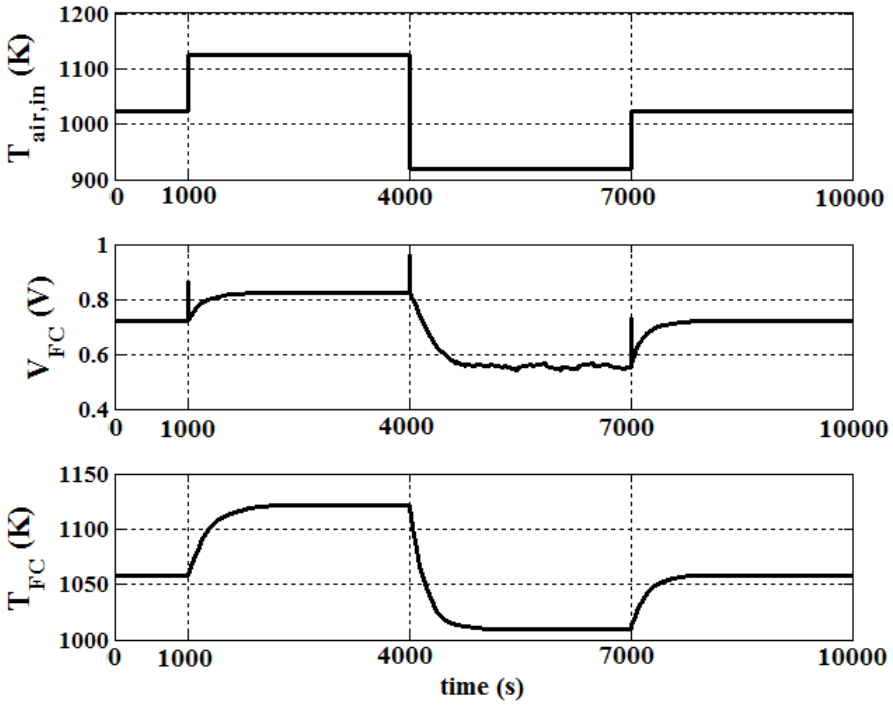

Figure 5. 3 The responses of the voltage and cell temperature due to step changes in the inlet temperature of air ($T_{air,in}$).

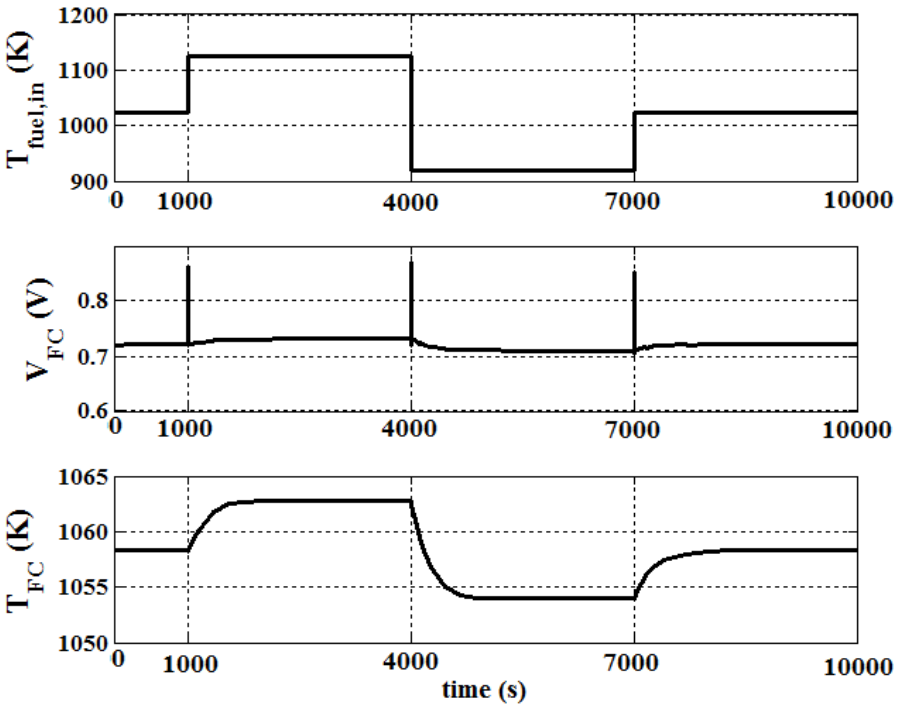

Figure 5. 4 The responses of the voltage and cell temperature due to step changes in the inlet temperature of fuel ($T_{fuel,in}$).

Furthermore, the transient responses due to the inlet molar flow rates of air and fuel in term velocity are shown in Figures 5.5 and 5.6, respectively. The inlet flow rates of air and fuel can be expressed in terms of air and fuel velocity that calculated from air ratio and fuel utilization factor, respectively. The transient responses of fuel cell voltage and cell temperature for the step changes of ±10% in the inlet flow rate of air and fuel are investigated. The inputs such as the current density and the inlet temperatures of air and fuel are kept constant. When the molar flow rates are changed, the fuel cell voltage and cell temperature changed are observed. The inlet molar flow rate of fuel increased causes an increase in hydrogen production rate associated with increase in reforming reaction rate. Because of the endothermic steam reforming reaction, heat for reformer provided by heat produced in a fuel cell results in the decrease of the cell temperature. However, the fuel cell voltage increases due to partial pressure of hydrogen increased and partial pressure of water decreased as a result of an increase in the fuel flow rate. The overshoots occurred in step changes could be described by the numerical errors, which are generated by the discontinuity in time (Chaisantikulwat et al., 2008).

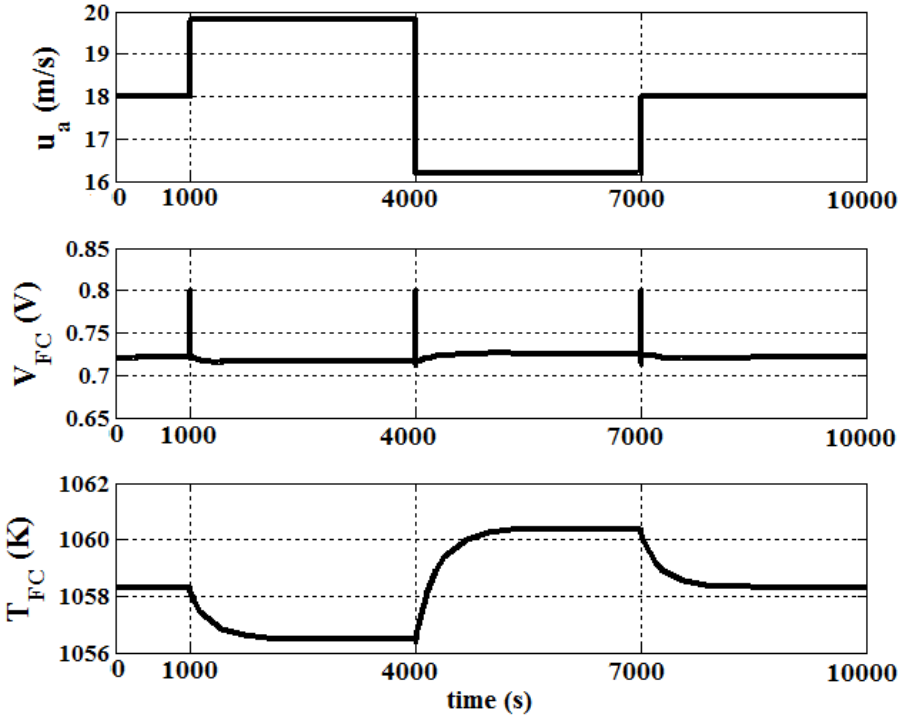

Figure 5. 5 The responses of the voltage and cell temperature due to step changes in the molar flow rate of air in term velocity (u_a).

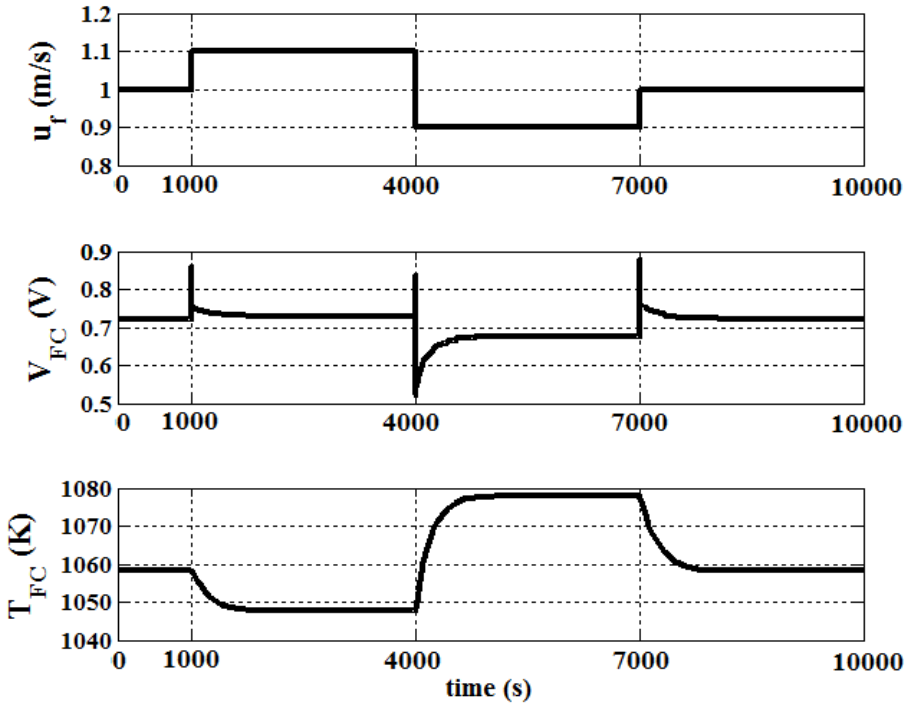

Figure 5. 6 The responses of the voltage and cell temperature due to step changes in the molar flow rate of fuel in term velocity (u_f).

5.3 Conclusions

In this study, the steady state analysis was analyzed to design the optimal operating condition for a planar solid oxide fuel cell. The results showed the optimal point was selected near maximum power density and voltage was equal to 0.72 V. The dynamic behavior of the cell voltage and cell temperature were considered by changing the input parameters. The simulation results indicated that the fuel cell temperature increases at high current densities because of the increased hydrogen consumption, leading to high exothermic reaction. However, the voltage drops immediately when the current density increases because of the concentration losses due to the insufficiency of hydrogen at the reaction sites. When the inlet temperature of air and fuel are increased, the cell temperature also increases leading to the gain of cell voltage due to decreasing of the internal resistance. Moreover, the cell voltage and cell temperature also depended on the inlet molar flow rate of air and fuel.

CHAPTER VI

CONTROL STRUCTURE DESIGN FOR A SOLID OXIDE FUEL CELL

This chapter focuses on the implementing of control structure design and controllability analysis for SOFC to design a good control system. A procedure for select an active constraint and a self-optimizing variables is presented. Moreover, the relative gain array (RGA) considered as a controllability index for the selection of input-output pairings is also implemented.

6.1 Introduction

Due to the direct internal reforming of solid oxide fuel cell, a temperature gradient due to the endothermic cooling effect in the fuel cell stack, especially at the cell inlet may be occurred. In addition, the coupling of the reforming and electrochemical reactions results in a complicated dynamic response that requires an efficient control system.

In recent years, SOFC has received much attention on its operation and design, but less focus has been given to the control study, including control structure design, controllability analysis, and the design and tuning of the controllers. Controllability analysis can offer insights for identifying the inherent properties of a process and how they limit control performance (Skogestad and Postlethwaite, 1996). Morari (1983) has reported that controllability is an inherent property of the process itself and should be considered at the design stage before the control system design is fixed. The comparison and selection of different control structures and the validation of the controlled system were studied for the controllability analysis of decentralized linear controllers (García et al., 2010, Serra et al., 2005). In addition, a controllability analysis is generally applied for selection of the best controlled and manipulated variable pairing within one process and evaluation of control properties for two or more process alternatives (Skogestad and Postlethwaite, 1996). Therefore, the theory of controllability analysis is interesting and challenging for SOFC.

The selection of manipulated variables, controlled variables, control configuration, and controller type and what to control and how to pair the variables to form control loops were described by Skogestad and Postlethwaite (1996) to achieve an effective control system. The proposed structures were tested to verify their performance. The self-optimizing control is implemented to select the good controlled variable which can be kept constant at setpoints without the need to reoptimize when disturbance occur. Moreover, the understanding of steady-state and dynamic behavior is an essential necessity for the nonlinear control system design (See detail in Chapter 5). Simple and accurate SOFC dynamic model is very important for optimizing the system as well as for developing control strategies (Kang et al., 2009). Compared with a very detailed model of SOFC, the developed SOFC model can captures the dynamics of the SOFC and thus the lumped parameter model can be used to design a control structure.

The purpose of this chapter is to study the control structure design and controllability analysis of an SOFC with direct internal reforming of methane. The control structure of the SOFC is determined and its controllability property is investigated by considering a relative gain array (RGA). The self-optimizing control concept is investigated and implemented to select economic controlled variables for SOFC.

6.2 Control structure design for SOFC

The most important control structure decision is usually to identify good controlled variables (CVs). The first is to find the active constraints at optimal operation, which should be controlled to operate the plant optimally. We here follow the stepwise procedure of Skogestad (2004). A process flow diagram of the direct internal solid oxide fuel cell is illustrated in the Figure 6.1. The goal is to control cell temperature to its desired value.

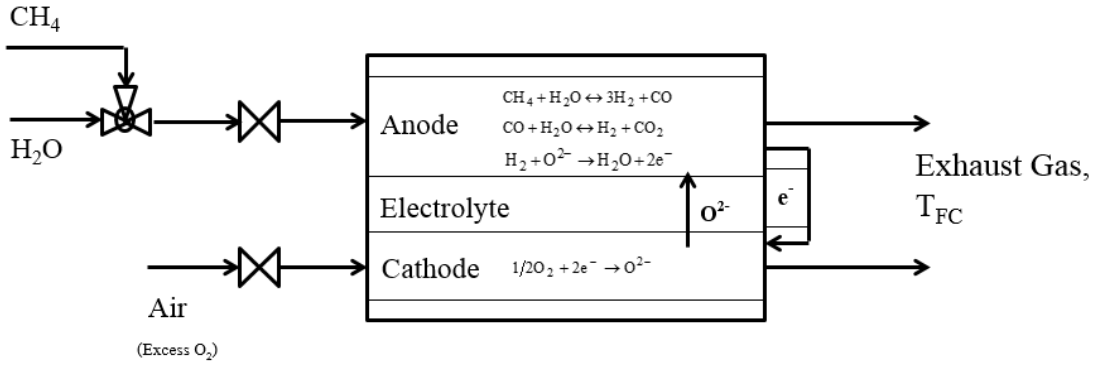

Figure 6. 1 Process flow diagram of the direct internal solid oxide fuel cell.

Step 1: Define cost function J and constraints.

With a given load (current density), the cost function *J* to be minimized is the cost of the fuel feed minus the value of the power, subject to satisfying constraints on the cell temperature kept at 1058 K (active constraint).

The objective function is defined as:

Cost = Steam price * total steam supply - Product price * total product

Step 2: Identify optimal operation as a function of disturbances.

At steady-state, there are two operational degrees of freedom (DOFs); the molar flow rates of air and fuel, MVs = [$\dot{n}_{air}^{in}$, $\dot{n}_{fuel}^{in}$]. The current density (*j*) is the main disturbance, and it is also the throughput manipulator (TPM) for the system. We have optimized the system in detail and found that the fuel cell temperature constraint of T_{FC} = 1058 K is always active. There is then one remaining unconstrained degree of freedom, which is related to the excess of air.

Step 3: Identify economic CVs.

The self-optimizing control idea is used to select the economic CVs. Self-optimizing control is achieved when an acceptable loss *L* result is achieved with a constant setpoint values for the controlled variables, without the need to reoptimize when disturbances occur (Skogestad, 2004). The loss *L* is defined for a given disturbance as the difference between the actual value of the cost function ($J(d)$) and the optimal value ($J_{opt}(d)$),

$$\text{Loss } L = J(d) - J_{opt}(d) \tag{6.1}$$

Table 6.1 shows the four disturbance variables used in this study. For selecting economic CVs, the fraction of methane (x_{CH4}) and hydrogen (x_{H2}) is considered. To find the loss, the candidate CV is kept constant when a process is disturbed by the disturbances. The fraction of methane and hydrogen need to kept constant at 0.0226 and 0.088, respectively. The loss results are shown in Table 6.2. The loss with constant x_{CH4} is acceptable, and it is found that x_{CH4} is a better self-optimizing controlled variable than x_{H2} when disturbances move away from their nominal operating points.

Table 6. 1 Disturbances to select economic CVs.

Disturbances		Nominal	Expected variation
d_1	current density	0.45 A/cm^2	± 10%
d_2	inlet temperature of fuel	1023 K	± 30 K
d_3	inlet temperature of air	1023 K	± 30 K
d_4	cell temperature	1058 K	+ 30 K

Table 6. 2 Evaluation of loss.

Disturbances				Optimal	Loss using	Loss using
d_1	d_2	d_3	d_4	Cost	constant x_{CH4}	constant x_{H2}
0.45	1023	1023	1058	-0.0832		
+10%	1023	1023	1058	-0.0873	0.0002	0.0028
-10%	1023	1023	1058	-0.0640	0.0014	0.0052
0.45	+30K	1023	1058	-0.0732	0.0000	0.0016
0.45	-30K	1023	1058	-0.0849	0.0000	0.0125
0.45	1023	+30K	1058	-0.0818	0.0009	0.0036
0.45	1023	-30K	1058	-0.0833	0.0040	0.0073
0.45	1023	1023	+30K	-0.0749	0.0017	0.0088

In summary, we select CV = [T_{FC}, x_{CH4}]. The first CV is the active constraint which is the optimally constrained variable and should be controlled at its setpoint. As a "self-optimizing" variable for the unconstrained degree of freedom, we select the fraction of unconverted methane in the exhaust gas (x_{CH4}) which was found to result in a small economic loss.

Step 4: Select the throughput manipulator.

As already mentioned, it is the current density.

Step 5: Structure of stabilizing control layer.

An important decision is to select the "stabilizing" controlled variables CV2, including inventories and other drifting variables that need to be controlled on a fast time scale. In this case, one need to control the temperature tightly to avoid material stresses and other needs to prevent cell voltage drop due to depletion of fuel. Fortunately, in this case the economic controlled variables (CV1) are also acceptable as stabilizing variables (CV2 = CV1), so a separate regulatory layer is not needed.

Step 6: Select structure for control of CV1.

This is the pairing issue which is discussed in Section 6.3 on "controllability analysis".

6.3 Controllability analysis for SOFC

The controllability analysis that computes zeros, poles, and relative gain array requires a linear dynamic model. The measurements of open-loop right half plane (RHP) zeros and poles are independent of the controller and the control configuration and thus reflect the controllability of the plant. The RHP-zeros and poles are also considered due to its presence limiting on the achievable control performance (Havre and Skogestad, 1998). Unstable (RHP) zeros may result in serious control problems and affect the achievable transient performances of feedback loops. The closed-loop poles can change to unstable if the open-loop zeros are lying in RHP. When a system has one pole lying in the right half plane, it also means an unstable system. The system will move away from the steady state in open-loop instability system. Figure 6.2 shows the open-loop poles and zeros location in the complex plane the dynamic system; all the zeros are in LHP. Small stable zeros with stable poles show that a very large amount of overshoot will be predicted. Small stable poles show a small amount of overshoot may be predicted. The unstable zeros and poles do not appear here and thus, the open-loop RHP zeros and poles may not affect the closed loop performance.

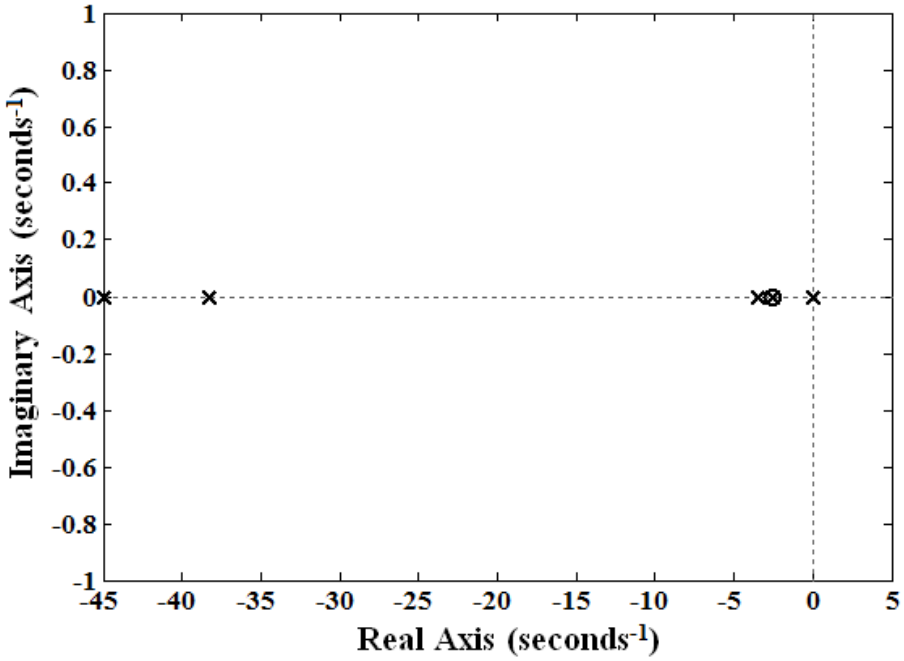

Figure 6. 2 Pole and Zero location for the dynamic model of SOFC.

The controllability of a process is the ability to achieve acceptable control performance; that is, to preserve the outputs with in specified bounds. It offers a numerical indication of the sensitivity balance to provide a qualitative assessment of the control properties of the alternative designs. To perform the controllability analysis of the SOFC, we consider the lumped parameter models with two inputs: the inlet molar flow rates of air (u_1) and fuel (u_2). The fuel cell temperature (y_1) and the fraction of methane (y_2) are selected as outputs. Next, the relative gain array (RGA) is considered a controllability index for the selection of input-output pairings and to describe the interactions among inputs and outputs. Generally, a RGA matrix close to the unity matrix is preferred and in particular control structures with high RGA elements should be avoided. The RGA of a non-singular square complex matrix (G) is defined as indicated in Eq. (6.2), where x denotes element by element multiplication (the Hadamard or Schur product).

$$\mathrm{RGA}(G) = \Lambda(G) = G \times \left(G^{-1}\right)^{T} \tag{6.2}$$

The selection of the controlled and manipulated variables for the investigated system is analyzed at the control structure design part. According to the RGA, the steady-state RGA is 1.94 for the diagonal pairings (u_1-y_1, u_2-y_2), which is close to 1 as

desired. This pairing is also reasonable from a dynamic point of view because the molar flow rate of fuel at inlet (u_2) has a direct effect on the fraction of methane (y_2). Moreover, the RGA at zero frequency for different cases are shown in Table 6.3. The 10% input increases while the other inputs are kept at the nominal point. The results show that the pairing choice is accepted by RGA_{11}. In all the case studies, the inlet molar flow rates of air and fuel are used as manipulated variable to control the cell temperature and the concentration of fuel, respectively.

Table 6. 3 Controllability index RGA at zero frequency (ω=0 rad/s) for different cases.

Case	ΔIncrement	RGA_{11}= RGA_{22}	RGA_{12}= RGA_{21}
1	Nominal Operation	1.94	-0.94
2	+10% u_f	1.92	-0.92
3	+10% u_a	1.87	-0.87
4	+10% T_f^0	1.89	-0.89
5	+10% T_a^0	2.02	-1.02
6	+10% j	1.94	-0.94

At steady state, the controllability analysis is completed with the investigation at different cases and the good control structure is identified as u_1-y_1, u_2-y_2. The frequency range from 10^{-3} to 10^{1} rad/s is considered. Figure 6.3 shows the result for RGA_{11} of difference cases during a wide frequency range. It can be observed that the pairing between u_1-y_1, u_2-y_2 is also suitable for all case.

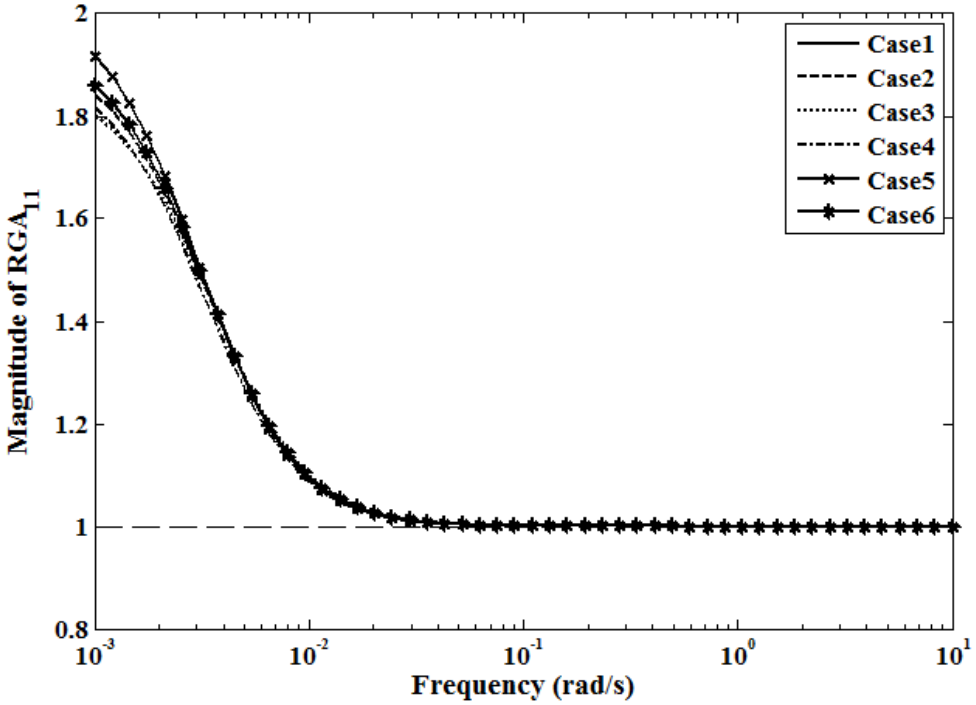

Figure 6. 3 Relative gain array (RGA_{11}) of SOFC for different cases in the frequency range of 10^{-3} to 10^{1} rad/s.

6.4 Conclusions

This work focused on a control structure design and controllability analysis of SOFC operated under a direct internal reforming of methane. The lumped-model represented zero dimensional nonlinear ODEs was implemented for dynamic and control design. The control structure design was implemented to identify good controlled variable. We found the cell temperature was the active constraints that should be controlled at its setpoint. Moreover, the fraction of unconverted methane was a good CV for the remaining unconstrained variable by the self-optimizing concept. The controllability analysis based on RGA at zero frequency was performed to pairing between manipulated variables and controlled variables. The result showed the inlet molar flow rates of air and fuel were manipulated variables to control the cell temperature and the unreacted fraction of methane, respectively. Moreover, the open-loop zeros and poles were calculated to investigate RHP zeros and poles.

CHAPTER VII

CONTROL OF THE INTERNAL REFORMING SOLID OXIDE FUEL CELL

As mentioned above, the dynamic behavior is implemented to describe their response by lumped-parameter model and the control structure design can define the good controlled variables with their manipulated variables. Therefore, it is interesting to implement controller to the process. This chapter presents the controller design for control the internal reforming solid oxide fuel cell. Control studies on the conventional PID controller strategy are investigated. The simulation result of the PID controllers is discussed.

7.1 Introduction

Recently, the several works have been concentrated on the dynamic models for process control of solid oxide fuel cell. In the work (Li et al., 2005), a dynamic model was derived and a control of a SOFC power was studied by implementing proportional-integral (PI) controller to maintain fuel utilization and voltage when the stack current changes. Whereas a SOFC dynamic model and a feedback control scheme can maintain output voltage despite load changes and the SOFC output voltage controlled by implementing a PI controller (Chaisantikulwat et al., 2008). A PID controller was implemented to maintain the outlet fuel temperature and the fuel utilization during load changes (Aguiar et al., 2004). Stiller et al. (2006) has developed a dynamic model for control of a SOFC and gas turbine hybrid system. The proportional–integral–derivative (PID) type controller was used for controlling the SOFC power, fuel utilization, air flow, and cell temperature.

In this work, we concentrate on the implementing of the PID controller for the internal reforming solid oxide fuel cell. Performance of the SOFC control using a conventional control methodology with the designed control structure is studied.

7.2 PID controller strategy

The most popular type of feedback stabilization control is Proportional-Integral-Derivative gain feedback. A proportional-integral-derivative controller (PID controller) is a control loop controller widely used in industrial control systems and is very effective and easy to implement. The PID controller calculates an error value between a measured variable (output variable) and a desired setpoint value. The controller attempts to minimize the error by adjusting a manipulated variable. The proportional depends on the present error, the integral involves the accumulation of past error, and the derivative is a prediction of future error. The PID controller is used to adjust the process via a final control element.

By tuning the three parameters in the PID controller algorithm, the controller can provide control action designed for specific process requirements. The response of the controller can be described in terms of the responsiveness of the controller to an error, the degree to which the controller overshoot the setpoint, and the degree of system oscillation.

The PID control scheme is to calculate the manipulated variable (MV). The proportional, integral, and derivative terms are summed to calculate the output of the PID controller, $u(t)$. The final form of the PID algorithm can be expressed as:

$$u(t) = u_0 + K_c\left(e(t) + \frac{1}{\tau_I}\int_0^t e(\tau)d\tau + \tau_D \frac{de}{dt} \right) \tag{7.1}$$

where

K_c is proportional gain

τ_I is integral gain

τ_D is derivative gain

e is error (setpoint value - measured value)

t is time

τ is variable of integration

The result of a high proportional gain shows a large change in the output for a given change in the error. If the proportional gain is too high, the system can become unstable. In contrast, if the proportional gain is too low, the control action may be too small when responding to system disturbances.

The integral term accelerates the movement of the process towards setpoint and eliminates the residual steady-state error that occurs with a pure proportional controller. However, since the integral term responds to accumulated errors from the past, it can cause the present value to overshoot the setpoint value.

A derivative action predicts system behavior and thus improves settling time and stability of the system. Derivative control action produces more robust behavior by the controlled processes. The implementation of PID controllers includes an additional low pass filtering to limit the high frequency gain and noise. Derivative action is occasionally used in practice though by one estimate in only 20% of deployed controllers because of its variable impact on system stability in real-world applications (Ang et al., 2005).

To obtain PID-tuning gains, there has been many works concentrated on Ziegler–Nichols method (Ziegler and Nichols, 1942) and Internal Model Control (IMC) PID-tuning rule (Rivera et al., 1986). The result for first method showed a very good disturbance response for integrating processes, but it was poor performance for processes with a dominant delay. For second method, it was found that a disturbance response was poor for integrating processes but was robust and gave very good responses for setpoint changes. Therefore, in this study, the SIMC (Skogestad IMC) PID tuning rules are implemented because they are simple and easy to memorize and work well on a wide range of processes (Skogestad, 2003). The second-order time delay model for PID –control can be expressed in form *g(s)*:

$$g(s) = \frac{k}{(\tau_1 s + 1)(\tau_2 + 1)} e^{-\theta s} \tag{7.2}$$

where k denotes the plant gain ($k=\Delta y(\infty)/\Delta u$), τ_1 denotes the time constant, τ_2 denotes the second-order lag time constant and θ denotes the time delay without output changes.

The SIMC PID tuning rules for the second-order time delay process in Eq. (7.2) are defined as:

$$K_c = \frac{1}{k}\frac{\tau_1}{\tau_c + \theta} \tag{7.3}$$

$$\tau_I = \min\{\tau_1, 4(\tau_c + \theta)\} \tag{7.4}$$

$$\tau_D = \tau_2 \tag{7.5}$$

where τ_c is the closed-loop response time constant and $\tau_2 > \theta$ for dominant second-order process. The selection of tuning parameter, τ_c, is determined between tight control that wants the fastest possible control with good robustness and smooth control that requires slowest possible control with acceptable disturbance rejection. This work focuses on the tight control of active constraints; therefore, the SIMC rule for fast response is expressed as $\tau_c = \theta$.

7.3 Results and discussion

The control structure with two feedback loops for solid oxide fuel cell is shown in Figure 7.1. Two proportional integral derivative controllers (PID controller) were implemented with controller parameters obtained using the SIMC method (Skogestad, 2003). According to control structure design, the inlet molar flow rates of air and fuel are used as manipulated variables to control the fuel cell temperature and the fraction of methane, respectively. To control cell temperature by using the flow rate of air, in this case the process gain Kc is negative (direct-acting control), if the cell temperature increases, the air flow rate must be increased to maintain the desired temperature. On the other hand, if the fraction of methane increases, the fuel flow rate must be decreased to maintain the desired value. This is called reverse-acting control (Kc>0).

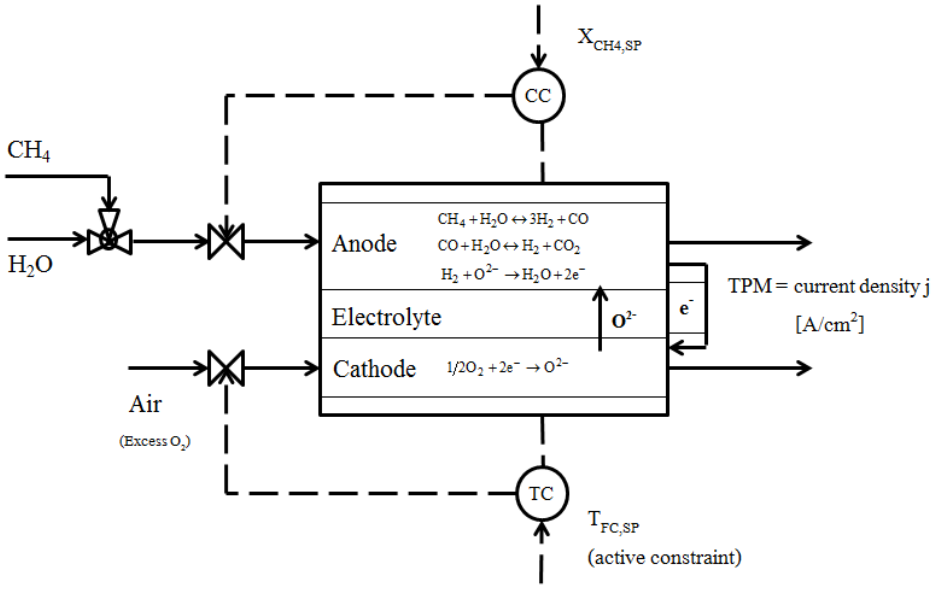

Figure 7. 1 Process flowsheet with control loops for SOFC.

In this study, the current density is the disturbance which effects on the SOFC. The controller design is carried out on the dynamic models of the SOFC. The first PID controller is implemented to control the cell temperature by using the inlet molar flow rate of air as manipulated variable. Moreover, the fraction of methane is controlled by manipulating the inlet molar flow rate of fuel using another PID controller. The step changes in the current density at 100s is simulated. The SIMC tuning technique is implemented and the controller gains are showed in Table 7.1.

Table 7. 1 The controller parameter for controlling the cell temperature and fraction of methane.

Controller tuning parameter	Cell temperature	Fraction of methane
Controller gain, *Kc*	5	1
Integral time, τ_I	4	8
Derivative time, τ_D	1	0.1

Figure 7.2 shows closed-loop responses for two controlled variables when the current density (disturbance) changes from 0.45 A/cm^2 to 0.47 A/cm^2 and 0.43 A/cm^2. The response of cell voltage due to step changes in the current density can be shown in Figure 7.3.

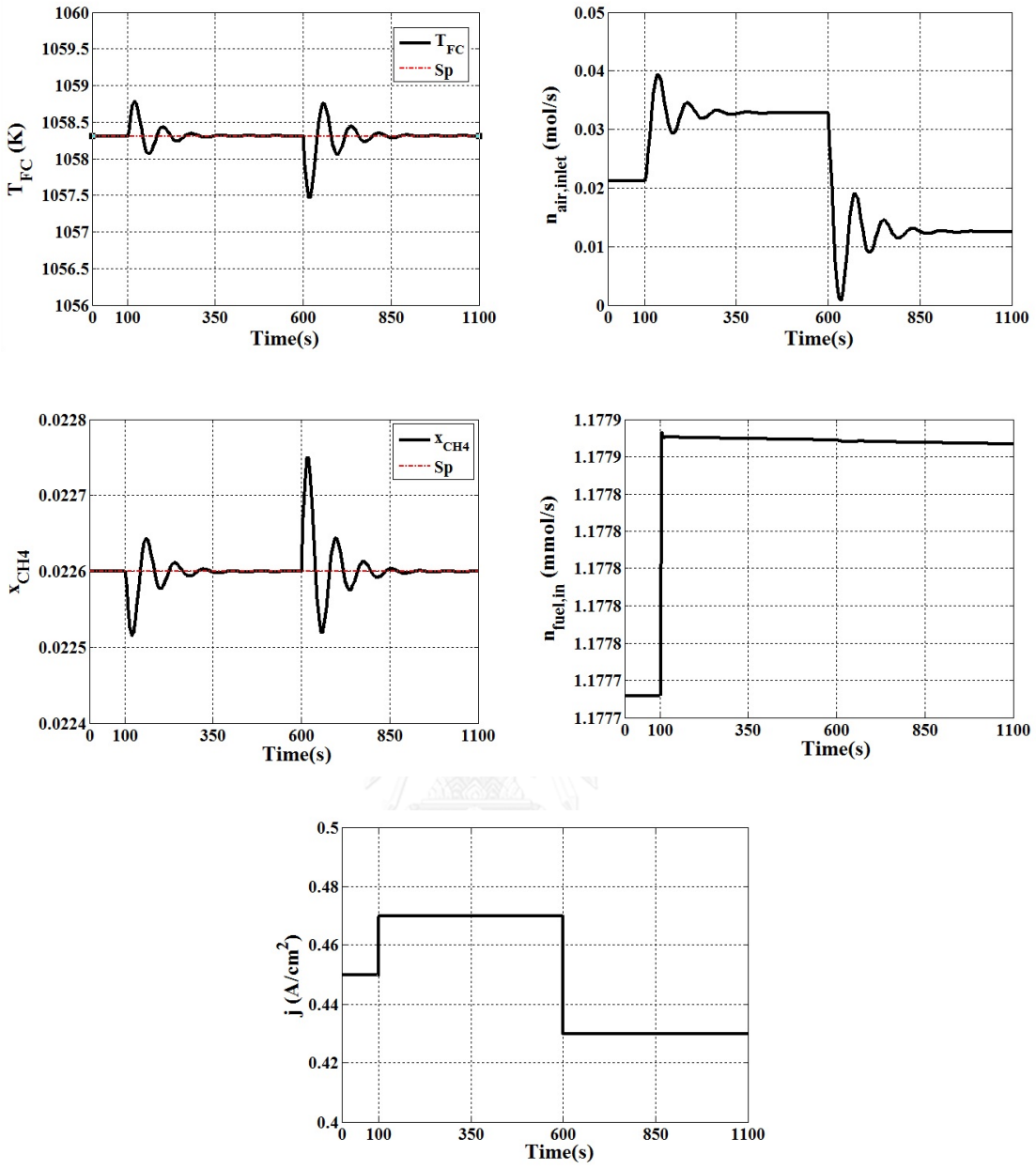

Figure 7. 2 Closed-loop responses of the cell temperature and fraction of methane due to step changes in the current density.

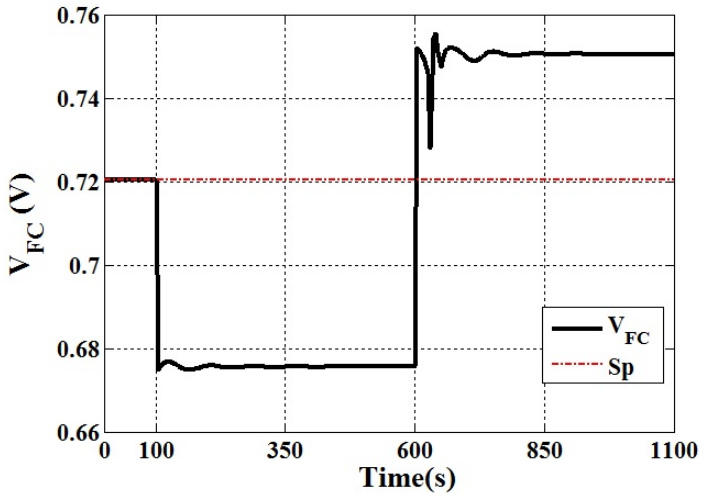

Figure 7. 3 The response of cell voltage due to step changes in the current density.

After the current density is changed at 100s, the cell temperature increases and the fraction of methane decreases due to the increased amount of hydrogen reacted in the fuel cell. The two PID controllers successfully maintain the cell temperature and fraction of methane to their desired setpoint. On the other hand, the cell voltage immediately drops due to the ohmic losses and fuel starvation. The controller performance of the two PID controller in term the IAE values is shown in Table 7.2. It observes that the IAE value for the PID controller of the fraction of methane is very small.

Table 7. 2 The controller performance in term the IAE values from controlling the cell temperature and the fraction of methane.

Variables	IAE
Cell temperature	14.6317
Fraction of methane	3.3131×10^{-6}
Cell voltage	7.5535

According to the operational objective, the cost function *J* to be minimized involves cost. Therefore, the fraction of methane is selected as economic controlled variable. However, it is importance for the SOFC to maintain the cell voltage to its setpoint value. Then, the cell voltage is selected as controlled variable replaces the fraction of methane by the inlet molar flow rate of fuel. The controller parameter tuning used in the fraction of methane is implemented for controlling the cell voltage. Figure 7.4 shows closed-loop responses for the cell temperature and the cell voltage when the current density (disturbance) changes from 0.45 A/cm^2 to 0.47 A/cm^2 and 0.43 A/cm^2. The response of fraction of methane due to step changes in the current density can be shown in Figure 7.5. The simulation results show the cell temperature and cell voltage can back to their setpoints by manipulating the inlet molar flow rate of air and fuel, respectively. When the step increases in the current density is applied, hydrogen reacted in the fuel cell increases. Therefore, the hydrogen production rate is increased by supplying more fuel in the fuel cell to avoid the fuel starvation.

The controller performance of the two PID controller in term the IAE value is shown in Table 7.3. It observes that the IAE values in Table 7.3 for all variables is better than the IAE values in Table 7.2.

Table 7. 3 The controller performance in term the IAE values from controlling the cell temperature and the cell voltage.

Variables	IAE
Cell temperature	7.7823
Fraction of methane	0.2917
Cell voltage	0.3669

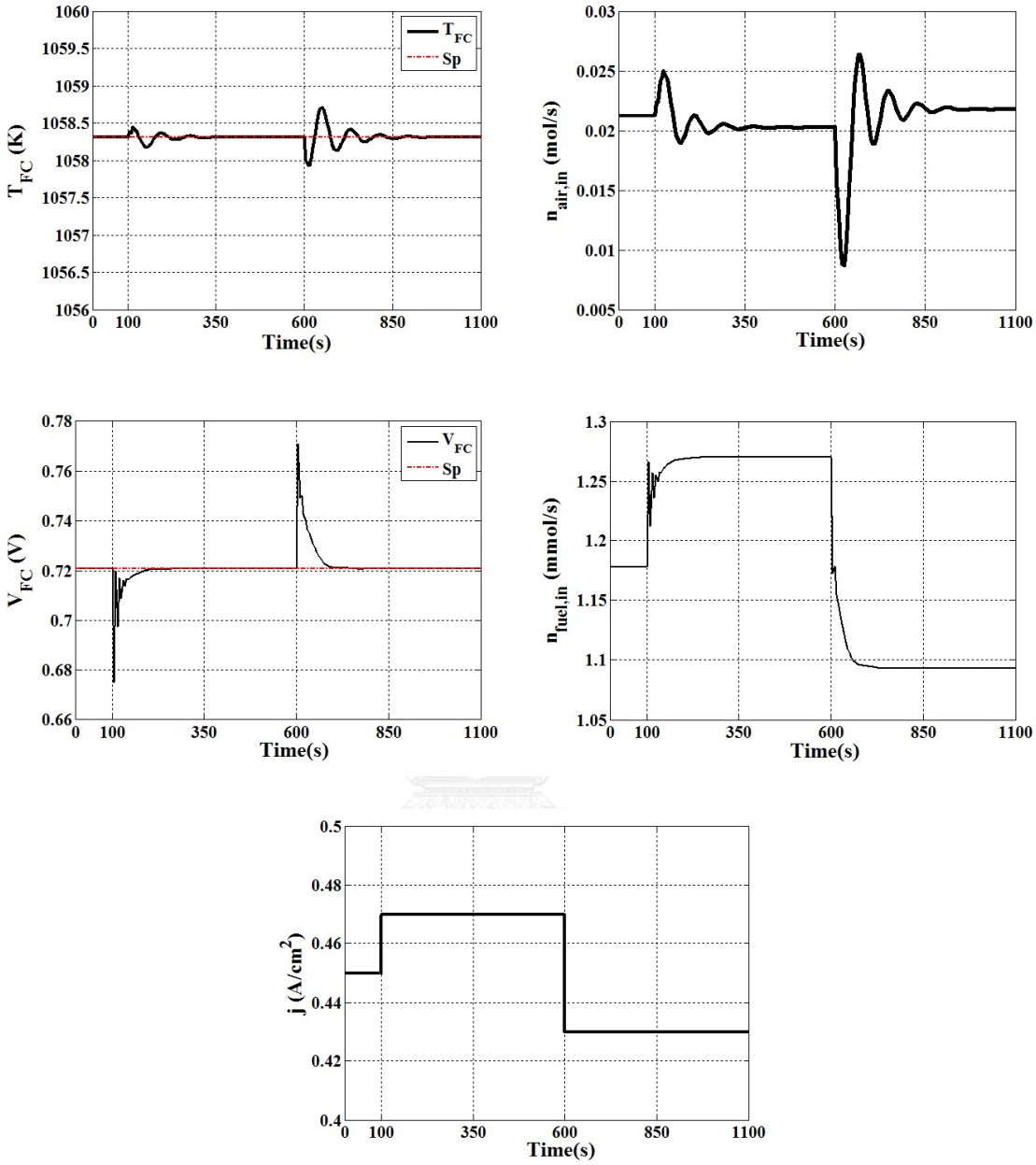

Figure 7. 4 Closed-loop responses of the cell temperature and cell voltage due to step changes in the current density.

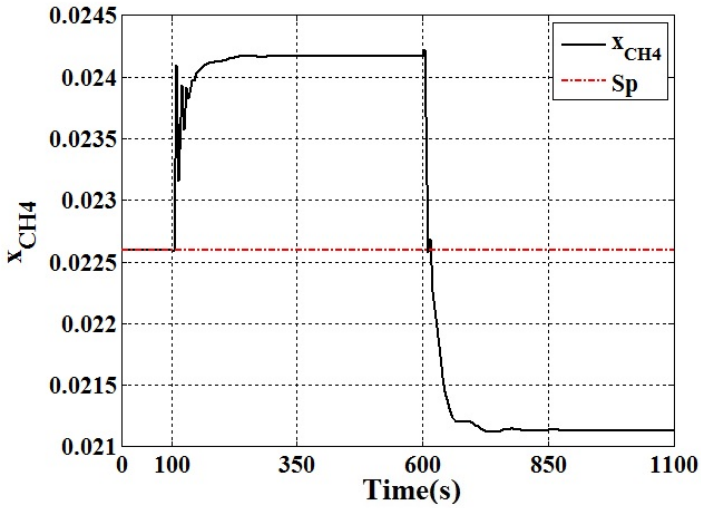

Figure 7. 5 The response of fraction of methane due to step changes in the current density.

7.4 Conclusions

In this chapter, we concentrated on the implementing of the two PID controller for the internal reforming solid oxide fuel cell. Performance of the SOFC control using a conventional control methodology with the designed control structure was studied. The cell temperature and the fraction of methane were controlled by manipulating the inlet molar flow rate of air and fuel, respectively. The controller parameter tunings were obtained by using the SIMC (Skogestad IMC) PID tuning rule. The simulation result showed the PID controllers successfully control two controlled variable to their setpoints. However, the cell voltage was needed to maintain constant. Therefore, the cell voltage was controlled by using the same controller tuning parameter. The result showed good control performances by investigating the IAE value. However, the use of the PID controller algorithm for controlled variables under a large step increases in the current density cannot guarantee optimal control of the system.

CHAPTER VIII

AN OFF-LINE ROBUST MODEL PREDICTIVE CONTROL ALGORITHM FOR THE INTERNAL REFORMING SOFC

This chapter describes the implementation of an off-line robust model predictive control algorithm based on uncertain polytopic approach using linear time-varying (LTV) and linear parameter varying (LPV) systems for controlling the internal reforming SOFC. The state feedback control law is defined to synthesis the robust MPC algorithm and are implemented to the process.

8.1 Introduction

Among many advanced control techniques, a model predictive control (MPC) technique is one of the most studied control algorithm. MPC is an effective control algorithm for dealing with multivariable constrained control problems. The overall objectives of an MPC controller have been summarized (Qin and Badgwell, 2003) such as to prevent violations of input and output constraints, to drive some output variables to their optimal set points, while maintaining other outputs within specified ranges. MPC can be designed to guarantee its stability, independence of the controlled plant. The MPC controller was implemented to prevent oxidant starvation of fuel in the fuel cell process due to load changes or decoupling the desired load from the effective load (Danzer et al., 2009). Moreover, the nonlinear model predictive control (NMPC) was studied and implemented by using the unscented Kalman filter to utilize estimated states for the solid oxide fuel cell system (Murshed et al., 2010). The linear MPC can stabilize the system for a small load change. It cannot control the system for higher load disturbances.

According to a model-based control, it is difficulty for MPC to handle with an uncertain plant model. There are many real chemical processes which are rigorously nonlinear model and uncertain. The control technique base on MPC is incompetence to deal with the plant model uncertainly (Kothare et al., 1996). As a result, the several

works focus on the development of MPC technique called robust MPC to handle nonlinear systems and the problem of robust stability.

Linear matrix inequalities (LMIs) involved the convex optimization problem is used to solve the problem of minimizing objective function. This approach can guarantee robust stability. Moreover, an algorithm of robust MPC for uncertain polytopic discrete-time systems is studied and implemented the state feedback control law to the process (Bumroongsri and Kheawhom, 2012). Robust model predictive control (RMPC) algorithm is presented to stabilize any linear time-varying (LTV) system (Pannocchia, 2004). Recently, the controller synthesis based on a linear parameter varying (LPV) system has been received considerable attention (Bumroongsri and Kheawhom, 2012). Casavola et al. (2012) proposed the MPC for feedback regulation problems. The LPV model was used to explain a nonlinear plant in the MPC algorithm. According to an on-line synthesis approach, the resulting on-line computation will grow significantly when MPC incorporates model uncertainty. With the off-line approach, the computation of robust MPC is reduced significantly with minor loss in performance. Therefore, the off-line computational is implemented for the robust model predictive control.

Because the SOFC model involves many uncertain parameters, the control design should sustain this model uncertainty. The performance of the developed MPC based on LPV and LTV models was compared.

The aim of this study is to develop the robust constrained MPC with a state feedback control law for the direct internal reforming SOFC. Uncertain polytopic discrete-time linear time varying (LTV) and linear parameter varying (LPV) models are employed to explain the SOFC behavior and to design the MPC control. Performance of the MPC based on the two different linear models are investigated and compared.

8.2 Robust MPC Algorithm for LTV and LPV systems

8.2.1 Model Description

For a Linear Time Varying (LTV) system

To synthesize a robust controller, a linear time-varying (LTV) system is defined for multi-model paradigm or polytopic uncertainty.

$$x(k+1) = A(k)x(k) + B(k)u(k) \tag{8.1}$$

$$y(k) = Cx(k)$$

$$\left[A(k) \quad B(k)\right] \in \Omega$$

where *x(k)* is the state of the plant, *u(k)* is the control input and *y(k)* is the plant output. Furthermore, we define that the set Ω is the polytope for polytopic systems.

$$\Omega = \mathrm{Co}\{[A_1 \quad B_1], [A_2 \quad B_2], ..., [A_L \quad B_L]\} \tag{8.2}$$

where Co represents the convex hull and [A_i B_i] are vertices in the convex hull. λ is the uncertain parameter vector (for some nonnegative summing of λ to one).If the system is the nominal linear time-invariant (LTI) model, it shows that L=1.

For other cases, [*A(k) B(k)*]$\in\Omega$ defined by L vertices, we have

$$\left[A(k) \quad B(k)\right] = \sum_{i=1}^{L} \lambda_i [A_i \quad B_i] \tag{8.3}$$

$$\sum_{i=1}^{L} \lambda_i = 1, \qquad 0 \le \lambda_i \le 1$$

For a Linear Parameter Varying (LPV) system

Consider the discrete-time polytopic linear parameter varying system

$$x(k+1) = A(p(k))x(k) + B(p(k))u(k) \tag{8.4}$$

$$y(k) = Cx(k)$$

$$\left[A(p(k)) \quad B(p(k))\right] \in \Omega$$

The scheduling parameter $p(k)$ is measurable on-line at each sampling time k. Furthermore, we define the set Ω which is the polytope for polytopic systems.

$$\Omega = \mathrm{Co}\{[A_1 \quad B_1], [A_2 \quad B_2], ..., [A_L \quad B_L]\} \tag{8.5}$$

where [$A(p(k))$ $B(p(k))$] are the linear combination of the vertices

$$[A(p(k)) \quad B(p(k))] = \sum_{j=1}^{L} p_j(k)[A_j \quad B_j] \tag{8.6}$$

$$\sum_{j=1}^{L} p_j(k) = 1, \qquad 0 \le p_j(k) \le 1$$

8.2.2 Model Predictive Control (MPC) Formulation

At each sampling time *k*, the robust performance objective is a min-max problem (minimization of worst-case performance cost) in term of the quadratic objective as given in Eqs. (8.7) and (8.8) for the LTV and LPV systems, respectively.

$$\min_{u(k+i|k),i=0,1,...,m} \max_{[A(k+i) \quad B(k+i)]\in\Omega,\, i\ge 0} J_\infty(k) \tag{8.7}$$

$$\min_{u(k+i|k),i=0,1,...,m} \max_{[A(p(k+i)) \quad B(p(k+i))]\in\Omega,\, i\ge 0} J_\infty(k) \tag{8.8}$$

$$J_\infty(k) = \sum_{i=0}^{\infty} \left[x(k+i|k)^T Q_1 x(k+i|k) + u(k+i|k)^T R u(k+i|k) \right] \tag{8.9}$$

where $Q_1 > 0$ and $R > 0$ are the symmetric weighting matrices.
subject to

$$|u_h(k+i|k)| \le u_{h,\max}, \quad h = 1, 2, 3, ..., n_u \tag{8.10}$$

$$|y_r(k+i|k)| \le y_{r,\max}, \quad r = 1, 2, 3, ..., n_y \tag{8.11}$$

The performance cost, Eq (8.9) at each sample time step is formulated as the convex optimization problem with linear matrix inequalities (LMIs) constraints (Kothare et al., 1996). The Lyapunov function is presented to guarantee the stability for the MPC algorithm.

The state-feedback control law can be stabilized as Eqs. (8.12) and (8.13) for the LTV and LPV systems, respectively.

$$u(k) = Fx(k), \; i \ge 0 \tag{8.12}$$

$$u(k) = F(p(k))x(k), \; F(p(k)) = \sum_{j=1}^{L} p_j(k) F_j \tag{8.13}$$

8.2.3 Off-line robust MPC algorithm using ellipsoidal invariant sets

For a Linear Time Varying (LTV) system

The state feedback gains F in the control law are defined as $F=Y_iQ_i^{-1}$ to stabilize the closed-loop system with in the ellipsoidal invariant set $\varepsilon = \{x/x^TQ^{-1}x\leq 1\}$. The matrix variables $Q_i>0$ and Y_i are achieved from the result of the linear objective minimization problem $J_\infty(k)$ with the upper bound γ on the worst-case MPC. The symbol * represents the corresponding transpose of the lower block part of symmetric matrices.

$$\min_{\gamma,Q_i,Y_i} \gamma \tag{8.14}$$

subject to

$$\begin{bmatrix} 1 & * \\ x_i & Q_i \end{bmatrix} \geq 0 \tag{8.15}$$

and

$$\begin{bmatrix} Q_i & * & * & * \\ A_jQ_i + B_jY_i & Q_i & * & * \\ Q_1^{1/2}Q_i & 0 & \gamma I & * \\ R^{1/2}Y_i & 0 & 0 & \gamma I \end{bmatrix} \geq 0, \quad j = 1,2,...,L \tag{8.16}$$

For input constraints, it is the limitations in the process equipment that inflict hard constraints on the manipulated variable $u(k)$. Boyd et al. (1994) showed the basic ideal for continuous-time systems. However, we present here in (discrete-time) robust MPC as follows:

$$\begin{bmatrix} X & * \\ Y_i^T & Q_i \end{bmatrix} \geq 0, \tag{8.17}$$

with

$$X_{hh} \leq u_{h,\max}^2, \quad h = 1,2,...,n_u \tag{8.18}$$

Performance terms inflict constraints on the process output *y(k)* for output constraints.

$$\begin{bmatrix} S & * \\ \left(A_j Q_i + B_j Y_i\right)^T C^T & Q_i \end{bmatrix} \geq 0, \tag{8.19}$$

with

$$S_{rr} \leq y_{r,\max}^2, \quad r = 1,2,...,n_y \tag{8.20}$$

Eq. (8.17) is expressed for input constraint satisfaction and Eq. (8.19) is expressed for output constraint satisfaction.

For a Linear Parameter Varying (LPV) system

The state feedback gains F_i in the control law are defined as $K_i = Y_i G_i^{-1}$ (Wada et al., 2006) to stabilize the closed-loop system. The matrix variables Q_i, G_i, and Y_i are achieved from the result of the linear objective minimization problem with the upper bound γ on the worst-case MPC. The symbol * represents the corresponding transpose of the lower block part of symmetric matrices.

$$\min_{\gamma, Q_i, G_i, Y_i} \gamma \tag{8.21}$$

subject to

$$\begin{bmatrix} 1 & * \\ x_i & Q_i \end{bmatrix} \geq 0 \tag{8.22}$$

and

$$\begin{bmatrix} G_i + G_i^T - Q_i & * & * & * \\ A_j G_i + B Y_i & Q_i & * & * \\ Q_1^{1/2} G_i & 0 & \gamma I & * \\ R^{1/2} Y_i & 0 & 0 & \gamma I \end{bmatrix} \geq 0, \quad j = 1,2,...,L \tag{8.23}$$

Input constraint

$$\begin{bmatrix} X & * \\ Y_i^T & G_i + G_i^T - Q_i \end{bmatrix} \geq 0, \quad X_{hh} \leq u_{h,\max}^2, \quad h = 1,2,...,n_u \tag{8.24}$$

Output constraint

$$\begin{bmatrix} S & * \\ \left(A_j G_i + B Y_i\right)^T C^T & G_i + G_i^T - Q_i \end{bmatrix} \geq 0, \tag{8.25}$$

$$S_{rr} \leq y_{r,\max}^2, \quad r = 1,2,...,n_y$$

8.3 Results and discussion

In this part, the implementation of the ellipsoidal off-line robust MPC algorithm for LTV systems is presented and performed using SeDuMi (Sturm, 1998) and YALMIP (Löfberg, 2004) within Matlab R2012a. The control algorithm is considered to the nonlinear model of SOFC. For the LTV system, the cell voltage, V_{FC} is considered as the uncertain parameter and assumed as an arbitrarily time-varying in the indicated range of variation. Whereas the scheduling parameter, *p(k)* for LPV system can be calculated from temperature.The lumped-parameter model represented by nonlinear ODEs of mass and energy balances of SOFC is linearized as follows:

$$\dot{x} = Ax + Bu \tag{8.26}$$

$$y = cx$$

where *x* are the state variables of SOFC. They include the mole contents of fuel and air and the cell temperature. Whereas *u* are the input variables or manipulated variables that are the inlet molar flow rate of air and fuel. Matrix *A* and *B* are obtained from linearization, and *y* are the output variables.

Then the linearized model is discretized using Euler first-order approximation into discrete-time model (expressed in Eq. 8.27) with a sampling period of 5 second. Let $\bar{x} = x - x_{ss}$ and $\bar{u} = u - u_{ss}$ where the subscript *ss* denotes the corresponding variable at steady state condition.

$$\bar{x}(k+1) = A(k)\bar{x}(k) + B(k)\bar{u}(k) \tag{8.27}$$

$$\bar{y}(k) = c\bar{x}(k)$$

Due to the cell temperature increased, the material stresses could potentially be a problem that can result in cracking of the anode and electrolyte materials. The objective is to control the state variables to their desired value by manipulating the input variables with $Q_1=I$ and $R=0.1I$.

In this study, the polytopic uncertain model includes two vertices due to one uncertain parameter, V_{FC} for LTV system. The uncertain parameter is randomly time-varying between 0.6 and 0.8 V. While the scheduling parameter for LPV system can be calculated from temperature at each sampling time.

Figure 8.1 shows schematic diagram of control system between robust MPC and SOFC. The solid line refers to on-line computational and the dash line refers to off-line computational. From SOFC model that is non-linear model is linearized, (the state, input, and output variables are expressed in term the deviation variables) and then discretized using Euler first-order approximation into discrete-time model. After we get LTV and LPV systems, they are implemented with robust MPC algorithm. To get gain F, we find matrix Q_i, G_i, and Y_i from the result of optimization. Lastly, the state feedback control, u can be calculated and used to adjust the final control element.

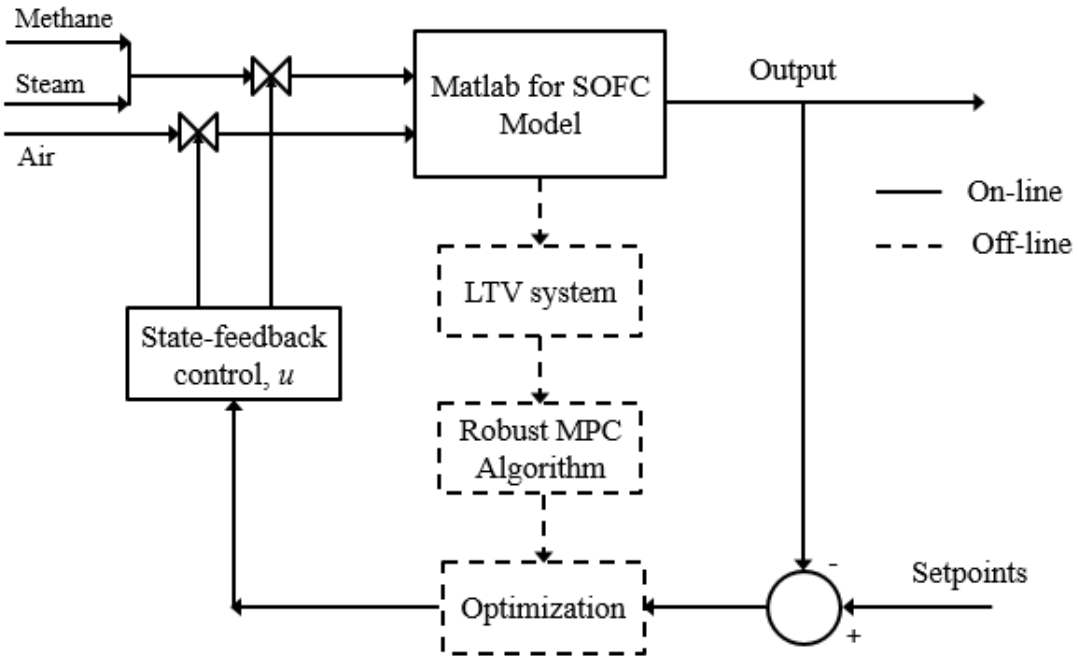

Figure 8. 1 Schematic diagram of control system.

The robust MPC using LTV model with the state feedback control is implemented as controller to maintain the state variables to their setpoints when the disturbance occurs. The closed-loop response of cell temperature and cell voltage due to the current density changes from 0.45 to 0.47 A/cm^2 is shown in Figures 8.2 and 8.3, respectively. Moreover, the responses of the moles of methane, water, carbon monoxide, hydrogen, carbon dioxide, and oxygen are shown in Figure 8.4. The reactions of the inlet molar flow rate of air and fuel in term velocity as the control input can be seen in Figure 8.5.

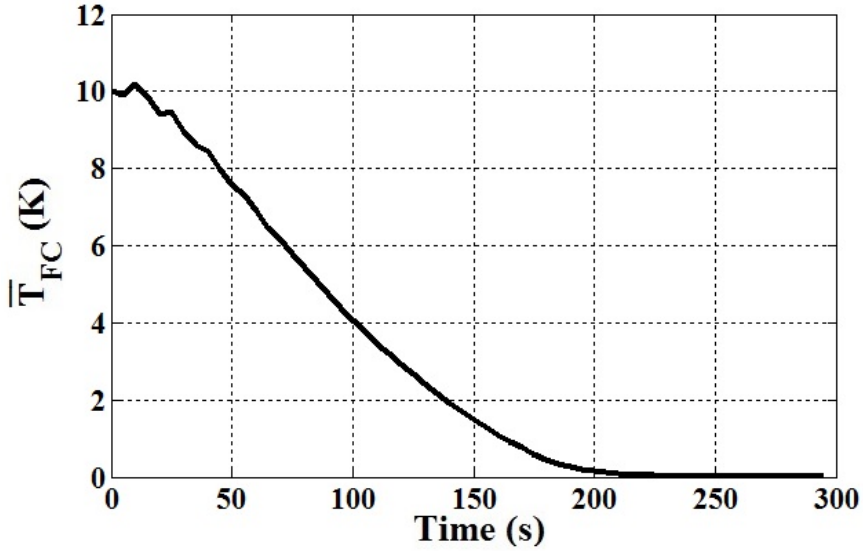

Figure 8. 2 The closed-loop response of SOFC temperature.

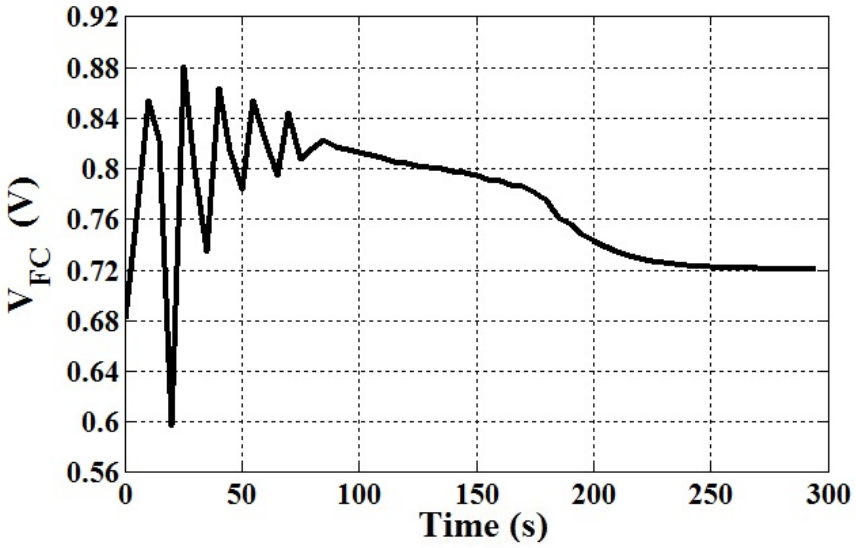

Figure 8. 3 The closed-loop response of the cell voltage.

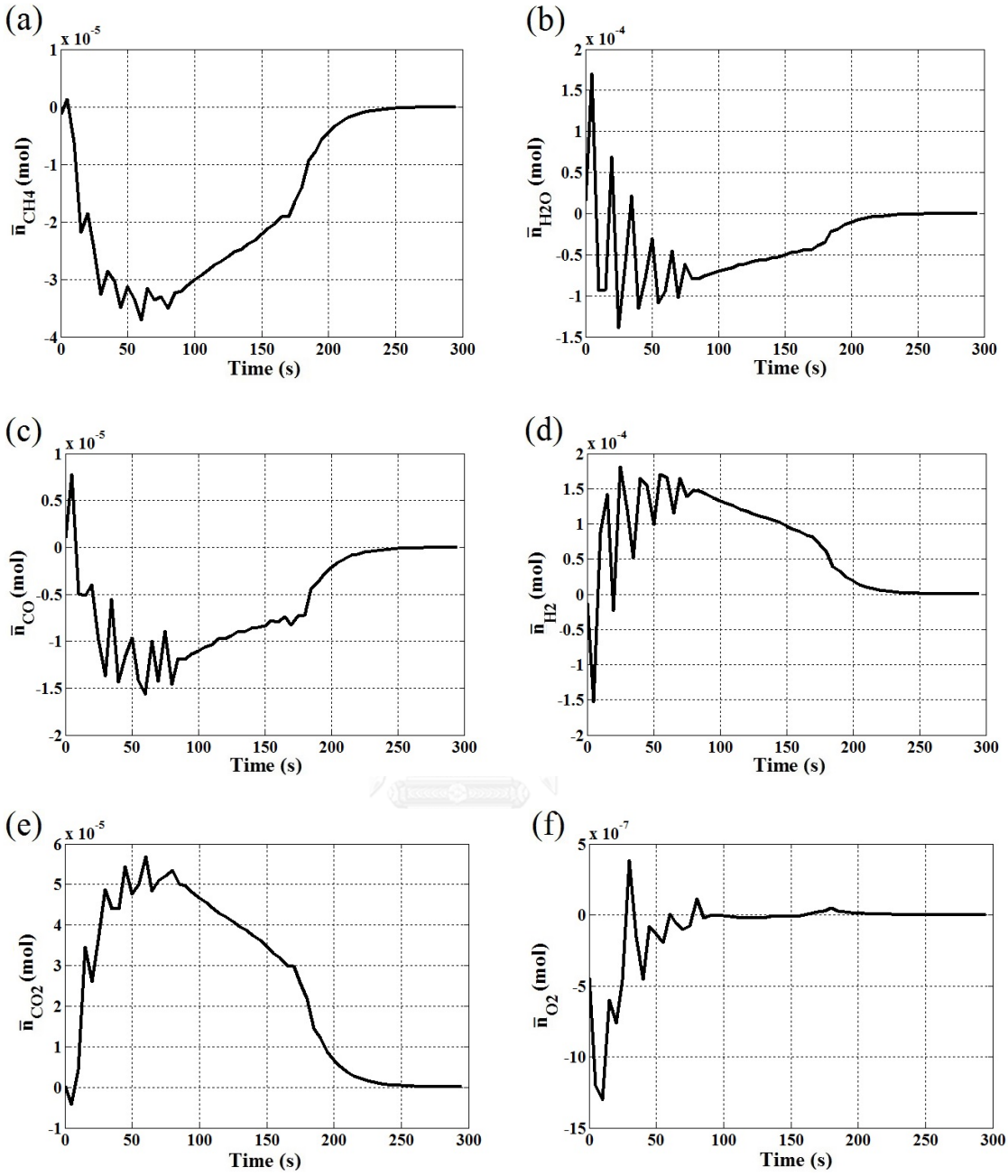

Figure 8. 4 The regular output in term mole contents of fuel and air.
(a) mole of methane, (b) mole of water, (c) mole of carbon monoxide, (d) mole of hydrogen, (e) mole of carbon dioxide, and (f) mole of oxygen.

The results show the inlet molar flow rate of air and fuel in term velocity can maintain the cell voltage and the state variables that are the cell temperature and the content of fuel and air to their setpoints when the process is changed due to current

density changes. The robust MPC controller with model uncertainty can control the SOFC and guarantee the stability of the SOFC.

(a) The inlet molar flow rate of fuel in term velocity

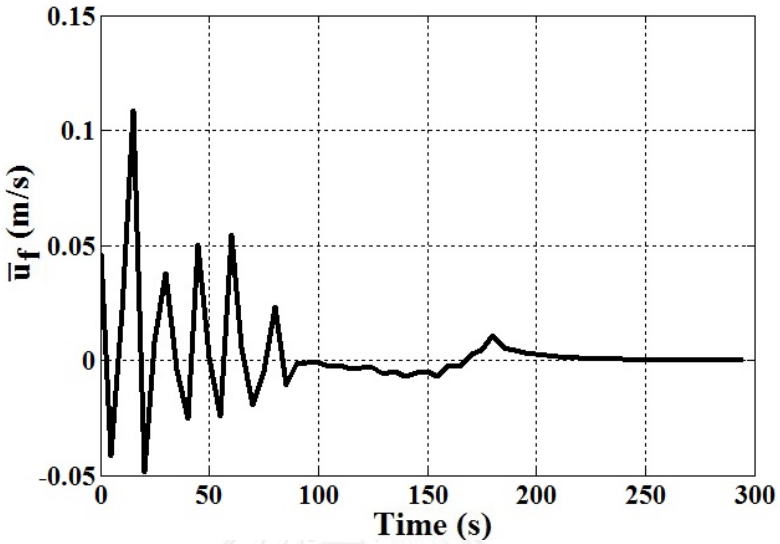

(b) The inlet molar flow rate of air in term velocity

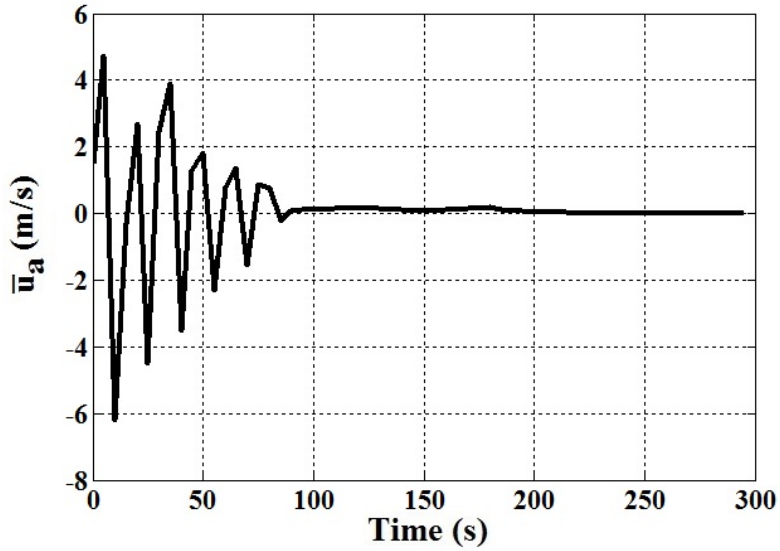

Figure 8. 5 The control input for LTV system (a) inlet molar flow rate of fuel in term velocity and (b) inlet molar flow rate of air in term velocity.

The robust MPC algorithm using LTV and LPV systems with the state feedback control is implemented for the SOFC. The comparison between LTV system and LPV system is investigated when the cell temperature (deviation variable) start at 10 K from setpoint.

Figure 8.6 shows the closed-loop responses of the cell temperature for the robust MPC based on the (a) LTV and (b) LPV systems. The regular output in term mole contents of fuel and air based on LTV and LPV systems can be shown in Figure 8.7 and 8.8, respectively. The results show that the proposed control algorithm can reach good results. The MPC controller for LTV and LPV systems can maintain the regular outputs to their setpoints by manipulating the control inputs.

(a) LTV system

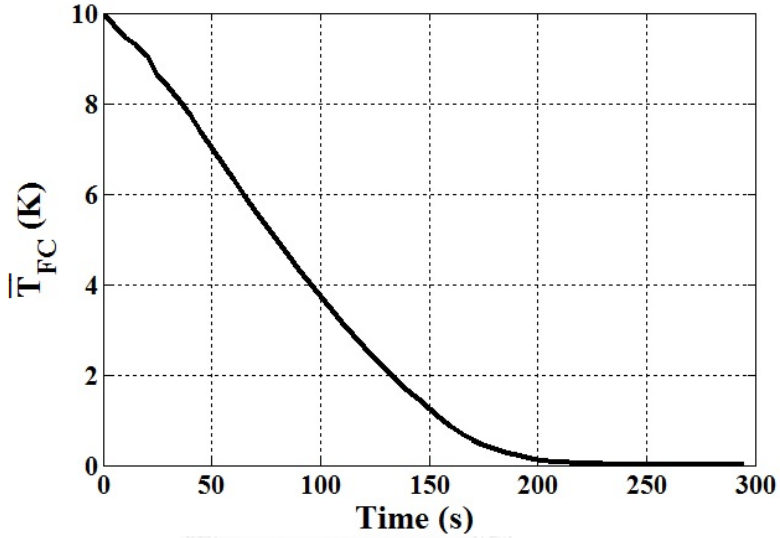

(b) LPV system

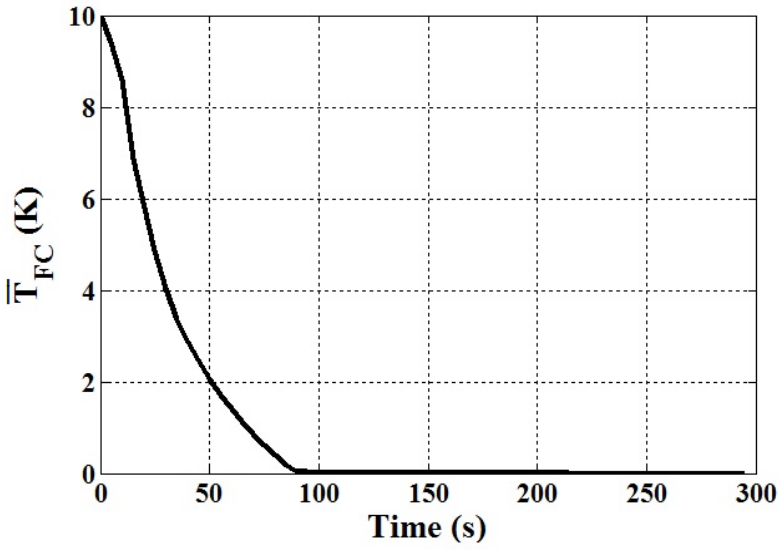

Figure 8. 6 The closed-loop responses of SOFC temperature: (a) LTV system, (b) LPV system.

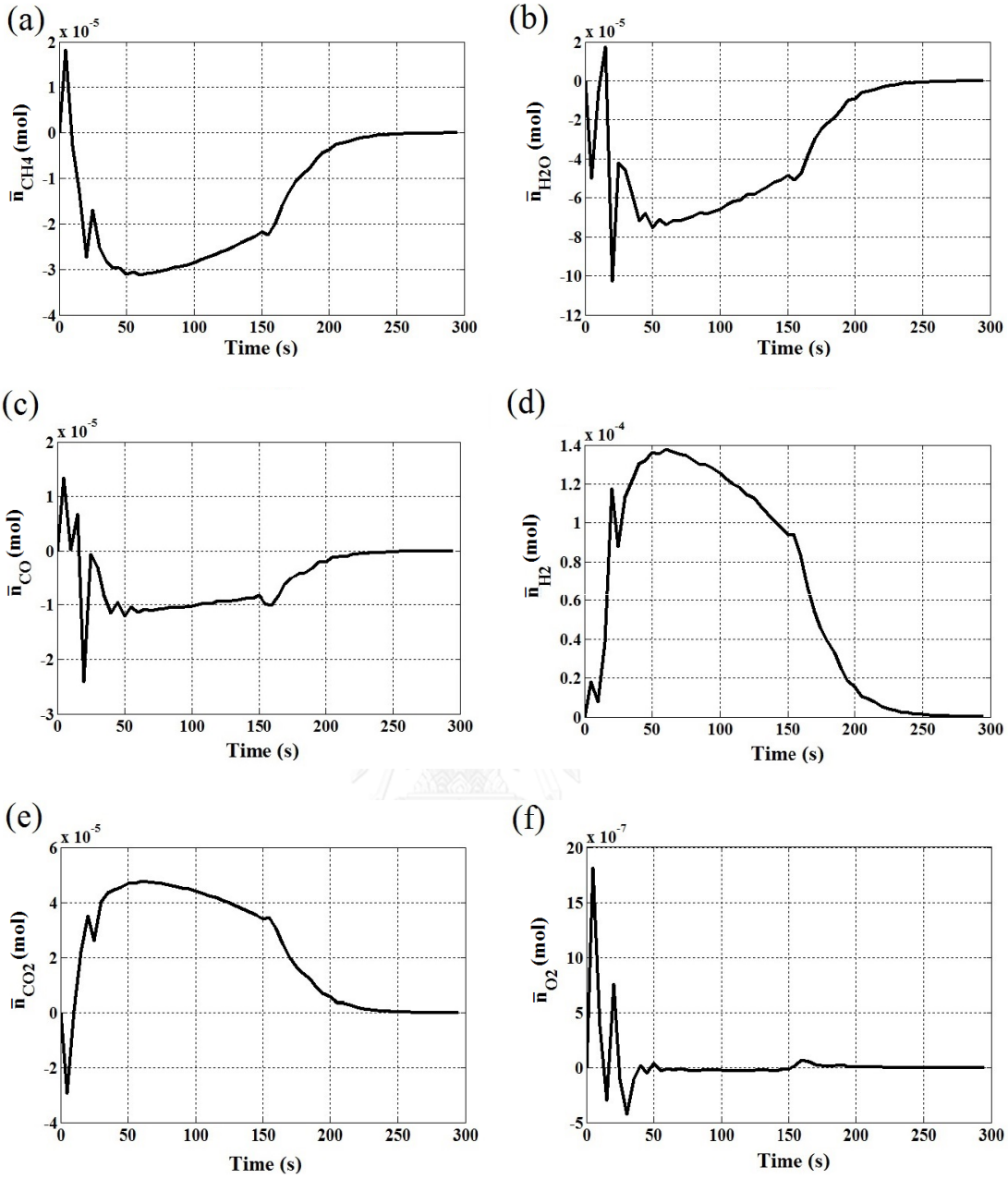

Figure 8. 7 The regular output in term mole contents of fuel and air based on LTV system.

(a) mole of methane, (b) mole of water, (c) mole of carbon monoxide, (d) mole of hydrogen, (e) mole of carbon dioxide, and (f) mole of oxygen.

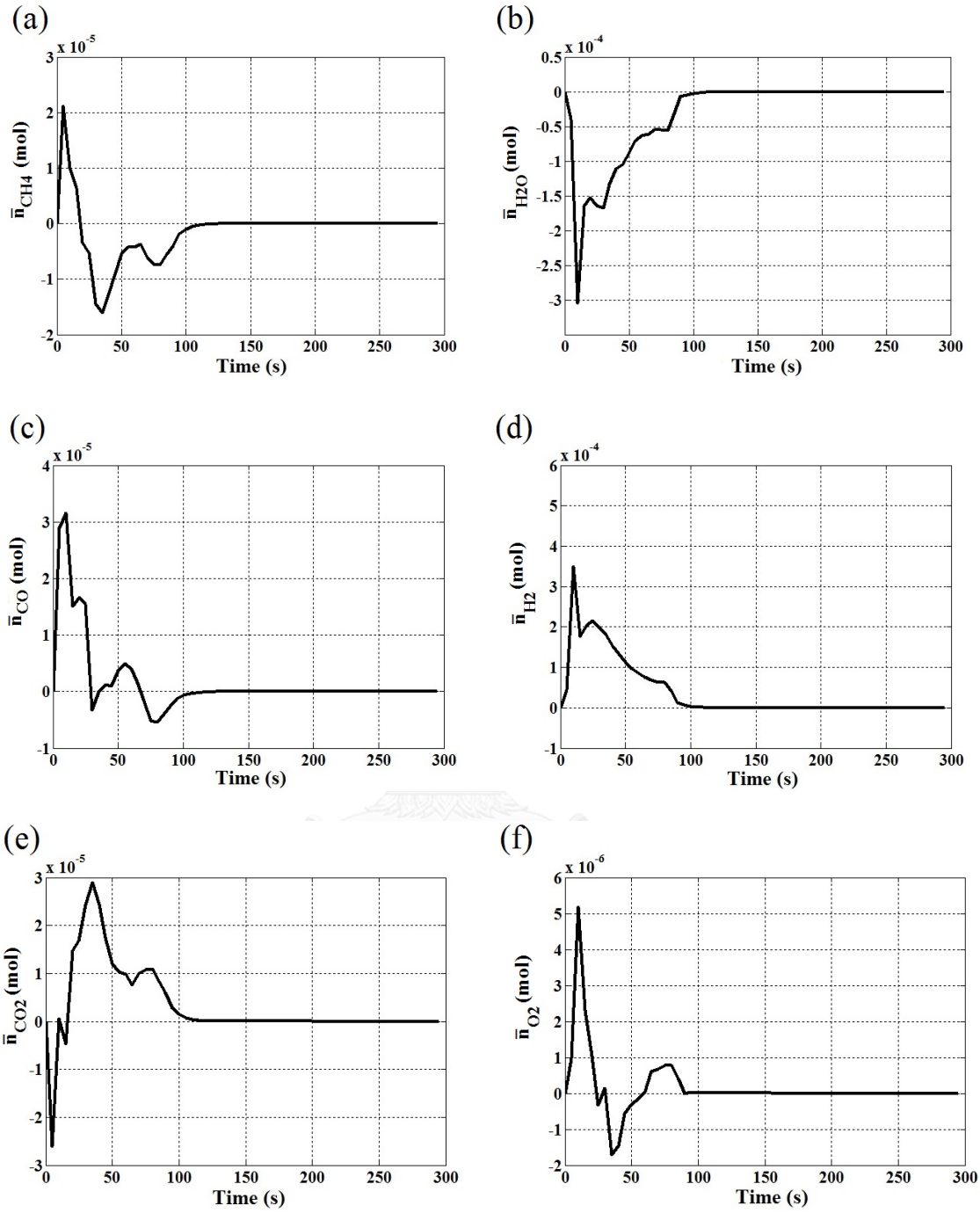

Figure 8. 8 The regular output in term mole contents of fuel and air based on LPV system.

(a) mole of methane, (b) mole of water, (c) mole of carbon monoxide, (d) mole of hydrogen, (e) mole of carbon dioxide, and (f) mole of oxygen.

The control inputs for closed-loop response of the SOFC based on LTV and LPV systems can be shown in Figure 8.9 and 8.10, respectively.

(a) The inlet molar flow rate of fuel in term velocity

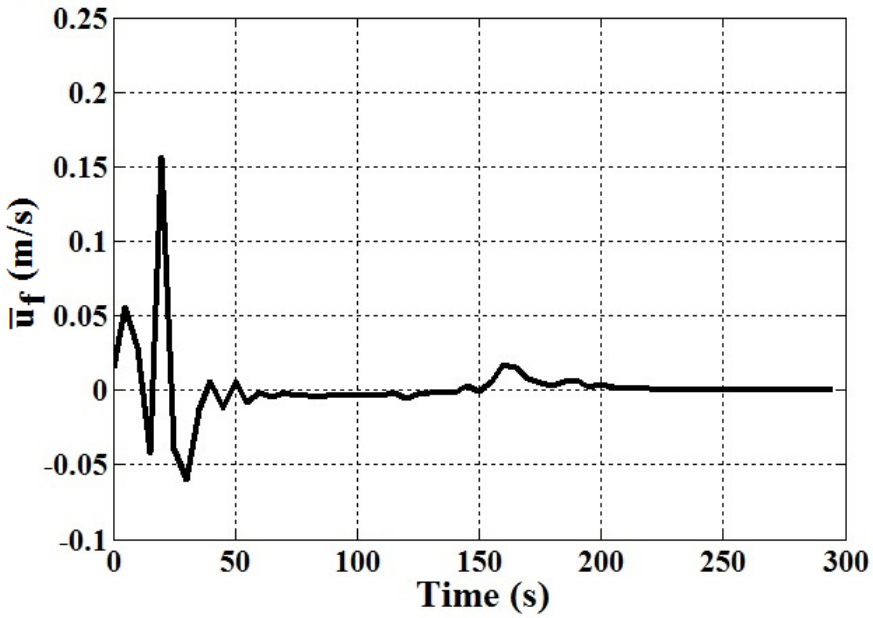

(b) The inlet molar flow rate of air in term velocity

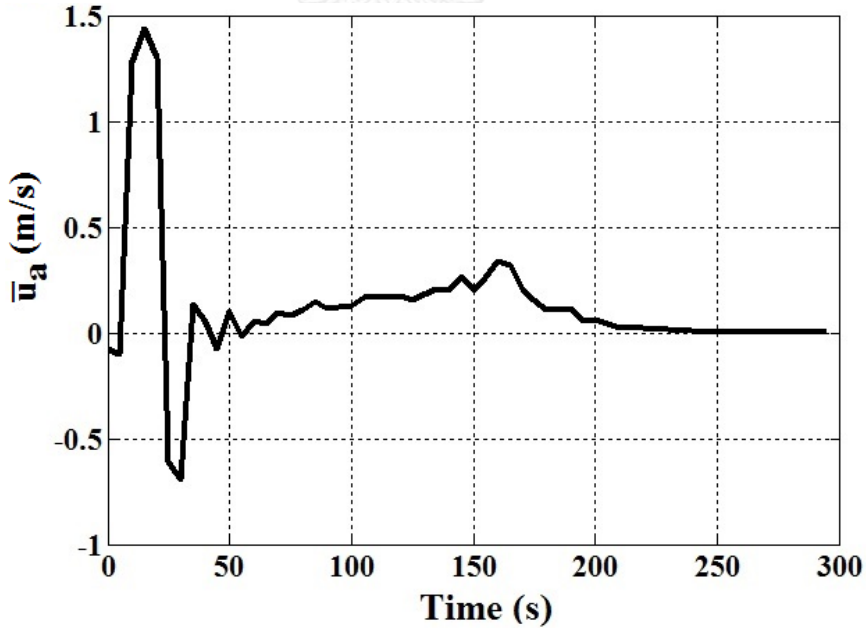

Figure 8. 9 The control input for LTV system.

(a) The inlet molar flow rate of fuel in term velocity

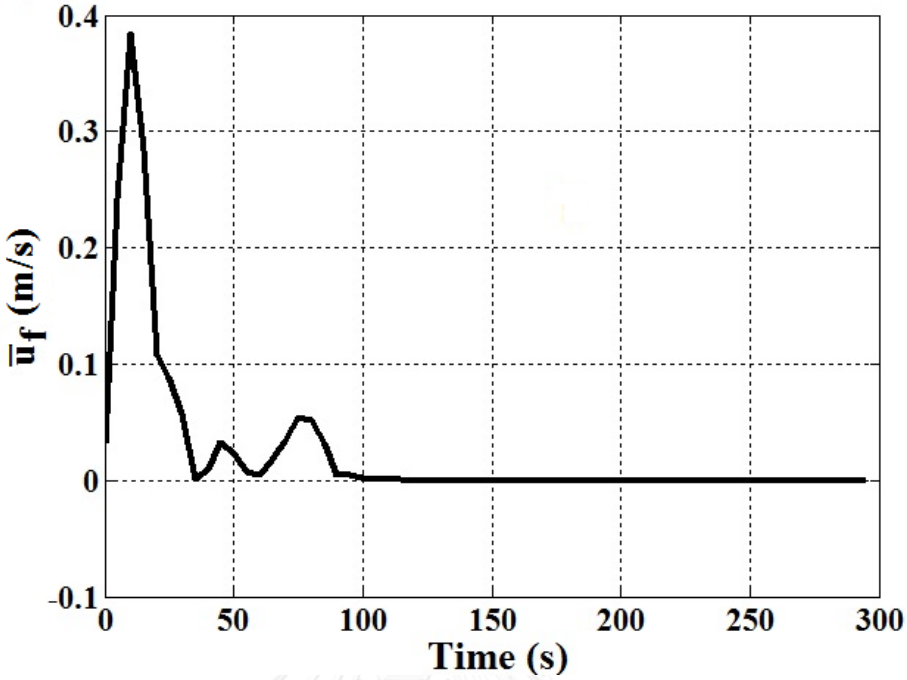

(b) The inlet molar flow rate of air in term velocity

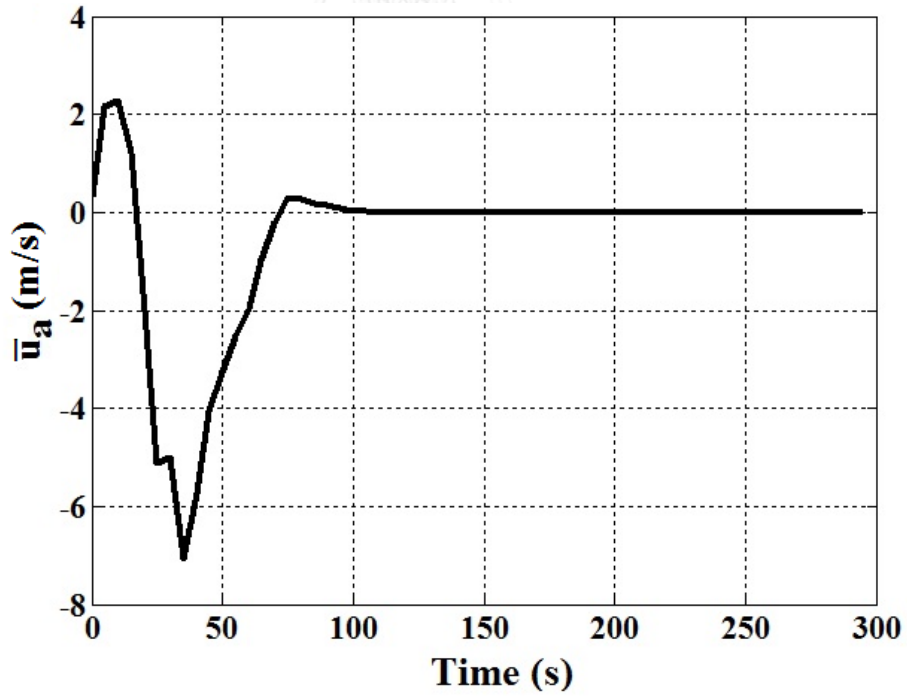

Figure 8. 10 The control input for LPV system.

Moreover, it is observed that the cell voltage (V_{FC}) also moves to its desired value (Figure 8.11). By comparing the MPC design based on the LTV and LPV systems, it seems that the MPC with the LPV system can achieve a better control performance because the scheduling parameter is taken into the controller synthesis.

(a) LTV system

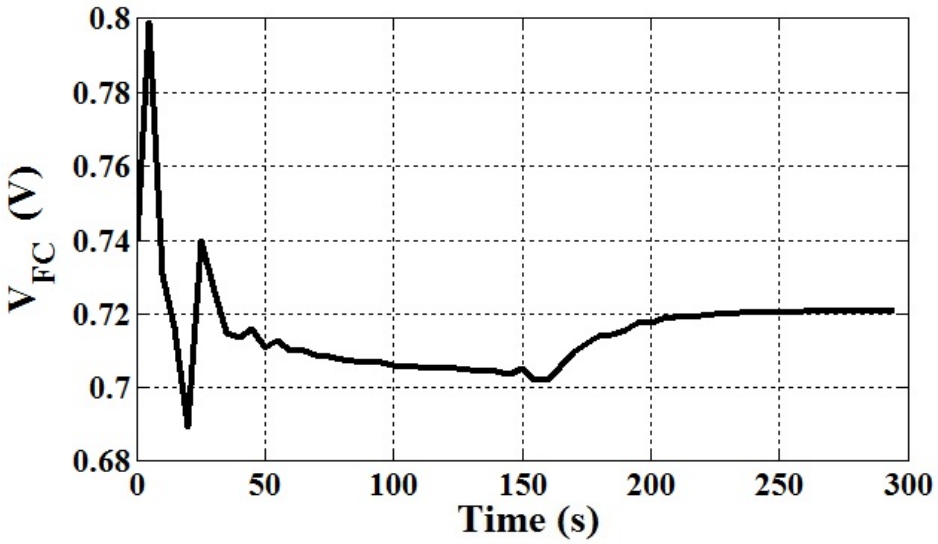

(b) LPV system

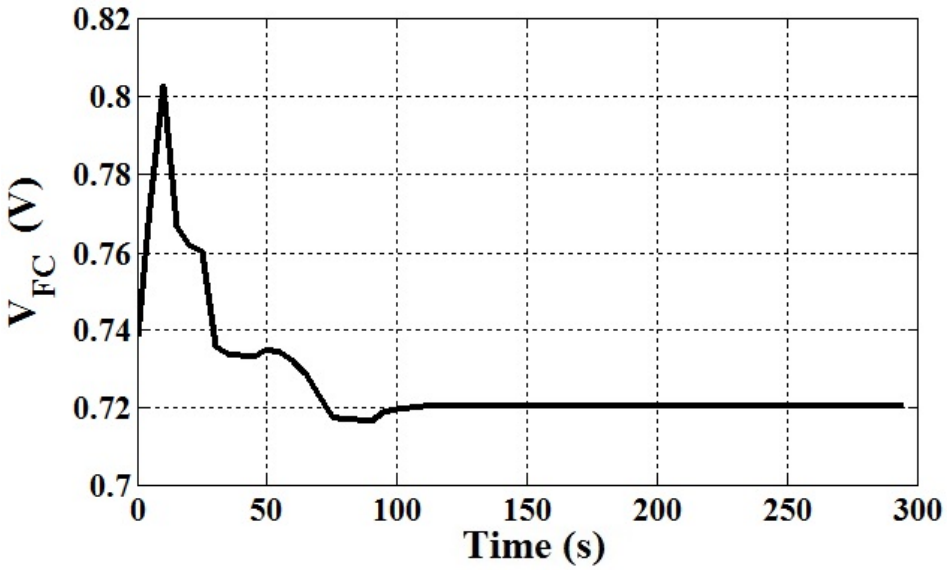

Figure 8. 11 The closed-loop responses of the cell voltage: (a) LTV system, (b) LPV system.

8.4 Conclusions

In this work, the robust constrained MPC algorithm based on uncertain polytopic discrete-time LTV and LPV systems was synthesized for controlling the direct internal reforming SOFC. The state feedback control law minimizing an upper bound on the worst-case objective function was implemented. The lumped-parameter model was used to explain the SOFC dynamic behavior and employed to design the MPC controller. The performance of the MPC controller using the proposed different models was compared. The simulation results showed that under model uncertainties, the proposed robust MPC can control the cell voltage and temperature to its setpoint. The proposed controller can guarantee the stability of the SOFC. The results also showed the control performance of the robust MPC algorithm based on LPV system was better than LTV system.

CHAPTER IX

CONCLUSIONS AND RECOMMENDATIONS

This work studies on the performance of the direct internal reforming solid oxide fuel cell using methane as fuel. The steady state analysis is studied to desire the optimal operating condition. The dynamic behavior using the lumped parameter model of mass and energy balances is investigated to explain the dynamic responses. The effect of the input variables such as the inlet temperatures of fuel and air, the molar flow rates of fuel and air in term velocity, and current density on the cell voltage and cell temperature are explained. Moreover, the control structure design is implemented to select the good controlled variable, manipulated variable, and control configuration by using the procedure of Skogestad (2004). The controllability analysis using the relative gain array as the controllability index is studied for the selection of input-output pairings. The implementation of conventional PID controller to control the cell temperature and the fraction of methane is presented. Finally, the off-line robust model predictive control using linear time varying and linear parameter varying systems is proposed for the internal reforming solid oxide fuel cell. The performance of robust MPC based on two different models is compared.

9.1 Conclusions

In this study, the methane is fed as fuel for the planar solid oxide fuel cell (SOFC) with the direct internal reforming. The electrochemical model, mass and energy balances were performed in Matlab to study the steady state analysis, dynamic behavior, control structure design as well as the controller design. The lumped parameter model of the mass and energy balances was implemented. The steady state analysis was performed for the SOFC and reformer in order to the select operating condition that is near the maximum power density and voltage near 0.7V. The cell temperature, cell voltage, and power density were determined as a function of current density. The results showed an increase in the current density cause a reduction of cell voltage and an increasing of cell temperature because of the increased hydrogen consumption. Moreover, the dynamic responses due to step changed of the different

input were investigated by using the operating condition as the initial condition. The cell temperature and cell voltage depend on, the inlet temperature of air and fuel as well as the current density. An increase in the inlet temperature of air and fuel resulted in the cell temperature increased leading to the gain of cell voltage due to decreasing of the internal resistance. At the high current densities, the cell operating temperature increased due to an increase in hydrogen consumption in the cell; however, the fuel cell voltage also sudden dropped associated with the ohmic losses.

After the dynamic behavior was analyzed, the implementing of control structure design and controllability analysis for the planar SOFC to design a good control system was studied. The cost function needed to be minimized was defined subject to satisfying constraints. A procedure for selecting an active constraint and a self-optimizing variables was presented. The results found the cell temperature was the active constraint variable needed to maintain at its desired value and the fraction of methane was found as the self-optimizing variable by investigating the loss, L. The inlet molar flow rate of air and fuel were selected as manipulated variables and the main disturbance variable was the current density. Moreover, the relative gain array (RGA) considered as a controllability index for the selection of input-output pairings was also implemented. The pairing result showed that the steady-state RGA was 1.94 for pairing the inlet molar flow rate of air with the cell temperature and the inlet molar flow rate of fuel with the fraction of methane. This mean the inlet molar flow rates of air and fuel were the manipulated variables to control the cell temperature and the fraction of methane at the outlet, respectively.

As mentioned above, the control structure design defined the good controlled variables with their manipulated variables. Therefore, it was interesting to implement controller design for control the internal reforming solid oxide fuel cell. Control studies on the conventional Proportional-Integral-Derivative (PID) controller was investigated and the SIMC (Skogestad Internal Model Control) PID tuning rule was id to find tuning parameters (K_c, τ_I, and τ_D). The simulation studies of the two PID controller with the designed control structure was discussed. The cell temperature and the fraction of methane were controlled by manipulating the inlet molar flow rate of air and fuel, respectively. The simulation result showed the PID controllers successfully maintained two controlled variable to their setpoints. When the current density was changed at

100s, the cell temperature increases and the fraction of methane decreases due to the increased amount of hydrogen reacted in the fuel cell. The inlet molar flow rate of air increased to reduce the cell temperature. The changing of the fraction of methane was very small and can be observed from the IAE value. However, the cell voltage was necessary to constant for SOFC. Therefore, the cell voltage was controlled by using the same controller tuning parameter. The simulation result showed the cell voltage was controlled to its desired value. The performance of two PID controller showed the good control performances by investigating the IAE value. However, the PID controller algorithm for controlled variables under a large step increases in the current density cannot guarantee optimal control of the system.

According to controller design, the model predictive control (MPC) is interesting to implement for the internal reforming SOFC. However, it is incompetent to deal with plant model uncertainties. Several works have been focused on the development of robust MPC to handle nonlinear systems and guarantee its stability. Therefore, an off-line robust model predictive control algorithm based on uncertain polytopic approach using linear time-varying (LTV) and linear parameter varying (LPV) systems was implemented for controlling the internal reforming SOFC. The minimization of an upper bound on the worst-case performance cost with the state feedback control law was implemented to the process. The state feedback control law is used to calculate the control input that was implemented to the process. The lumped-parameter model of SOFC was linearized and discretized using Euler first-order approximation into discrete-time model. The voltage was uncertain parameter for the LTV system. Whereas the scheduling parameter for LPV system can be calculated from the cell temperature. The control performance of the robust MPC controller using the proposed different models was compared. The simulation result showed the proposed robust MPC can control the output variables to their setpoints. The proposed controller can guarantee the stability of the internal reforming SOFC. The result also showed the control performance of the robust MPC algorithm based on LPV system was better than LTV system because the scheduling parameter was taken into the controller synthesis.

9.2 Recommendations

1. In this study, we only considered the solid oxide fuel cell (SOFC) single cell. When comparing the controlling of an SOFC system, variable parameters of SOFC system affecting the system performance and efficiency are more than that of the SOFC single cell. It is a challenge in the implementation of the control structure design on the SOFC system in order to achieve the good control system. Therefore, the selection of control structure and the increase variable parameters should be considered to find the suitable condition for controlling the SOFC system
2. A development of control strategies to control the important variables of SOFC should be investigated. The robust model predictive control (MPC) based on the ellipsoidal approximation implemented for the SOFC (proposed in Chapter 8) only considered small number of vertices. The offline robust MPC handling more uncertain parameter and using a polyhedral invariant set is interesting for the SOFC. Moreover, disturbance variables should be included.

REFERENCES

Achenbach, E. (1994). Three-dimensional and time-dependent simulation of a planar solid oxide fuel cell stack. Journal of Power Sources 49: 333-348.

Aguiar, P., Adjiman, C. S.and Brandon, N. P. (2004). Anode-supported intermediate temperature direct internal reforming solid oxide fuel cell. I: model-based steady-state performance. Journal of Power Sources 138: 120-136.

Aguiar, P., Adjiman, C. S.and Brandon, N. P. (2005). Anode-supported intermediate-temperature direct internal reforming solid oxide fuel cell: II. Model-based dynamic performance and control. Journal of Power Sources 147: 136-147.

Andrade, G. V. N.and Lima, E. L. (2009). Control Structure Design for an Ethanol Production Plant. 10th International Symposium on Process Systems Engineering: 1551-1556.

Ang, K. H., Chong, G. C. Y.and Li, Y. H. (2005). PID control system analysis, design, and technology. IEEE Transactions on Control Systems Technology 13: 559-576.

Araújo, A.and Skogestad, S. (2008). Control structure design for the ammonia synthesis process. Computers & Chemical Engineering 32: 2920-2932.

Balas, G. J. (2003). Flight Control Law Design: An Industry Perspective. European Journal of Control 9: 207-226.

Boyd, S., Ghaoui, L. E., Feron, E.and Balakrishnan, V. (1994). Linear Matrix Inqualities in System and Control Theory. Society for Industrial and Applied Mathematics 15.

Bristol, E. H. (1996). On a new measure of interactions for multivariable process control. IEEE Transactions on Automatic Control: 133-134.

Bumroongsri, P.and Kheawhom, S. (2012). An ellipsoidal off-line model predictive control strategy for linear parameter varying systems with applications in chemical processes. Systems & Control Letters 61: 435-442.

Bumroongsri, P.and Kheawhom, S. (2012). An off-line robust MPC algorithm for uncertain polytopic discrete-time systems using polyhedral invariant sets. Journal of Process Control 22: 975-983.

Cao, H., Deng, Z., Li, X., Yang, J.and Qin, Y. (2010). Dynamic modeling of electrical characteristics of solid oxide fuel cells using fractional derivatives. International Journal of Hydrogen Energy 35: 1749-1758.

Casas, Y., Dewulf, J., Arteaga-Pérez, L. E., Morales, M., Van Langenhove, H.and Rosa, E. (2011). Integration of Solid Oxide Fuel Cell in a sugar–ethanol factory: analysis of the efficiency and the environmental profile of the products. Journal of Cleaner Production 19: 1395-1404.

Casavola, A., Famularo, D., Franzè, G.and Garone, E. (2012). A fast ellipsoidal MPC scheme for discrete-time polytopic linear parameter varying systems. Automatica 48: 2620-2626.

Chaisantikulwat, A., Diaz-Goano, C.and Meadows, E. S. (2008). Dynamic modelling and control of planar anode-supported solid oxide fuel cell. Computers & Chemical Engineering 32: 2365-2381.

Chan, S. H., Khor, K. A.and Xia, Z. T. (2001). A complete polarization model of a solid oxide fuel cell and its sensitivity to the change of cell component thickness. Journal of Power Sources 93: 130-140.

Chang, H., Krieger, A., Astolfi, A.and Pistikopoulos, E. N. (2014). Robust multi-parametric model predictive control for LPV systems with application to anaesthesia. Journal of Process Control 24: 1538-1547.

Danzer, M. A., Wittmann, S. J.and Hofer, E. P. (2009). Prevention of fuel cell starvation by model predictive control of pressure, excess ratio, and current. Journal of Power Sources 190: 86-91.

Dwivedi, D., Halvorsen, I. J.and Skogestad, S. (2013). Control structure selection for four-product Petlyuk column. Chemical Engineering and Processing: Process Intensification 67: 49-59.

García, C. E.and Morari, M. (1985). Internal Model Control Design Procedure for Multivariable. Ind. Eng. Chem. Res. 24: 472-484.

García, C. E., Prett, D. M.and Morari, M. (1989). Model predictive control: theory and practice - a survey. Automatica 25: 335-348.

García, V. M., López, E., Serra, M., Llorca, J.and Riera, J. (2010). Dynamic modeling and controllability analysis of an ethanol reformer for fuel cell application. International Journal of Hydrogen Energy 35: 9768-9775.

García, V. M., Serra, M.and Llorca, J. (2011). Controllability study of an ethanol steam reforming process for hydrogen production. Journal of Power Sources 196: 4411-4417.

Georgis, D., Jogwar, S. S., Almansoori, A. S.and Daoutidis, P. (2011). Design and control of energy integrated SOFC systems for in situ hydrogen production and power generation. Computers & Chemical Engineering 35: 1691-1704.

Golbert, J.and Lewin, D. R. (2004). Model-based control of fuel cells. Journal of Power Sources 135: 135-151.

Haberman, B. A.and Young, J. B. (2004). Three-dimensional simulation of chemically reacting gas flows in the porous support structure of an integrated-planar solid oxide fuel cell. International Journal of Heat and Mass Transfer 47: 3617-3629.

Hajimolana, S. A.and Soroush, M. (2009). Dynamics and Control of a Tubular Solid-Oxide Fuel Cell. Ind. Eng. Chem. Res. 48: 6112-6125.

Hajimolana, S. A., Tonekabonimoghadam, S. M., Hussain, M. A., Chakrabarti, M. H., Jayakumar, N. S.and Hashim, M. A. (2013). Thermal stress management of a solid oxide fuel cell using neural network predictive control. Energy 62: 320-329.

Hall, J.and Kerr, R. (2003). Innovation dynamics and environmental technologies: the emergence of fuel cell technology. Journal of Cleaner Production 11: 459-471.

Havre, K.and Skogestad, S. (1998). Effect of RHP zeros and poles on the sensitivity functions in multivariable systems. Journal of Process Control 8: 155-164.

Hu, Q., Wang, S.and Wen, T.-L. (2008). Analysis of processes in planar solid oxide fuel cells. Solid State Ionics 179: 1579-1587.

Jayasankar, B. R., Ben-Zvi, A.and Huang, B. (2009). Identifiability and estimability study for a dynamic solid oxide fuel cell model. Computers & Chemical Engineering 33: 484-492.

Kakac, S., Pramuanjaroenkij, A.and Zhou, X. (2007). A review of numerical modeling of solid oxide fuel cells. International Journal of Hydrogen Energy 32: 761-786.

Kandepu, R., Imsland, L., Foss, B. A., Stiller, C., Thorud, B.and Bolland, O. (2007). Modeling and control of a SOFC-GT-based autonomous power system. Energy 32: 406-417.

Kaneko, T., Brouwer, J.and Samuelsen, G. S. (2006). Power and temperature control of fluctuating biomass gas fueled solid oxide fuel cell and micro gas turbine hybrid system. Journal of Power Sources 160: 316-325.

Kang, Y., Li, J., Cao, G., Tu, H., Li, J.and Yang, J. (2009). One-dimensional Dynamic Modeling and Simulation of a Planar Direct Internal Reforming Solid Oxide Fuel Cell. Chinese Journal of Chemical Engineering 17: 304-317.

Kothare, M. V., Balakrishnan, V.and Morari, M. (1996). Robust Constrained Model Predictive Control using Linear Matrix Inequalities. Automatica 32: 1361-1379.

Kouramas, K., Varbanov, P. S., Georgiadis, M. C., Klemeš, J. J.and Pistikopoulos, E. N. (2011). Explicit/Multi-Parametric Model Predictive Control of a Solid Oxide Fuel Cell. 29: 773-777.

Kulikovsky, A. A. (2009). A model for SOFC anode performance. Electrochimica Acta 54: 6686-6695.

Laurencin, J., Lefebvre-Joud, F.and Delette, G. (2008). Impact of cell design and operating conditions on the performances of SOFC fuelled with methane. Journal of Power Sources 177: 355-368.

Li, Y. H., Choi, S. S.and Rajakaruna, S. (2005). An Analysis of the Control and Operation of a SOFC power plant. IEEE Transactions on Energy Conversion 20: 381-387.

Liu, R. W. (1968). Convergent systems. IEEE Transactions on Automatic Control: 384-391.

Löfberg, J. (2004). YALMIP : A toolbox for modeling and optimization in MATLAB. IEEE International Symposium on Computer Aided Control Systems Design: 284-289.

Mayne, D. Q., Rawlings, J. B., Rao, C. V.and Scokaert, P. O. M. (2000). Constrained model predictive control Stability and optimality. Automatica 36: 789-814.

Morari, M. (1983). Flexibility and resiliency of process systems. Computers & Chemical Engineering 7: 423-437.

Muller, F., Gaynor, R., Auld, A. E., Brouwer, J., Jabbari, F.and Samuelsen, G. S. (2008). Synergistic integration of a gas turbine and solid oxide fuel cell for improved transient capability. Journal of Power Sources 176: 229-239.

Murshed, A. M., Huang, B.and Nandakumar, K. (2007). Control relevant modeling of planer solid oxide fuel cell system. Journal of Power Sources 163: 830-845.

Murshed, A. M., Huang, B.and Nandakumar, K. (2010). Estimation and control of solid oxide fuel cell system. Computers & Chemical Engineering 34: 96-111.

Ni, M. (2011). Electrolytic effect in solid oxide fuel cells running on steam/methane mixture. Journal of Power Sources 196: 2027-2036.

Ni, M., Leung, D. Y. C.and Leung, M. K. H. (2009). Electrochemical modeling and parametric study of methane fed solid oxide fuel cells. Energy Conversion and Management 50: 268-278.

O'Hayre, R., Cha, S. W., Colella, W.and Prinz, F. B. (2006). Fuel cell Fundamentals. New York, Wiley&Sons.

Panahi, M., Karimi, M., Skogestad, S., Hillestad, M.and Svendsen, H. F. (2010). Self-Optimizing and Control Structure Design for a CO2 Capturing Plant. 331-338.

Pannocchia, G. (2004). Robust model predictive control with guaranteed setpoint tracking. Journal of Process Control 14: 927-937.

Patcharavorachot, Y., Arpornwichanop, A.and Chuachuensuk, A. (2008). Electrochemical study of a planar solid oxide fuel cell: Role of support structures. Journal of Power Sources 177: 254-261.

Pinheiro, C. I. C.and Kershenbaum, L. S. (1999). Model predictive control of reactor temperature in a CSTR pilot plant operating at an unstable steady-state. Computers & Chemical Engineering: 859-862.

Pirkandi, J., Ghassemi, M., Hamedi, M. H.and Mohammadi, R. (2012). Electrochemical and thermodynamic modeling of a CHP system using tubular solid oxide fuel cell (SOFC-CHP). Journal of Cleaner Production 29-30: 151-162.

Qin, S. J.and Badgwell, T. A. (2003). A survey of industrial model predictive control technology. Control Engineering Practice 11: 733-764.

Rahimpour, M. R.and Lotfinejad, M. (2008). A comparison of co-current and counter-current modes of operation for a dual-type industrial methanol reactor. Chemical Engineering and Processing: Process Intensification 47: 1819-1830.

Rawlings, J. B.and Muske, K. R. (1993). The Stability of Constrained Receding Horizon Control. IEEE Transactions on Automatic Control 38: 1512-1516.

Rivera, D. E., Skogestad, S.and Morari, M. (1986). Internal Model Control 4: PID Controller Design. Ind. Eng. Chem. Res. 25: 252.

Saebea, D., Patcharavorachot, Y.and Arpornwichanop, A. (2012). Analysis of an ethanol-fuelled solid oxide fuel cell system using partial anode exhaust gas recirculation. Journal of Power Sources 208: 120-130.

Salogni, A.and Colonna, P. (2010). Modeling of solid oxide fuel cells for dynamic simulations of integrated systems. Applied Thermal Engineering 30: 464-477.

Sammes, N. M. (2006). Fuel Cell Technology: Reaching Towards Commercialization, Springer-Verlag London.

Seborg, D. E., Edgar, T. F.and Mellichamp, D. A. (2003). Process dynamics and control. New York, John Wiley & Sons.

Seki, H., Ogawa, M., Ooyama, S., Akamatsu, K., Ohshima, M.and Yang, W. (2001). Industrial application of a nonlinear model predictive control to polymerization reactors. Control Engineering Practice 9: 819-828.

Serra, M., Aguado, J., Ansede, X.and Riera, J. (2005). Controllability analysis of decentralised linear controllers for polymeric fuel cells. Journal of Power Sources 151: 93-102.

Skogestad, S. (2003). Simple analytic rules for model reduction and PID controller tuning. Journal of Process Control 13: 291-309.

Skogestad, S. (2004). Control structure design for complete chemical plants. Computers & Chemical Engineering 28: 219-234.

Skogestad, S.and Postlethwaite, I. (1996). Multivariable Feedback Control: Analysis and Design. New York, Wiley.

Sorrentino, M., Pianese, C.and Guezennec, Y. G. (2008). A hierarchical modeling approach to the simulation and control of planar solid oxide fuel cells. Journal of Power Sources 180: 380-392.

Stiller, C., Thorud, B., Bolland, O., Kandepu, R.and Imsland, L. (2006). Control strategy for a solid oxide fuel cell and gas turbine hybrid system. Journal of Power Sources 158: 303-315.

Sturm, J. F. (1998). Using Sedumi 1.02, a MATLAB toolbox for optimization over symmetric cones.

Temeng, K. O., Schnelle, P. D.and McAvoy, T. J. (1995). Model predictive control of an industrial packed bed reactor using neural networks. Journal of Process Control 5: 19-27.

Van den Hoed, R. (2007). Sources of radical technological innovation: the emergence of fuel cell technology in the automotive industry. Journal of Cleaner Production 15: 1014-1021.

Varbanov, P. S.and Friedler, F. (2009). Boosting energy conversion efficiency using fuel cells.

Wada, N., Saito, K.and Saeki, M. (2006). Model predictive control for linear parameter varying systems using parameter dependent Lyapunov function. IEEE Transactions on Circuits and Systems 53: 1446-1450.

Wan, Z.and Kothare, M. V. (2003). An efficient off-line formulation of robust model predictive control using linear matrix inequalities. Automatica 39: 837-846.

Xi, H., Varigonda, S.and Jing, B. (2010). Dynamic modeling of a solid oxide fuel cell system for control design. American Control Conference: 423-428.

Xin, X., Lü, Z., Huang, X., Sha, X., Zhang, Y.and Su, W. (2006). Anode-supported solid oxide fuel cell based on dense electrolyte membrane fabricated by filter-coating. Journal of Power Sources 159: 1158-1161.

Yamamoto, O. (2000). Solid oxide fuel cells: fundamental aspects and prospects. Electrochimica Acta 45: 2423-2435.

Yang, Y., Du, X., Yang, L., Huang, Y.and Xian, H. (2009). Investigation of methane steam reforming in planar porous support of solid oxide fuel cell. Applied Thermal Engineering 29: 1106-1113.

Zhang, X., Chan, S., Ho, H., Li, J., Li, G.and Feng, Z. (2008). Nonlinear model predictive control based on the moving horizon state estimation for the solid oxide fuel cell. International Journal of Hydrogen Energy 33: 2355-2366.

Zhang, X., Li, J., Li, G.and Feng, Z. (2006). Development of a control-oriented model for the solid oxide fuel cell. Journal of Power Sources 160: 258-267.

Zhao, F.and Virkar, A. (2005). Dependence of polarization in anode-supported solid oxide fuel cells on various cell parameters. Journal of Power Sources 141: 79-95.

Ziegler, J. G.and Nichols, N. B. (1942). Optimum Settings for Automatic Controller. Transactions of the A.S.M.E.: 759-768.

APPENDIX

APPENDIX A

PROOF OF LINEAR OBJECTIVE MINIMIZATION PROBLEM

Let $x(k)=x(\ k\ |\ k\ )$ be the state of the uncertain system (A.1) measured at sampling time k.

$$x(k+1) = A(k)x(k) + B(k)u(k) \tag{A.1}$$

$$y(k) = Cx(k)$$

$$\begin{bmatrix} A(k) & B(k) \end{bmatrix} \in \Omega$$

An upper bound on the robust performance cost is given as:

$$\max_{[A(k+i)\ \ B(k+i)]\in\Omega} J_{\infty}(k) \le V\left(x(k|k)\right)$$

Therefore, minimization of $V = x^T Px$, $P>0$ is equivalent to

$$\min_{\gamma,P} \gamma \tag{A.2}$$

subject to

$$x^T Px \le \gamma$$

Defining $Q = \gamma P^{-1} > 0$

$$x^T x \le \gamma P^{-1}$$

$$Q - x^T x \ge 0$$

Convert to LMI form using Schur complements

$$\begin{bmatrix} 1 & x^T \\ x & Q \end{bmatrix} \ge 0 \tag{A.3}$$

To guarantee the robust stability to the closed-loop, the state feedback gain, F is proved to satisfy the Lyapunov stability constraint.

Derivation of the upper bound, assume V satisfies the following inequality for all $x(k+i \mid k)$, $u(k+i \mid k)$, $i \geq 0$ satisfying (A.1), and for any $[A(k+i) \;\; B(k+i)] \in \Omega$, $i \geq 0$. We get

$$V\left(x\left(k+i+1|k\right)\right)-V\left(x\left(k+i|k\right)\right) \leq -\left[x\left(k+i|k\right)^T Q_1 x\left(k+i|k\right)+u\left(k+i|k\right)^T Ru\left(k+i|k\right)\right] \tag{A.4}$$

Substituting

$$u(k+i|k) = Fx(k+i|k) \tag{A.5}$$

$$V\left(x\left(k|k\right)\right) = x\left(k|k\right)^T Px\left(k|k\right) \tag{A.6}$$

$$x(k+i+1|k) = \left(A\left(k+i\right)+B\left(k+i\right)F\right)x(k+i|k) \tag{A.7}$$

The quadratic function V required to satisfy (A.4) becomes

$$\begin{aligned} &x(k+i+1|k)^T Px(k+i+1|k) - x(k+i|k)^T Px(k+i|k) \\ &\leq -\left[x\left(k+i|k\right)^T Q_1 x\left(k+i|k\right)+Fx(k+i|k)^T RFx(k+i|k)\right] \end{aligned} \tag{A.8}$$

$$\begin{aligned} &\left[\left(A\left(k+i\right)+B\left(k+i\right)F\right)x(k+i|k)\right]^T P\left[\left(A\left(k+i\right)+B\left(k+i\right)F\right)x(k+i|k)\right] \\ &- x(k+i|k)^T Px(k+i|k) \leq -\left[x\left(k+i|k\right)^T \left[Q_1+F^T RF\right]x\left(k+i|k\right)\right] \end{aligned} \tag{A.9}$$

$$\begin{aligned} &x(k+i|k)^T \left[\left(A\left(k+i\right)+B\left(k+i\right)F\right)^T P\left(A\left(k+i\right)+B\left(k+i\right)F\right)-P\right]x(k+i|k) \\ &\leq -\left[x\left(k+i|k\right)^T \left[Q_1+F^T RF\right]x\left(k+i|k\right)\right] \end{aligned} \tag{A.10}$$

$$x(k+i|k)^T \begin{bmatrix} \left(A\left(k+i\right)+B\left(k+i\right)F\right)^T P\left(A\left(k+i\right)+B\left(k+i\right)F\right) \\ -P+Q_1+F^T RF \end{bmatrix} x(k+i|k) \leq 0 \tag{A.11}$$

That is satisfied for all i ≥ 0 if

$$\left(A\left(k+i\right)+B\left(k+i\right)F\right)^T P\left(A\left(k+i\right)+B\left(k+i\right)F\right)-P+Q_1+F^T RF \leq 0 \tag{A.12}$$

Substituting

$$P = \gamma Q^{-1}, \quad Q > 0 \tag{A.13}$$

and

$$Y = FQ \tag{A.14}$$

Then pre- and post- multiplying by Q

$$\begin{aligned} &\left(A(k+i)Q + B(k+i)FQ\right)^T \gamma Q^{-1}\left(A(k+i)Q + B(k+i)FQ\right) \\ &- Q\gamma Q^{-1}Q + QQ_1Q + QF^T RFQ \le 0 \end{aligned} \tag{A.15}$$

$$\begin{aligned} &-\left(A(k+i)Q + B(k+i)Y\right)^T \gamma Q^{-1}\left(A(k+i)Q + B(k+i)Y\right) \\ &+ Q\gamma - QQ_1Q + Y^T RY \ge 0 \end{aligned} \tag{A.16}$$

Convert to LMI form using Schur complements

$$\begin{bmatrix} Q & QA(k+i)^T + Y^T B(k+i)^T & QQ_1^{1/2} & Y^T R^{1/2} \\ A(k+i)Q + B(k+i)Y & Q & 0 & 0 \\ Q_1^{1/2}Q & 0 & \gamma I & 0 \\ R^{1/2}Y & 0 & 0 & \gamma I \end{bmatrix} \ge 0 \tag{A.17}$$

Using Schur complement, let $Q(x) = Q(x)^T$, $R(x) = R(x)^T$, and $S(x)$ defend affinely on x. The matrix inequalities

$$R(x) > 0, \quad Q(x) - S(x)R(x)^{-1}S(x)^T > 0 \tag{A.18}$$

or,

$$Q(x) > 0, \quad R(x) - S(x)^T Q(x)^{-1} S(x) > 0 \tag{A.19}$$

This is equivalent to the linear matrix inequalities (LMIs)

$$\begin{bmatrix} Q(x) & S(x) \\ S(x)^T & R(x) \end{bmatrix} > 0 \tag{A.20}$$

APPENDIX B
LIST OF PUBLICATIONS

International publications

1. **Chatrattanawet, N.,** Skogestad, S., Arpornwichanop, A., (2014). Control Structure Design and Controllability Analysis for Solid Oxide Fuel Cell. Chemical Engineering Transactions, 39, 1291-1296.

2. **Chatrattanawet, N.,** Kheawhom, S., Arpornwichanop, A., (2015). Robust Model Predictive Control Strategy for LTV and LPV Systems of the Internal Reforming Solid Oxide Fuel Cell. Computer Aided Chemical Engineering, 37, 1733-1738.

3. **Chatrattanawet, N.,** Skogestad, S., Arpornwichanop, A., (2015). Control structure design and dynamic modeling for a solid oxide fuel cell with direct internal reforming of methane. Chemical Engineering Research and Design, 98, 202-211.

International conferences

1. **Chatrattanawet, N.,** Skogestad, S., and Arpornwichanop, A. (2014). Control Structure Design and Controllability Analysis for Solid Oxide Fuel Cell. 17th Conference Process Integration, Modelling and Optimisation for Energy Saving and Pollution Reduction (PRES 2014), 23-27 August 2014, Prague, Czech Republic.

2. **Chatrattanawet, N.,** Kheawhom, S., Arpornwichanop, A. (2014). Off-Line Robust Model Predictive Control of the Internal Reforming Solid Oxide Fuel Cell. The 4th TICHE International Conference 2014 "Changes: Cleaner Energy, Leaner Processes, Better Living" (TICHE 2014), 18-19 December 2014, Chiang Mai, Thailand.

3. **Chatrattanawet, N.,** Kheawhom, S., Arpornwichanop, A. (2015). Robust Model Predictive Control Strategy for LTV and LPV Systems of the Internal Reforming Solid Oxide Fuel Cell. 12th International Symposium on Process Systems Engineering and 25th European Symposium on Computer Aided Process Engineering (PSE2015/ESCAPE25), 31 May - 4 June 2015, Copenhagen, Denmark.

National conference

1. **Chatrattanawet, N.** and Arpornwichanop, A. (2012). Performance Analysis and Dynamic Modeling of Solid Oxide Fuel Cell with Methane Steam Reforming. RGJ-Ph.D. Congress XIII "From Green Revolution to Green Innovation", 6-8 April 2012, Pattaya, Thailand

VITA

Miss Narissara Chatrattanawet was born in Songkhla, Thailand, on July 14, 1986. She received her Bachelor of Engineering Degree (with first class honours) in Chemical Engineering from Prince of Songkla University in 2008. She directly continued her graduate studies at Chulalongkorn University in Control and Systems Engineering Research Center, Department of Chemical Engineering, Faculty of Engineering in June 2008 and received Ph.D. scholarship from Thailand Research fund (TRF) through the Royal Golden Jubilee Ph.D. program. During her graduate studies, she spent a period of 9 months in the Department of Chemical Engineering, Norwegian University of Science and Technology (NTNU), Norway, to do some parts of the Ph.D. research.